COMPARISON OF DIFFUSION TENSOR IMAGING, SUSCEPTIBILITY-WEIGHTED IMAGING AND DYNAMIC SUSCEPTIBILITY CONTRAST-ENHANCED MRI IN DIFFERENTIATING HIGH-GRADE INTRA-AXIAL CEREBRAL TUMORS

THESIS

SUBMITTED IN PARTIAL FULFILLMENT FOR DEGREE OF DM (NEUROIMAGING AND INTERVENTIONAL NEURORADIOLOGY)

(2013-2015)

OF THE

SREE CHITRA TIRUNAL INSTITUTE FOR MEDICAL SCIENCES AND TECHNOLOGY

TRIVANDRUM, KERALA, INDIA

Dr. SWETA SWAIKA

DEPARTMENT OF IMAGING SCIENCES & INTERVENTIONAL RADIOLOGY

SREE CHITRA TIRUNAL INSTITUTE FOR MEDICAL SCIENCES AND TECHNOLOGY

TRIVANDRUM, KERALA, INDIA

SREE CHITRA TIRUNAL INSTITUTE FOR MEDICAL SCIENCES AND TECHNOLOGY, TRIVANDRUM

CERTIFICATE

This is to certify that the study incorporated in this thesis titled ***"Comparison of diffusion tensor imaging, susceptibility-weighted imaging and dynamic susceptibility contrast-enhanced MRI in differentiating high-grade intra-axial cerebral tumors"*** *for the degree of* ***DM (Neuroimaging and Interventional Neuroradiology)*** *has been done by Dr. Sweta Swaika under my supervision and guidance. The work done related to this thesis has been carried out by the candidate herself and is genuine.*

(Dr. Bejoy Thomas)	***(Dr. Krishna Kumar K)***	***(Dr. Santhosh Kumar K)***
Additional Professor	***Associate Professor***	***Assistant Professor***
Department of IS&IR	***Department of Neurosurgery***	***Department of IS&IR***
Principal Guide	***Co-Guide***	***Co-Guide***

Dr. Kapilamoorthy TR

Professor and HOD

Department of Imaging Sciences and Interventional Radiology (IS&IR)

SCTIMST, Trivandrum

DECLARATION

I hereby declare that this thesis titled ***"Comparison of diffusion tensor imaging, susceptibility-weighted imaging and dynamic susceptibility contrast-enhanced MRI in differentiating high-grade intra-axial cerebral tumors"*** *has been prepared by me under the supervision and guidance of Dr. Bejoy Thomas (Additional Professor), Dr. Santhosh Kumar K (Assistant Professor) and Dr. Kapilamoorthy TR (Professor & HOD), Department of Imaging Sciences and Interventional Radiology and Dr. Krishna Kumar K (Associate Professor), Department of Neurosurgery, Sree Chitra Tirunal Institute for Medical Sciences and Technology, Trivandrum.*

Date: ***Dr. Sweta Swaika***

Place: Trivandrum

ACKNOWLEDGEMENT

- *I would like to express my deep gratitude and indebtedness to my honorable teachers and guides* ***Dr. Bejoy Thomas, Dr Krishna Kumar K, Dr. Santhosh Kumar K and Dr. Kapilamoorthy TR*** *for their continuous support, proficient supervision, useful criticism, helpful observations and benevolent guidance which were of paramount help throughout the course of the study.*

- *I am highly grateful to my teachers Dr. Kesavadas C and Dr. Jayadevan ER for their invaluable help and immense support throughout the study.*

- *I truly appreciate the constructive help and cooperation of my past and present colleagues. I also acknowledge the favorable help and support of all the technicians and staff members of my department.*

- *I am enormously grateful to my patients and their relatives who have made this study possible.*

- *It will never be enough to thank my family members for their unconditional and precious support, care and motivation which have been the driving force throughout my life.*

Dr. Sweta Swaika

Senior Resident

Department of IS&IR

SCTIMST

CONTENTS

INTRODUCTION

The common high-grade intra-axial tumors of brain include glioblastoma multiforme, anaplastic glioma, metastasis and lymphoma. These tumors have grim prognosis in spite of improvements in surgery, chemotherapy and radiotherapy. Accurate diagnosis is of utmost importance in clinical decision making and estimating patient's prognosis.

Conventional magnetic resonance imaging (MRI) is not always helpful in differentiating between these high-grade lesions as they may have similar imaging findings. Classification and grading of the gliomas cannot always be accurately done based on conventional MRI findings. Contrast-enhanced MRI is useful for detection and structural characterization of brain tumors. However, contrast enhancement signifies blood–brain barrier interruption and not tumor vascularity which is a marker of tumor aggressiveness.

Advanced MRI techniques including diffusion tensor imaging (DTI), susceptibility-weighted imaging (SWI), perfusion MRI and magnetic resonance spectroscopy (MRS) could further help in this regard. Infiltrating gliomas usually spread in the course of white matter tracts and DTI is the single noninvasive imaging method which can quantitatively evaluate the white matter tracts for their microstructural integrity. SWI is a gradient-echo method that shows tissue magnetic susceptibility. It has the potential to assess intratumoral microvascularity and

hemorrhage commonly seen in these tumors. Dynamic susceptibility contrast-enhanced perfusion MRI (DSC-MRI) yields functional information regarding neoangiogenesis in brain tumors.

This study aims to evaluate and compare the efficacy of diffusion tensor imaging, susceptibility-weighted imaging and dynamic susceptibility contrast-enhanced MRI in accurately diagnosing high-grade intra-axial cerebral tumors with histo-pathological evaluation as gold standard.

AIMS AND OBJECTIVES

This study evaluates and compares DTI (using diffusion tensor metrics), SWI and DSC-MRI in distinguishing intra-axial high-grade cerebral tumors with histopathological assessment considered as gold standard. Both retrospective (January 2009 - May 2013) and prospective (June 2013 - June 2015) observational studies were done for patients referred to our department and satisfying the inclusion criteria.

Study Hypothesis: The use of DTI, SWI and DSC-MRI enhances the diagnostic accuracy in differentiating high-grade intra-axial cerebral tumors.

Objectives:

- To accurately diagnose the intra-axial cerebral high-grade lesions preoperatively and thus help in surgical and chemotherapy/radiotherapy planning.
- To reliably distinguish the peritumoral white matter infiltration from peritumoral edema and determine the choice of biopsy site.
- To find the highest predictive value among the different parameters used in DTI, SWI and DSC-MRI for differentiating these high-grade lesions.

REVIEW OF LITERATURE

Brain tumors represent a group of neoplasm arising either from the brain structures (primary) or secondary due to metastasis from extracranial tumor. These tumors comprise less than 1.5% of all body tumors but have high morbidity and mortality.[1] The incidence of primary brain tumors is escalating due to increasing age of population and better diagnostic techniques.[2] These tumors are seen in all age groups with predilection of certain tumor types in children and adults. Due to the difference in pathology and location of brain tumors between children and adults, they are studied separately. The brain tumors differ in management approach and thus require accurate imaging diagnosis.

EPIDEMIOLOGY

In adults, the commonest primary brain tumor is glioma which constitutes over 70% of entire brain tumors.[2] The revised World Health Organization (WHO) classification of glioma divides it into four grades (grade I - IV) based on tumor cellularity, nuclear atypia, pleomorphism, necrosis and mitosis.[3] Grade I glioma includes pilocytic astrocytoma, pleomorphic xanthoastrocytoma and subependymal giant cell astrocytoma. Diffuse astrocytoma is classified as grade II glioma and anaplastic astrocytoma is classified as grade III glioma. Glioblastoma multiforme represents grade IV glioma. Grade I and grade II gliomas are grouped together as

low-grade gliomas. The grade III and grade IV gliomas are considered as high-grade gliomas. More than 50% of all gliomas are high-grade lesions.

The low-grade gliomas are most frequent in young adults and anaplastic astrocytoma is mostly seen in middle-aged adults (40-60 years).[4] Glioblastoma multiforme is most common in elderly population, occurring mostly in the fifth and sixth decades of life. It exhibits worst prognosis among all gliomas.[1] Glioma is the most prevalent primary brain tumor in adult males. In females, meningioma is the most common tumor encompassing 20% of all intracranial tumors in adults.

High-grade gliomas cause direct local brain infiltration, tissue destruction and secondary changes such as edema and raised intracranial pressure. The patients present mostly with headache, seizures and focal neurological deficits like hemiparesis or aphasia. Around 6% of patients may develop acute symptoms due to tumor bleed. Only 1% of patients will be asymptomatic and incidentally detected.[5]

Metastasis is among the most common intracranial neoplastic lesion in adults. The most common primary sources are lung cancer, breast cancer and melanoma.[6] The patients usually present with headache, focal neurological deficits, cognitive dysfunction and seizures.[7] It is difficult to differentiate solitary metastatic lesion with unknown primary malignant lesion from high-grade glioma based on conventional MRI findings due to their similar appearance.[8]

The other malignant parenchymal lesion is primary central nervous system lymphoma (PCNSL). It constitutes 1-5% of the entire primary brain tumors.[9] It occurs in both immunocompetent and immunocompromised patients. It peaks in the fourth decade in immunocompromised patients and between the fifth and seventh decades of life in immunocompetent patients. It is bilateral in around 40% of patients. The most common clinical symptoms of these patients are cognitive dysfunction, personality changes, altered mental status, features of raised intracranial pressure and seizures.[10]

PATHOLOGY

Anaplastic astrocytoma is a grade III glioma which develops either de novo or from malignant transformation of low-grade glioma. It is mostly found in the cerebral hemispheres and is usually solitary. It causes diffuse infiltration and expansion of the involved brain parenchyma. It appears rubbery to fleshy in consistency. It is moderate to markedly cellular with inconstant amount of nuclear atypia and mitosis. It lacks necrosis and hemorrhage. Mean survival in the patient is 2-3 years.[11]

Anaplastic oligodendroglioma is a grade III glioma and constitutes 25-35% of all oligodendrogliomas. It is characterized by pleomorphism, endothelial proliferation, high cellularity, high mitotic activity (mitoses counts ≥ 4 per 10 high-power fields) and necrosis. It has predilection for frontotemporal lobes. It is associated with

poorer prognosis than low-grade oligodendrogliomas. The proliferation index is 7-10%. Mean survival in the patient is about 4 years.[11, 12]

Anaplastic oligoastrocytoma is also a grade III glioma with tumor cells resembling astrocytoma (> 30% of tumor cell population) and oligodendroglioma. It has pleomorphism, nuclear atypia, increased cellularity and increased mitotic activity. It is most commonly located in the frontotemporal lobes. The median survival time is nearly 2.8 years.[11, 12]

These two anaplastic tumors (anaplastic oligodendroglioma and anaplastic oligoastrocytoma) differ from low-grade oligodendroglioma and low-grade oligoastrocytoma as studied by Sepulveda Sanchez et al[12]. They found that anaplastic oligodendroglioma and anaplastic oligoastrocytoma have older age of onset, clinical presentation other than seizure (like focal neurological deficits, headaches), more contrast enhancement, significantly lower postsurgical Karnofsky Performance Scale (KPS) score and more frequent incomplete excision compared to the low-grade oligodendroglioma and oligoastrocytoma. The presence of calcification, gender of the patient and location of the lesion did not correlate with the tumor grade.[12]

Glioblastoma multiforme is a poorly differentiated WHO grade IV tumor and develops either de novo or from pre-existing low-grade glioma or anaplastic astrocytoma. It has rapid progression with mean survival of less than 12 months. It

is most commonly located in the cerebral parenchyma involving the subcortical and deep periventricular white matter. It has high propensity to spread through the corpus callosum and corticospinal tracts. It usually appears as a reddish gray "rind" of tumor with a central necrotic core. It has high neovascularity, hemorrhage and mitotic rate. Intratumoral calcification is rare within it. The proliferation index is > 10%.[11, 13, 14, 15]

PCNSL is an uncommon form of extranodal non-Hodgkin lymphoma, 95% of which is diffuse large B-cell lymphoma. The other types are T-cell lymphoma; mucosa associated lymphoid tissue type and the lymphoplasmacytic lymphoma. The disease is absent outside the central nervous system. It can affect brain, meninges, spinal cord and eye. About 95% of it is located in contact with cerebrospinal fluid (CSF) surface. It is most commonly located in the cerebral hemispheres, usually in periventricular white matter. It can also involve the basal ganglia and thalamus. It can be solitary (40-60%) or multiple. It may be unilateral or bilateral. It is mostly a solid pale lesion on gross examination. It forms lymphoid clustering around the cerebral small vessels and extends into the adjacent parenchyma. The lymphoid cells are most commonly high-grade with immature blastic cells and large pleomorphic nuclei. It has very high proliferation index (MIB-1> 50%).[16]

Brain metastasis can arise from extracranial (hematogenous route) or intracranial tumors. Direct extension from adjacent structures (nasopharyngeal carcinoma), along neural foramina, perineural or perivascular spread can occur, though less common. In about 10% of metastasis, there is an unknown primary source at the time of diagnosis. In adults, the primary site is usually lung cancer (most frequently adenocarcinoma and small cell carcinoma), breast carcinoma, melanoma, renal carcinoma and colon cancer. It mostly occurs in the cerebral parenchyma (around 80%). Other sites are basal ganglia, cerebellum, skull, dura mater and leptomeninges. It may be single (50%) or multiple (50%). It frequently occurs at the arterial border zones and at the cortical-subcortical junction. It is usually 0.5-1.5 cm in size. Grossly, it is a round, well-defined lesion with variable perilesional edema and necrosis. Hemorrhage can occur in metastasis when the primary source is renal cell carcinoma, melanoma and choriocarcinoma. There may be more mitoses and labeling index in metastatic lesion compared to the primary source. The prognosis is better for solitary lesions.[17, 18]

TREATMENT

Anaplastic astrocytoma is treated by resection followed by adjuvant chemotherapy and radiotherapy with improved progression-free survival. Glioblastoma multiforme is usually treated with gross total excision with adjuvant chemotherapy and radiotherapy. This significantly improves median survival.[11, 19, 20]

Surgery is the primary treatment with chemotherapy and radiotherapy for residual or recurrent tumor in cases of anaplastic oligodendroglioma and anaplastic oligoastrocytoma.[11]

Lymphoma needs histopathological confirmation done by stereotactic biopsy. Treatment can be done by chemotherapy, radiotherapy and corticosteroids. It has a good response to treatment but has a high rate of relapse. Autologous stem cell transplantation can be useful in younger patients.[16] Management options for brain metastases are surgical resection, radiotherapy, chemotherapy and stereotactic radiosurgery.[18]

CONVENTIONAL MRI FINDINGS

MRI is the primary modality for diagnosis of these tumors determining their location, extent and mass effect, directing biopsies and deciding the mode of treatment. It is also used for assessing the treatment response and monitoring the long-term outcome.[21, 22] The standard protocol for MRI is T1-weighted spin-echo sequence, T2-weighted fast spin-echo sequence, fluid-attenuated inversion recovery (FLAIR) sequence, proton density-weighted sequence, gradient-echo sequence and contrast-enhanced T1-weighted sequence taken in multiple planes.

High-grade gliomas:

High-grade gliomas show heterogeneous signal intensity on MRI with predominant hypointensity on T1-weighted images and hyperintensity on T2-weighted images with areas of necrosis, tumor bleed, peritumoral vasogenic edema and tissue infiltration. They show diffusion restriction and irregular contrast enhancement (which can be focal, nodular and ring-like). Glioblastoma multiforme can also spread along the CSF pathways (known as drop metastasis), white matter tracts and along the ependyma (seen as creeping tumor spread). It can also cause mass effect due to rapid growth causing features of raised intracranial pressure.[11]

PCNSL:

PCNSL is most frequently located in the periventricular or cerebral hemispheric white matter regions. In the immunocompetent patients, it is iso- to hypointense on T1-weighted images and iso- to hyperintense on T2-weighted images. It may be hypointense to gray matter on T2-weighted images. It may be of variable signal intensity on FLAIR images. It shows moderate to marked homogeneous or heterogeneous contrast enhancement. Linear contrast enhancement along the perivascular spaces highly suggests PCNSL. It rarely shows ring enhancement. There is usually mild perilesional edema. Petechial hemorrhage may be seen within the lesions (5-8%). Diffusion restriction is usually present. In the immunocompromised patients, ring enhancement with non-enhancing necrotic core is typically seen.[9, 16]

Metastasis:

Metastasis occurring within brain parenchyma appears usually iso- to mildly hypointense on T1-weighted images and has varied signal intensity on T2-weighted images (mostly isointense to mildly hyperintense). Melanoma metastasis is hyperintense on T1-weighted images. Hemorrhagic metastatic lesions are of heterogeneous T1 signal intensity with mixed areas of hyper- and hypointensities. Metastasis from highly cellular tumors appears hypointense to gray matter on T2-weighted and FLAIR images. Cystic metastasis appears mildly hyperintense on T2-weighted images. Metastasis shows moderate to marked contrast enhancement, which may be solid, nodular or ring-like enhancement. Diffusion restriction is usually not seen. There is usually some perilesional edema. Subacute hemorrhage may be seen in some cases.[17, 18]

Comparative imaging findings between different high-grade intra-axial lesions:

Chen et al[23] showed that the qualitative and quantitative analysis of T2 prolongation in the intratumoral and peritumoral regions can be helpful to distinguish between glioblastomas and metastases. They analyzed conventional T2 signal intensity in 45 cases of glioblastoma and 21 cases of solitary metastasis. They compared the peritumoral T2 prolongation areas with the intratumoral areas and graded each lesion into 2 types: 1) grade I – peritumoral prolongation area less than or equal to tumor area, 2) grade II – area of peritumoral prolongation more than

tumor area. They also measured the signal intensities of the peritumoral T2 prolongation areas and then normalized them to values of the contralateral normal tissue. This ratio of normalized signal intensity (nSI) was compared.

They found that grade I pattern was more common in glioblastomas and grade II pattern was more common in metastases ($P < 0.001$), thus indicating higher peritumoral T2 prolongation area in metastases. The nSI was significantly more in glioblastomas in comparison to metastases ($P < 0.001$) with AUC = 0.725. The higher nSI in glioblastomas was explained by the presence of tumor infiltration and glial changes in infiltrated tissue apart from vasogenic edema. Metastases only have vasogenic edema in peritumoral regions causing white matter tract compression and displacement with no tumor infiltration. However, there was no correlation between the cellularity of tumors with signal intensity on T2-weighted images likely due to involvement of multiple factors.[23]

Tang et al[24] assessed the usefulness of FLAIR images in differentiating gliomas from metastases. They found that the presence of abnormal signal intensity in adjacent cortex on FLAIR images had 44% sensitivity, 91% specificity and 84% positive predictive value for gliomas in comparison to metastases.

The neovascularity in glioblastoma is irregularly arranged with alternate foci of dilatation and constriction. Vessels in tumor bed are larger, more tortuous and disorganized. The draining veins are dilated. Christoforidis et al[25] visualized the

microvascularity in glioblastomas using 8T gradient-echo MRI with high spatial-resolution. They also found dilatation and tortuousness of the peritumoral transmedullary veins in glioblastomas.

All contrast-enhancing lesions are not high-grade tumors. Low-grade tumors may also have perilesional edema and mass effect mimicking high-grade lesions. The major factors for high-grade tumors are the histopathological findings of high tumor cellularity and vascularity. These factors are not reliably determined by conventional MRI. Contrast enhancement within lesions merely signifies blood-brain barrier disturbance and does not imply increased angiogenesis.[26] Hence advanced MRI techniques like diffusion-weighted and perfusion MRI are required to study tumor cellularity and vascularity respectively.

ADVANCED MRI IMAGING

i) Diffusion-weighted imaging (DWI):

Water molecules in tissues show random translational motion based on Brownian motion. DWI uses strong diffusion gradients to study the movement of water molecules within tissues. The pulse sequence consists of two sequential gradient pulses which are applied on each side of the 180° pulse in a 90°–180° spin-echo sequence. This causes loss of signal after the second gradient pulse due to the random motion of water. This signal loss (S/S_0) depends on: 1) time-span and strength of the diffusion gradients (or degree of diffusion weighting termed b) and

2) the diffusion coefficient of the substance (termed D). S implies the signal after application of diffusion gradients and S_0 represents the signal before use of diffusion gradients. The degree of signal loss (S/S_0) is represented by the equation: $S/S_0 \propto e^{-bD}$.[27, 28]

Apparent diffusion coefficient (ADC) is computed from the diffusion-weighted images and represented as a map. ADC describes the microscopic diffusibility of water in presence of factors that restrict it like cell membranes and tissue viscosity.[27]

Various reports have published mean ADC value in high-grade gliomas. Stadnik et al[29] reported mean ADC value of 1.14 x 10^{-3} mm^2/s and Sugahara et al[30] found ADC value to be 1.2 ± 0.4 x 10^{-3} mm^2/s. Calli et al[26] measured mean ADC value to be 0.92 ± 0.28 x 10^{-3} mm^2/s from contrast-enhancing solid portions of the tumor excluding the cystic and necrotic areas, which could be the reason for the ADC value to be lower compared to the other studies. Similarly, lower ADC values were reported by Yang et al[31] who found it to be 0.92 ± 0.27 x 10^{-3} mm^2/s in high-grade gliomas and by Kono et al[32] who calculated ADC values in glioblastomas to be 0.82 ± 0.13 x 10^{-3} mm^2/s. Also, anaplastic astrocytomas were reported by Yang et al[31] to have greater ADC values (1.1 ± 0.31 x 10^{-3} mm^2/s) compared to glioblastomas (0.80 ± 0.14 x 10^{-3} mm^2/s).

Studies have shown that there is a reverse correlation between the tumor cellularity and minimum ADC value.[30, 32] Thus, there is a significant dissimilarity in

the ADC values of low-grade and high-grade gliomas reflecting differences in cellular density and extracellular matrix. Low-grade gliomas are less cellular and appear iso- to mildly hyperintense on DWI images and markedly hyperintense on ADC maps suggestive of high ADC values. High-grade gliomas have high cellularity and less interstitial space which restricts the random motion of water molecules. This prevents the loss of signal and they appear as markedly hyperintense on DWI images and hypointense on ADC maps due to significantly lower ADC value. High-grade gliomas have lesser ADC value than low-grade gliomas and glioblastoma multiforme has lower ADC value than anaplastic astrocytoma.[30]

High-grade gliomas have heterogeneous morphology with different grades present within the same tumor. This causes variation in ADC values within a single lesion. Hence minimum ADC value corresponding to the high-grade changes should be used for grading the tumor. The minimum ADC value can help in choosing the site of biopsy and prevent sampling error.[30]

Pauleit et al[33] studied 22 gliomas and calculated the ADC maps. They correlated ADC values with the histological specimens taken after neuronavigation-guided biopsies. They did not find any significant disparity in absolute ADC values of the tumor and peritumoral regions in their study. They concluded that ADC values are not useful in differentiating tumor from peritumoral regions in gliomas.

In metastases, various authors have published ADC values. Krabbe et al[34] reported it to be 1.2 – 2.73 x 10^{-3} mm^2/s. It was not much different from high-grade gliomas in which ADC was found to be 0.72 – 2.61 x 10^{-3} mm^2/s. Kono et al[32] found mean ADC value to be 0.79 ± 0.23 x 10^{-3} mm^2/s in metastases (almost similar to the ADC value of 0.82 ± 0.13 x 10^{-3} mm^2/s seen in glioblastomas). Stadnik et al[29] reported it as 0.82 and 1.24 x 10^{-3} mm^2/s and Calli et al[26] found mean ADC value to be 0.68 ± 0.11 x 10^{-3} mm^2/s. There has been no considerable discrepancy in mean ADC values between metastases and high-grade gliomas in all reported studies at 1.5T MRI.

Lee et al[35] similarly stated that mean ADC values in the contrast-enhancing tumor regions were not significantly dissimilar between glioblastomas and metastases. The peritumoral minimum ADC values of glioblastomas however, were significantly more compared to metastases. They defined a cutoff value of 1.3 x 10^{-3} mm^2/s for the minimum ADC value in peritumoral regions with 82.9% sensitivity and 78.9% specificity for discriminating glioblastomas from metastases.

At 3T MRI, Chiang et al[36] reported a notable difference in mean ADC values between the tumor regions of high-grade gliomas and metastases. The ADC value in metastases was found to be 1.87 ± 0.73 x 10^{-3} mm^2/s and in high-grade gliomas was estimated to be 1.04 ± 0.42 x 10^{-3} mm^2/s ($P < 0.005$).

Lymphomas are found to have ADC values less than high-grade gliomas. Calli et al[26] reported mean ADC value in lymphomas to be 0.51 ± 0.09 x 10^{-3} mm^2/s which was remarkably lower than in high-grade gliomas. Stadnik et al[29] found it to be 0.55 and 0.58 x 10^{-3} mm^2/s in lymphomas. Similarly, Guo et al[37] found lower mean ADC ratio (1.15) in lymphomas compared to high-grade gliomas (1.68). However, there was considerable similarity in ADC values of lymphomas and metastases.[26]

Barajas et al[38] recently published that measurement of ADC values in intratumoral regions of PCNSL can predict the treatment outcome. They found that patients with PCNSL having lower pretreatment ADC values had shorter duration of progression-free and overall survival in posttreatment period. Significant reduction of ADC values posttreatment increased the overall and progression-free survival in these patients. However, ADC values alone cannot be used for making decisions in an individualized setting.[39]

ii) Diffusion Tensor Imaging (DTI):

DTI helps to characterize the orientation and integrity of white matter fibers in vivo.[40, 41] It perceives water diffusion along the white matter fibers i.e. anisotropic diffusion. In brain, anisotropic diffusion is due to many factors including lipid bilayer of myelin sheath which acts as a diffusion barrier and the collimated axon bundles and their subcomponents (microtubules, microfilaments and neurofilaments). Maximum diffusion of water takes place analogous to the

longitudinal configuration of axons and myelin sheaths. Water diffusion is minimal perpendicular to the axons.[3] Brain tumors are usually surrounded by vasogenic edema which is seen as perilesional T2/ FLAIR hyperintensity. DTI shows altered parameters in this region due to increased extracellular edema with or without tumor infiltration.

The tumor cells of high-grade gliomas can infiltrate into the surrounding tissue (peritumoral region). The immediate peritumoral region is the transitional zone which may show contrast enhancement. Beyond it is the region of tumor infiltration which shows abnormalities on MRS and DSC-MRI. Outside this region is the zone of peritumoral edema which can be detected by DTI. And beyond this is the normal appearing white matter which may still have tumor cells but is not detected by the advanced MRI techniques.[42]

In DTI, echoplanar imaging (EPI) sequence is acquired by applying diffusion gradients in 30 non-collinear planes. The diffusion tensor is measured by applying the source data onto the software which utilizes Stejskal-Tanner equation. Three eigenvalues (λ_1, λ_2, λ_3) are determined per voxel. DTI quantifies the comparative amount of water diffusion along three mutually perpendicular planes (known as eigenvectors). The eigenvector of the biggest eigenvalue (λ_1) represents the major course of water diffusion and thus demonstrates the orientation of white matter bundles. The other two eigenvalues (λ_2, λ_3) are at right angles to λ_1.[40]

There are a number of diffusion indices (or metrics).[40, 43] These are: 1) MD - mean diffusivity 2) FA - fractional anisotropy 3) p - pure isotropic component of diffusion 4) q - pure anisotropic component of diffusion 5) L - total magnitude of diffusion tensor 6) CL - linear anisotropy 7) CP - planar anisotropy 8) CS - spherical anisotropy. Quantitative maps of these parameters can be obtained. In the normal gray matter, FA and MD are low. In the normal white matter, FA is high and MD is low. In the CSF, FA is low and MD is high. The diffusion tensor metrics are calculated using the following formulae:

$$MD = (\lambda_1 + \lambda_2 + \lambda_3)/3$$

$$FA = \sqrt{\frac{3}{2}} \times \frac{q}{L}$$

$$p = \frac{\lambda_1 + \lambda_2 + \lambda_3}{\sqrt{3}}$$

$$q = \sqrt{[(\lambda_1 - D)^2 + (\lambda_2 - D)^2 + (\lambda_3 - D)^2]}$$

$$L = \sqrt{p^2 + q^2}$$

$$CL = (\lambda_1 - \lambda_2)/(\lambda_1 + \lambda_2 + \lambda_3)$$

$$CP = 2(\lambda_2 - \lambda_3)/ (\lambda_1 + \lambda_2 + \lambda_3)$$

$$CS = 3\lambda_3/(\lambda_1 + \lambda_2 + \lambda_3)$$

The applications of DTI include**:** 1) presurgical assessment of interval between the lesion and eloquent areas of brain to assess the risk of postsurgical disabilities 2) to choose patients requiring intraoperative monitoring and 3) to decide on the use of neuronavigation during biopsy or surgery.

The limitations of DTI are: 1) it is largely affected by the maximum value of water diffusion at each voxel 2) it is sensitive to distortion and susceptibility artifacts 3) data quality is affected by head motion of the patient 4) positioning of the ROI is operator dependent 5) lack of standardized DTI processing protocols 6) it cannot differentiate tumor from inflammation 7) it cannot identify singly located tumor cells at a little distance from the lesion.

DTI tractography creates diagrammatic representation of the white matter bundles superimposed on high-resolution anatomical data. Three-dimensional illustration of white matter tracts is obtained by tractography. It detects the involvement of the white matter fibers in both tumor and peritumoral regions. Direction encrypted color maps are created using red, green and blue colors. The white matter fibers running in the x-direction (left-right) are colored red, tracts in y-direction (anterior-posterior) appear green, and bundles running in z-direction (superior-inferior) are colored blue. FA determines the intensity of the voxels.[43]

FA describes the course of water movement along the white matter tracts. Its value ranges from 0 to 1. In a completely anisotropic tissue, FA is 1 as all the water

molecules diffuse in the same direction. In a completely isotropic tissue, FA is 0. High FA is seen in normal brain white matter and reduces with destruction of white matter tracts.[44] As FA is a ratio of *q* and *L*, it can be altered by changes in either *q* or *L*.[45] Reduced FA value is seen as hypointensity in the quantitative FA maps. MD measures the magnitude of the water movement.

Toh et al[46] calculated mean FA and ADC values in 10 patients of glioblastoma and 10 patients of PCNSL. They found that the mean FA and ADC values were remarkably less in PCNSL in comparison to glioblastomas ($P < 0.001$). They suggested cutoff value of 0.192 for FA (having sensitivity 100%, specificity 80% and accuracy 90%) and 0.818 for ADC (sensitivity 100%, specificity 90% and accuracy 95%) to differentiate between the two tumors.

The reduction in FA and ADC was attributed to the more cellularity of PCNSL compared to glioblastoma.[46] However, FA is also dependent on integrity of white matter tracts, tumor vascularity, edema, microcysts, extracellular space and ratio of extracellular to intracellular space. FA and ADC are thus determined by different factors and are independent parameters.[47]

Le Bihan et al[48] and Morita et al[49] found increase in MD in the peritumoral region in high-grade gliomas compared to low-grade gliomas. This increase in diffusivity was postulated to be due to destruction of the extracellular matrix by the infiltrating

lesions. This was reflected by reduced glutamate levels in MRS by a study done by Kimura et al[50].

Lu et al[21] showed that increase in MD in peritumoral region was more in metastases compared to high-grade gliomas. This was explained by the presence of higher extracellular water in peritumoral region in metastases compared to high-grade gliomas. They found reduced peritumoral FA in both metastases and high-grade gliomas. The reduction in FA in metastases was attributed solely to the increased extracellular water but for high-grade gliomas, it was also caused by infiltrating cells destroying the extracellular matrix. However, there was no significant disparity in peritumoral FA between the two lesions. They explained this by the fact that the increase in extracellular water in case of metastases was equivalent to the peritumoral changes (peritumoral edema and infiltration) in high-grade gliomas. Since MD depends solely on the amount of extracellular water it was higher in metastases but FA is determined by more than one factor.

A new metric, Tumor Infiltration Index (TII) was suggested by Lu et al[51] for defining the extent of the tumor infiltration in high-grade gliomas. They reported that the high-grade gliomas had mean TII of 64 owing to perilesional infiltration whereas metastases and meningiomas showed mean TII equal to 0.

Kinoshita et al[52] also assessed the usefulness of TII in 14 patients (gliomas 8, meningiomas 5 and metastases 1) comparing it with C-11 methionine PET. The

mean TII in gliomas ranged from -127 to 96 (mean ± SD, 5.4 ± 65). For meningiomas and metastases, it ranged from -24 to 44 (mean ± SD, 6.8 ± 29). There was no statistically significant difference in TII between these tumors. They concluded that TII was not useful for differentiating tumor-infiltrated edema from vasogenic edema in peritumoral edematous regions. But they could identify tumor infiltration in nonedematous regions. There was a positive correlation between TII and C-11 methionine PET which suggested that PET could also be used as an adjunctive modality for detecting tumor infiltration.

Deng et al[44] studied the correlation of DTI with degree of tumor invasion in 20 cases of gliomas. The degree of peritumoral tumor infiltration was quantified under high-power magnification. They estimated the ratio of tumor cells to normal cells. The extent of tumor invasion was divided into 4 types based on percentage of tumor cells: 1) no invasion 2) mild invasion (tumor cells < 20%) 3) moderate invasion (tumor cells 20-40%) 4) severe invasion (tumor cells > 40%). The tumor invasion was studied in 5 areas: 1) intratumoral area 2) peritumoral edematous region 3) surrounding edematous region 4) adjacent white matter region 5) contralateral white matter area. They found that FA had a negative correlation with degree of tumor infiltration and increased outwards from the intratumoral region with maximum increase occurring between the peritumoral edema and surrounding edematous regions (area appearing normal in conventional MRI but detected in DTI). The ADC values in gliomas increased from intratumoral region to

peritumoral region and then decreased outwards. This increase in ADC in peritumoral edematous region was statistically significant but changes in other areas varied. They suggested that FA in peritumoral and surrounding edematous regions should be studied to measure the degree of peritumoral invasion. However, there was no correlation between FA and glioma grade.

Liang et al[53] carried out a meta-analysis on the role of FA to discriminate high-grade and low-grade gliomas. They analyzed 7 reports including 246 patients (142 cases of high-grade gliomas and 104 cases of low-grade gliomas). FA was notably more in high-grade gliomas in contrast to low-grade gliomas. FA showed 93% sensitivity, 85% specificity and diagnostic odds ratio of 55.41 in categorizing the gliomas.

Systematic review and meta-analysis recently published by Jiang et al[8] included 9 studies (3 prospective and 6 retrospective) from January 1980 to August 2014. These studies calculated and compared the mean FA with or without MD in high-grade gliomas (193 patients) and metastases (141 patients). The age of patients ranged from 50-64 years. The histopathological result was taken as the standard in 7 studies. Both 3T and 1.5T MRI scanners were used for imaging. The meta-analysis showed that FA in peritumoral edema in high-grade gliomas was considerably high in comparison to metastatic lesions ($P < 0.01$). The FA in peritumoral edema was not affected by the type of glioma, sample size, publication year, study region or

scanner type and remained significant in the subgroup analysis. The relatively high peritumoral FA in high-grade gliomas was related to the high degree of infiltration into the adjacent tumor regions with increased tumor specific extracellular matrix components causing adhesion and orientation of the tumor cells causing higher anisotropy. There was higher FA in intratumoral regions in high-grade gliomas in contrast to metastases in higher field strength (3T) scanner, prospective studies and studies with different types of high-grade gliomas. This was supposed to be due to higher cellularity in high-grade gliomas leading to higher anisotropy. Prospective studies reduced study bias and were considered higher evidence than retrospective studies. Also, DTI at 3T led to higher resolution and better performance and was also found to have a correlation though weak, in meta-regression analysis.

In the 4 studies which calculated MD in the peritumoral edema there was decrease in MD in high-grade gliomas in comparison to metastatic lesions ($P < 0.01$). 2 studies also reported intratumoral MD. They found no notable difference in intratumoral MD between the 2 tumors ($P = 0.59$). Further subgroup analysis for intra- and peritumoral MD was not done as there was less number of studies. The changes in MD were explained to be due to varying degrees of vasogenic edema in the extracellular compartment.[8]

Byrnes et al[54] studied 28 cases of glioblastomas and metastases with DTI. They found that mean MD was considerably more ($P = 0.020$) and mean FA was notably

lesser (P = 0.044) within the perilesional edema around metastases in comparison to glioblastomas. MD but not FA was appreciably more (P = 0.019) in the intratumoral areas of glioblastomas compared to metastases.

Wang et al[55] reported improved diagnostic accuracy in distinguishing glioblastomas and metastases with application of classification models utilizing FA and MD. They measured FA and MD in both tumor and peritumoral regions in glioblastomas (128 patients) and metastases (93 patients). They observed notably higher FA in tumor regions in glioblastomas in comparison to metastases (P < 0.01). This was explained by the notion that glioblastomas produce high amount of tumor-specific extracellular matrix components which cause adhesion, migration and orientation of the tumor cells leading to high anisotropy. This was considered similar to high anisotropy within fibroblastic meningiomas which have high collagen content. The low FA in metastases was elucidated to be due to degradation of the extracellular matrix and expansive growth of the lesion.

They also reported absence of any major discrepancy in MD between the 2 tumor groups which thus showed low sensitivity and low specificity when used alone. FA and MD had a negative correlation in glioblastomas but not in metastases (P < 0.05), though this could not be explained specifically. FA from enhancing tumor region was found to be the single best predictor for the discrimination and had 80% sensitivity, 76% specificity and AUC = 0.84. The Logistic Regression Model (LRM) (best classification model) of FA and MD was formed from multivariate logistic

regression analysis. The LRM had 84% sensitivity, 77% specificity and AUC = 0.86. By using the classification model, the diagnostic performance of 2 experienced neuroradiologists improved with AUC boosted from 0.90 to 0.96 for first neuroradiologist and from 0.85 to 0.93 for second neuroradiologist.[55]

Tumor invasion into the peritumoral white matter causes displacement, infiltration or destruction of the white matter tracts. This differentiation of extent of the white matter involvement can be studied by 3 metrics derived from DTI i.e. p, q and L.

A study done by Price et al[43] included 35 gliomas (18 high-grade gliomas, 17 low-grade gliomas) and 7 controls (normal volunteers). They analyzed the peritumoral white matter tracts in colored FA maps. The p and q values of the white matter tracts were also displayed on a graph simultaneously from each region of interest and different location of different tissues were plotted. The displaced peritumoral white matter tracts exhibited normal FA and normal tissue signatures. Infiltrated white matter tracts showed low FA, mean increase in p (isotropic component) of 50 ± 20% (in comparison to contralateral normal white matter) and a less significant reduction in q (anisotropic component) of 14 ± 9%. In tracts which were disrupted by tumor invasion, there was reduced FA, distinct increase in p (68 ± 17%) and decrease in q (42 ± 7%).

The glioma cells in the initial growth period form "secondary structures" which grow around and in between the neurons. In the later stages of growth, there is disruption and replacement of the neurons as described by Scherer[56] causing changes in diffusion indices. The increase in p in peritumoral regions is due to increased extracellular water from vasogenic edema. The decrease in q occurs due to interference in white matter tracts.

Price et al[43] also studied different grades of gliomas using these indices. They reported that the low-grade gliomas had remarkably higher p values (P = 0.01) and slightly higher q values (P = 0.08) compared to high-grade gliomas. The low-grade gliomas caused only intratumoral disruption of white matter tracts without affecting the peritumoral white matter. Normal controls showed similar diffusion indices and tissue signatures in comparable white matter regions. There was a little variation in p values taken from different white matter tracts. The p value was least within the internal capsule ($0.95 \pm 0.02 \times 10^{-3}$ mm^2/ sec) and maximum in corpus callosum ($1.24 \pm 0.07 \times 10^{-3}$ mm^2/sec).

There was more variation in q in different white matter tracts. It was found to be maximum in the corpus callosum ($1.07 \pm 0.05 \times 10^{-3}$ mm^2/sec) and least in the association fibers of frontal and occipital lobes and in the external capsule where it measured $0.43 \pm 0.06 \times 10^{-3}$ mm^2/sec.[43] The higher anisotropy in the commissural fibers have been proposed by Chepuri et al[57] to be caused by closer arrangement of

white matter bundles, decreased permeability of myelin or varied size of the white matter fibers.

Wang et al[58] measured DTI parameters (p, q, L and FA) in 49 tumors (30 glioblastoma multiforme and 19 metastases) in tumor region, peritumoral region and opposite cerebral hemispheric white matter. The peritumoral region was divided into the peritumoral margin (edematous region immediately next to the tumor) and the white matter region just beyond the peritumoral margin having normal signal intensity. The hemorrhagic areas and necrotic core within the tumor were excluded from the measurements. They found significant rise in the p and L values and considerable reduction in FA values in regions studied in comparison to comparative regions in the opposite cerebral hemisphere ($P < 0.001$). However, they reported no remarkable difference in mean q values in all regions studied in metastatic lesions and in adjacent normal signal intensity white matter in glioblastomas.

They also found that in tumor regions and peritumoral margins of metastases, there was a slight increase in the q values. They attributed this to the identical internal structure of metastases to the primary source and also to the increased compactness of the displaced white matter tracts that increased the anisotropy. They found that the FA and q values were appreciably reduced in intratumoral regions ($P < 0.001$) and q was also considerably less in peritumoral margins ($P <$

0.001) in glioblastomas compared to metastases. ROC analysis calculated AUC for intratumoral *q* values to be 0.804, for peritumoral *q* values to be 0.732 and for intratumoral FA to be 0.784. They found substantial similarity in values of all parameters in the tumor and peritumoral regions between the two groups. They also could not show a clear threshold to differentiate the infiltrated peritumoral margin from vasogenic edema.[58]

Smitha et al[59] compared the DTI parameters (FA, *p*, *q*, *L*) in different grades of gliomas. They showed that *p* and *L* values in the tumor regions were significantly higher as compared to the nontumoral regions in gliomas. High-grade gliomas had lowest range of *p* and *L* in comparison to low-grade gliomas. They found considerable decrease in intratumoral FA values in high-grade gliomas in comparison to the peritumoral regions and opposite cerebral hemispheric white matter. The mean FA values were significantly less in low-grade gliomas in comparison to high-grade gliomas ($P < 0.003$). High-grade gliomas had significantly lower *q* value as compared to low-grade gliomas ($P < 0.05$). ROC analysis showed sensitivity of 93.9%, 63.3%, 91.8% and 69.4% for *p*, *q*, *L* and FA respectively. ROC analysis also showed specificity of 53.3%, 66.7%, 53.3% and 66.7% for *p*, *q*, *L* and FA respectively. AUC for *p*, *q*, *L* and FA were 0.793, 0.622, 0.793 and 0.714 respectively. They observed significant disparity in all DTI parameters studied between low-grade and high-grade gliomas.

DTI metrics can be used in prognostication and treatment follow-up. Muthusami et al[60] found that with progression of glioma to higher grade, there was intratumoral increase in FA and reduction of MD and *CS*. Within the peritumoral region, there was elevation of MD, *p*, *L* and *CS* with decrease in FA, *q* and *CL* with transformation of low-grade to high-grade glioma.

Conventional MRI cannot adequately identify the tumor margins. T2-weighted images can identify only about 50% of the tumor margins accurately. DTI can be used for defining the tumor margins. Price et al[61] analyzed 20 patients with preoperative imaging diagnosis of glioma. DTI was done at 3T MRI scanner around 48 hours prior to MRI-guided tumor biopsy. Biopsy was taken using a 10 x 2 mm needle from the center of the lesion and at 1 cm interval alongside the trajectory of the needle. From each location at least 2 biopsy samples were taken. Regions of interest (ROIs) of 10 x 4 mm were taken from similar sites of biopsy for DTI analysis. The diffusion tensor data was used for computation of FA, *p* and *q* maps. The DTI metrics were normalized to the normal white matter of opposite cerebral hemisphere and ratios were calculated. The DTI metrics were correlated with histopathology.

The intratumoral regions had significant increase in *p* values and a notable reduction in *q* values (> 12% lower than normal side). The peritumoral infiltrated areas showed rise in *p* values (> 10% higher than opposite side) with a marginal

increase in q values (< 12% than opposite side). Using these thresholds, 42 of 43 areas of gross tumor were identified (areas of heavy calcification could not be identified). Based on these thresholds, 19 of 20 areas of peritumoral infiltration were correctly identified. The sensitivity of these thresholds was 98% and specificity was 81%. FA values were significantly lower in intratumoral regions in comparison to the peritumoral regions (P = 0.02) and normal brain (P < 0.001). They observed no considerable dissimilarity in FA values between the peritumoral regions and the normal opposite cerebral white matter. In their study, they concluded that DTI may be used for radiation planning of gliomas by accurately delineating the infiltrated peritumoral regions which would reduce the chance of tumor recurrence.[61]

It has been shown that dexamethasone can alter the DTI metrics. Sinha et al[62] reported considerable reduction in MD in the peritumoral edematous regions after use of steroids for 2-3 days in intracranial tumors. There was however no major alteration in peritumoral FA. These findings occur due to decrease in amount and movement of peritumoral extracellular water with use of steroids, leading to underestimation of size of the peritumoral regions by DTI.

iii) Perfusion MRI:

The malignant lesions have increased vascular proliferation (angiogenesis). Angiogenesis within the high-grade gliomas is characterized by increased microvascular density, endothelial permeability and vessel tortuosity.

Conventional MRI offers only the structural information of tumors. Perfusion MRI allows functional information that supplements conventional MRI. It assesses the tumor vascularity in vivo.[63] It is based on tracer kinetic theory. The tracer used may be endogenous (arterial water) or exogenous (deuterium oxide and gadopentetate dimeglumine). Arterial water and deuterium oxide show random movement but gadopentetate dimeglumine cannot disperse out of normal vessels.[64]

DSC-MRI measures the signal changes in brain parenchyma with initial pass of contrast agent to obtain physiological maps. With initial passage of the paramagnetic contrast agent through tumor vessels, the T2*-relaxation time of protons within the blood vessels and the adjacent tissue changes which causes variation in local magnetic field. The local magnetic susceptibility is different between the vessels and the surrounding tissue. This causes T2* decay causing sudden decrease in signal intensity.[28, 63, 64, 65, 66]

Dynamic T2*-weighted images are taken after giving contrast bolus of 0.1 mmol per kilogram of patient's body weight with flow rate of 5 ml/sec. Then 20 ml of saline is injected. T2*-weighted gradient-echo EPI sequence is capable of obtaining 10 sections per second and is used to obtain 50 dynamic scans. A set of images are acquired sequentially at around 1 second interval starting prior to contrast administration and continuing during and after the contrast bolus. The initial ten acquisitions are taken before contrast administration and are used to calculate the approximate mean normal baseline signal intensity. [64]

After acquisition of the dynamic data, postprocessing is done. Spatial smoothing is done to reduce noise. The gamma-variate function is used to decrease signal alteration due to contrast leakage. The signal intensity-time curve after leakage correction is more accurate. However, gamma-variate fitting is discordant.[64, 66] So the current recommendation is to use digital trapezoidal incorporation.[66] After baseline correction of the curve of relaxation rate change, the area under the curve is calculated. Arterial input function (AIF) is the specific input profile of the contrast to the tissue and is calculated by measuring contrast concentration in voxels near an artery. Deconvolution is the mathematical process which removes the AIF contribution from tissue contrast concentration. This is required for proper quantification of the perfusion parameters.[66]

The area beneath the tissue contrast concentration–time curve is equivalent to the cerebral blood volume (CBV). CBV is the amount of blood in a given tissue region and is measured in ml/100 g of tissue. Cerebral blood flow (CBF) is calculated as the preliminary peak of the deconvoluted tissue contrast concentration-time curve. It represents the amount of blood going within a particular tissue region in unit of time measured in ml/minute/100 g of tissue. Mean transit time (MTT) is determined by ratio of CBV and CBF. It is the mean time required for blood to go through a given tissue region and is measured in seconds. Percentage of signal-intensity recovery (PSR) is the proportion of retrieval of signal intensity at the finish

of primary passage of contrast in comparison to the precontrast signal intensity. It depends on the capillary permeability and cell volume fraction.[66]

Color overlay maps of CBV are processed. ROIs are selected for CBV calculation and the maximal CBV obtained from the ROIs have best reproducibility. To reduce the confusing factors in CBV analysis, ROIs of fixed sizes are used. There is still overestimation of CBV in areas of blood-brain barrier disruption. Therefore, in clinical practice, CBV of the tumor or peritumoral region is compared to the contralateral white matter and is termed as relative CBV (rCBV).[66]

MR perfusion measures tissue microcirculatory hemodynamic parameters. The rCBV map reflects overall lesion microvascular density and is a better predictor of lesion grade. It has been widely accepted for assessing the hemodynamic properties of tumors and helps in their classification and grading. It is also used for biopsy guidance and response of tumor to treatment.[66]

Signal intensity–time curve is generated from the areas of interest by loading the perfusion data from the particular slice into the software on the workstation. There is appreciable reduction in signal intensity at the time of initial passage of contrast bolus. There is subsequently complete or incomplete regain of signal back to the baseline. There may be a second smaller dip in signal intensity due to contrast recirculation.[64]

PSR is also determined relative to baseline signal intensity prior to contrast administration.[67, 68, 69, 70] It is dependent on factors affecting vascular leakiness, rate of blood flow and size of extravascular space. It can be measured directly on a workstation without need for dedicated software. It is measured by the equation:

$$PSR = 100\%\ x\ (S_1 - Smin)/(S_0 - Smin)$$

(S_0 - precontrast signal intensity, S_1 - postcontrast signal intensity, Smin - minimum signal intensity)

High-grade glioma has elevated microvascularity and neovascularity causing high intratumoral rCBV. It causes tumor infiltration into the adjacent normal tissue along the newly formed or pre-existing vascular channels leading to raised rCBV in peritumoral region. Also, there is altered capillary morphology in the peritumoral regions. However, due to breakdown of blood–brain barrier, there is extravasation of contrast agent into the extracellular extravascular space which decreases the susceptibility effects between intravascular and extravascular space. This can cause underestimation of the true tumor vascularity.[71]

Different authors have published the mean rCBV values in high-grade gliomas. Yang et al[31] reported it to be 6.1 ± 3.98, Sugahara et al[72] reported it to be 7.32, Knopp et al[73] measured it to be 3.64, Shin et al[74] calculated it to be 4.91 ± 1.81, Law et al[75] found it to be 5.18 and Aronen et al[76] found it equal to 5.07. Calli et al[26] reported mean maximum rCBV in glioblastomas to be 6.33 ± 2.03 and in anaplastic

astrocytomas to be 3.66 ± 1.79. Preul et al[77] calculated it to be 4.0 in anaplastic astrocytomas and 10.3 in glioblastomas. These different values were likely due to difference in sequences, location of ROIs, size of ROIs and different areas of comparison from contralateral white matter in various studies.

Cha et al[64] measured maximum rCBV in gliomas. In 51 cases of glioblastomas, they found a large variation in maximum rCBV ranging from 1.95 - 28.59 with mean of 5.5, suggesting internal inhomogeneity. In 19 cases of anaplastic astrocytomas, there was less variation in maximum rCBV ranging from 1.29 - 10.26 with mean of 4.03. The 13 cases of low-grade gliomas studied showed reduced rCBV ranging from 0.89 – 3.73 with an average of 1.86. Thus, there was significant similarity in rCBV among the glioma grades. Law et al[78] determined the cutoff value of 1.75 for rCBV with 95% sensitivity, 57.5% specificity, 87% positive predictive value and 79.3% negative predictive value for high-grade gliomas.

Some studies have published the mean rCBV values in metastases. It was reported by Cho et al[79] to range from 3.16 - 13.27 (mean ± SD, 8.34 ± 3.02). It was not significantly different from high-grade gliomas in which it ranged from 3.02 - 16.66 (mean ± SD, 9.33 ± 3.96). Calli et al[26] have found it to be 4.45 ± 1.87, not statistically different from high-grade gliomas and lymphomas.

Cha et al[64] studied 14 cases of solitary metastases and 25 cases of gliomas with DSC-MRI. They found that both the tumor groups had high rCBV in the tumor

regions ($P > 0.05$). However, they found the rCBV in the peritumoral regions was significantly higher in gliomas in comparison to metastases ($P < 0.001$). This occurred due to absence of tumor infiltration beyond the enhancing margin in metastases.

Cho et al[79] measured rCBV in lymphomas and found it to be 1.38 - 2.07 (mean ± SD, 1.80 ± 0.23). Calli et al[26] reported mean rCBVmax in lymphomas as 2.33 ± 0.68. The rCBVmax was significantly lower in lymphomas in both studies compared to glioblastomas. In 19 cases of PCNSL studied by Cha et al[64], the maximum rCBV was statistically lower than that of glioblastomas, ranging from 0.42 to 3.41 (mean ± SD, 1.44 ± 0.67). There is low rCBV in PCNSL with maximum rCBV lower than other brain tumors.[26, 70, 80] It was proposed that low rCBV in PCNSL is due to two factors. Firstly, there is low microvascular density in lymphomas compared to high-grade gliomas. Secondly, there is increased permeability causing underestimation of CBV in lymphomas.

K_2 is used in perfusion MRI as a measure of permeability but it reflects the combined effects of multiple factors on vascular leakiness like vascular surface area, blood flow, hydrostatic, interstitial, and osmotic gradients across the vascular endothelium and vascular permeability. Toh et al[81] found higher K_2 in PCNSL (15 cases) and glioblastomas (20 cases) in contrast to normal white matter of opposite cerebral hemisphere. It was found to be more in PCNSL indicating higher

permeability in PCNSL compared to glioblastomas ($P < 0.004$). This was explained by the ultrastructural structure in PCNSL characterized by thinned endothelial cells, endothelial fenestration and lack of endothelium between the lumen and basement membrane.

High-grade gliomas have increased permeability with contrast leakage causing signal intensity increase secondary to T1 effects masking the decrease in signal intensity in T2*-weighted images. This causes underestimation of CBV. It has been proposed that accuracy of CBV measurement can be increased by using mathematic leakage-correction model and corrected CBV had increased correlation with tumor grade.[82]

Toh et al[81] measured CBV ratio, corrected CBV ratio (normalized to opposite white matter) in 15 cases of PCNSL and 20 cases of glioblastoma. There was higher CBV ratio in glioblastomas compared to PCNSL ($P < 0.001$). They found that CBV increased significantly with leakage correction in both groups; however, it did not increase the diagnostic accuracy. In fact it had lower diagnostic accuracy than the CBV without leakage correction. When the effect of high vascular permeability which causes underestimation of CBV was removed by leakage correction, the leakage-corrected CBV increased. But it also caused decrease in difference between the CBV of the two tumor groups. It has been proposed that the T1 effects due to contrast leakage can also be corrected by preload contrast injection. However,

improved accuracy in CBV measurement was not associated with increased diagnostic accuracy.[81]

Microvascular permeability can also be assessed by dynamic contrast-enhanced MRI (DCE-MRI). It measures certain parameters like volume transfer constant, extracellular extravascular space volume, and flux rate constant between plasma and extravascular extracellular space. Kickingereder et al[83] studied 11 cases of PCNSL and 60 cases of glioblastoma with DCE-MRI at 3T MRI. Lymphomas were found to have higher permeability compared to glioblastomas as they had higher volume transfer constant and flux rate constant values ($P < 0.001$). The volume transfer constant demonstrated the best discriminative value for differentiating lymphomas from glioblastomas with sensitivity of 90.9% and specificity of 95.0%. They observed no statistical disparity in median values of extravascular extracellular space volume between the two groups. These findings correlated with the histological findings of intact vascular integrity in glioblastoma and disrupted vessel architecture in PCNSL.

The neoplastic cells of lymphoma cause formation of perivascular multiple thick layers and invasion into the endothelial cells and vascular lumen. There is hypercellularity with absent neoangiogenesis in lymphoma. Contrast agent causes T1 shortening as it passes into the extravascular extracellular space. The contrast within the tumor vessels causes T2* shortening effect. Due to less vascularity of

lymphoma, the T2* shortening effect is less in lymphoma. The contrast agent slowly extravasates into the extracellular extravascular space due to compact cellularity. The T1 shortening effect of contrast will not be manifested at the time of initial passage of contrast. After the primary passage of contrast, T1 shortening effect will overcome the T2* shortening effect. The signal intensity will increase and may also go above the baseline level causing higher PSR. The higher PSR depends on interplay between various factors like blood volume, rate of blood flow, interstitial space, vascular permeability, and the TR (time to repeat) and flip angle of the pulse sequence. If a preload of contrast is given, it may decrease or cancel the T1 effects and may cause apparent reduction of percentage signal recovery.[69, 84]

Metastases have high capillary permeability with rapid extravasation of contrast, increased volume of distribution and effective compartment size. This leads to higher T2* effects causing lower PSR. Similarly low PSR is manifested by intracranial extra-axial lesions lacking blood-brain barrier.

Cha et al[67] performed DSC-MRI in 27 cases of glioblastoma and 17 cases of metastasis in addition to conventional MRI. They studied the intratumoral and peritumoral regions of both tumor groups. They placed ROIs in both the regions in all the lesions and measured the signal intensity-time curves. The summit of the maximum signal intensity loss and PSR after preliminary passage of contrast was calculated. They found that the average summit in the peritumoral regions was

considerably more for glioblastomas compared to metastases (P = 0.04). The mean PSR was significantly reduced in metastases (78.4%) compared to glioblastomas (82.8%) in peritumoral regions (P = 0.02) and also in contrast enhancing tumor regions (62.5% in metastases and 80.9% in glioblastomas, P = 0.01).

Hartmann et al[68] studied 12 cases each of PCNSL and glioblastomas by using DSC-MRI. They analyzed the signal intensity-time curves and calculated the maximum rCBV of these tumors. They found that rCBVmax was notably lower in PCNSL in comparison to glioblastomas (P < 0.0001). The signal intensity-time curve in PCNSL had remarkable elevation beyond baseline (attributed to extensive contrast extravasation into the extravascular extracellular space and contrast enhancement); this was not seen in glioblastomas. They concluded that PCNSL can be differentiated by these two findings from glioblastomas.

Mangla et al[69] performed DSC-MRI in 22 patients each of glioblastoma, metastasis and PCNSL. They calculated mean PSR, minimum PSR, maximum PSR and rCBV. Mean PSR was statistically different (P < 0.000) in the three groups with highest values in lymphomas (mean ± SD, 113.15 ± 41.59). Glioblastomas had intermediate mean PSR of 78.22 ± 14.27 and metastases had lowest mean PSR of 53.46 ± 12.87. The maximum PSR was more accurate in distinguishing lymphomas from glioblastoma and metastases (AUC = 0.934) compared to rCBV (P < 0.01). They

found PSR > 136% to be 100% specific for lymphomas and PSR < 40% to be 100% specific for metastases.

Perfusion MRI and rCBV measurement help to envisage duration of tumor progression, glioma biology and treatment outcome.[78, 85] Law et al[78] evaluated the utility of perfusion MRI in assessing the clinical outcome of gliomas. They initially performed DSC-MRI in 189 patients and then carried out clinical and imaging follow-up in these patients for an average time of 334 days. They found that both low-grade and high-grade gliomas which had high rCBV (> 1.75) progressed faster (average progression time was 265 days) than gliomas with low rCBV (average progression time was 3585 days). The gliomas showing absolute response had rCBV less than gliomas having rapid clinical deterioration. Thus they observed that rCBV has implication in treatment planning for glioma patients. The low-grade gliomas with high rCBV are at higher risk for malignant transformation and hence require more extensive resection with postoperative chemotherapy and radiotherapy to improve survival.

Coban et al[86] also showed that maximum rCBV is useful as a prognostic indicator of overall survival in glioblastoma patients. They found that the maximum rCBV values were statistically less in glioblastomas having long survival (> 15 months) compared to glioblastomas with short survival (< 15 months) with $P < 0.05$. A cutoff

value of 5.79 had 89% sensitivity, 90% specificity and AUC = 0.93 in differentiating between the two groups ($P < 0.001$).

Spin-echo EPI (SE-EPI) rCBV maps denote the blood volume within vessels < 8 μ in size. Young et al[87] reported that this property of SE-EPI may help to distinguish metastases from high-grade gliomas with 88% sensitivity and 72% specificity. The average normalized CBV within high-grade gliomas was found to be 1.53 ± 0.79 compared with 0.82 ± 0.40 in metastases. The average PSR was found to be significantly different in high-grade gliomas (0.86) compared to metastases (0.75) with $P < 0.05$ but it had lower specificity (48%) than rCBV.[87]

Measurement of vascular tortuosity within gliomas was evaluated by Jackson et al[88] as a surrogate marker for antiangiogenic therapy. High-grade gliomas have rapid growth which is not sufficiently supplied by the neoangiogenic microvasculature. This causes regional hypoxia and hypoglycemia with increased cytokine production and further necrosis occurs within these tumors. Flow within these areas is therefore slow and erratic. This leads to aberrations during the recirculation stage of contrast measured as relative recirculation (rR). It may identify areas of inadequate flow adjacent to site of necrosis. Jackson et al[88] observed that it was elevated in high-grade gliomas with increased variability in distribution in glioblastomas compared to anaplastic astrocytomas. Thus, relative recirculation was proposed as an independent indicator of tumor grade.

iv) **Susceptibility-weighted imaging (SWI)**:

SWI has high sensitivity to tissue magnetic susceptibility variations and can identify blood products, microvenous structures and calcifications. It depends on blood oxygenation level dependent-induced difference in phase between the tissues. It can detect the vascular structures not appreciated in conventional MR sequences. It can be used in neurodegenerative diseases for detecting iron accumulation and in assessment of venous malformations.[65] Its use was described by Sehgal et al[89] for identifying intratumoral vascular structures, calcifications and blood products seen as low signal intensities.

Intratumoral susceptibility signals (ITSS) are described into 3 types: 1) very thin straight or point-like hypointensities, not detected on conventional MRI 2) grainy or small low signal intensities, easily detected on conventional MRI 3) frizzy or scattered hypointensities. There are four grades of the first type of ITSS: 1) Grade 0 - no ITSS 2) Grade I- 1-5 in number 3) Grade II- 6-10 in number 4) Grade III- ≥ 11 in number.[90]

Kim et al[91] assessed the usefulness of ITSS in differentiation of high-grade gliomas, lymphomas and metastases. They found that 100% of glioblastomas and 40% of anaplastic astrocytomas had ITSS due to increased tumor blood supply and angiogenesis. 73% of metastatic lesions had ITSS and none of the lymphomas had ITSS. The diagnostic accuracy of MRI increased from 67% to 78% on reviewing SWI

along with conventional MRI (P = 0.016). Grade III ITSS had 84% sensitivity and 60% specificity for differentiating glioblastomas from metastases (P = 0.012). ITSS had 86.7% sensitivity and 100% specificity in distinguishing high-grade gliomas from lymphomas (P < 0.0001). The absence of ITSS aided in diagnosis of lymphomas as these tumors did not have calcification and microbleeds.

Hemorrhage can be differentiated from intratumoral or peritumoral venous structures by performing SWI before and after contrast administration. Blood within the veins will have change in signal intensity on postcontrast SWI images but regions of tumoral bleed will appear similar to precontrast SWI images.[92]

v) Magnetic Resonance Spectroscopy (MRS):

MRS imparts the biochemical profile of brain tumors. It measures specific amino acids such as n-acetylaspartate (NAA), creatine (Cr), choline (Cho), lipids and lactate within the intratumoral regions and normal white matter. It also calculates their relative ratios. Most brain tumors have a non-specific spectrum with increased Cho/Cr and decreased NAA/Cr ratios due to disruption of neuronal integrity and high myelin turnover. Aggressive tumors also have lactate and lipid peaks due to increased anaerobic metabolism and cellular necrosis, respectively.[93] The lipid peak area (LPA) ratio can be used to separate glioblastomas from metastases. Opstad et al[94] showed a higher LPA ratio in metastases compared to glioblastomas (P < 0.0001).

COMBINATION OF ADVANCED MRI TECHNIQUES:

Combined use of advanced MRI methods complements the conventional MRI.[95] Previous studies have shown that combined use of rCBV and ADC values increases the efficiency of MRI and helps in glioma grading.[33, 96] It is known that 14-45% of high-grade gliomas do not enhance. Fan et al[71] studied nonenhancing gliomas (22 patients) based on diffusion-weighted and perfusion MRI. They reported that gliomas having lower ADC values in nonenhancing regions and higher rCBV values in the solid enhancing and peritumoral regions were high-grade in nature ($P < 0.01$). The peritumoral ADC values though low in both low-grade and high-grade gliomas, were not significantly different between the 2 groups.

Calli et al[26] evaluated the utility of DSC-MRI and DTI for diagnosing contrast-enhancing neoplastic brain tumors including 17 cases of glioblastoma, 14 cases of anaplastic astrocytoma, 9 cases of metastasis and 8 cases of lymphoma. They measured the minimum ADC values (ADCmin) and maximum rCBV values from each tumor. The ADCmin values (x 10^{-3} mm^2/s) were 0.75 ± 0.21 in anaplastic astrocytomas, 0.79 ± 0.21 in glioblastomas, 0.68 ± 0.11 in metastases and 0.51 ± 0.09 in lymphomas. The rCBVmax ratios were 6.33 ± 2.03 in glioblastomas, 3.66 ± 1.79 in anaplastic astrocytomas, 4.45 ± 1.87 in metastases and 2.33 ± 0.68 in lymphomas. There was statistical dissimilarity between the ADCmin values of glioblastomas and lymphomas ($P < 0.05$) and between anaplastic astrocytomas and lymphomas ($P <$

0.03) but not between metastases and lymphomas and between glioblastomas, anaplastic astrocytomas and metastases. The rCBVmax values were remarkably different between glioblastomas and lymphomas ($P < 0.0001$) and between glioblastomas and anaplastic astrocytomas ($P < 0.001$) but not between glioblastomas and metastases ($P < 0.083$). They concluded that though there was difference in ADCmin and rCBVmax between these high-grade lesions, there was some overlapping in the values.

Wang et al[97] used a combination of DTI metrics (FA, *CL*, *CP*, *CS*, ADC) and rCBV for differentiation of the high-grade intracranial lesions. Glioblastomas showed significantly increased FA, *CP*, *CL* and decreased *CS* in the enhancing tumor regions compared to lymphomas and metastases ($P < 0.001$). Their study demonstrated that the combination of FA, ADC, *CS* from the enhancing tumor regions and rCBV from the immediate peritumoral regions could differentiate glioblastomas from lymphomas and metastases (AUC = 0.938). They also observed that ADC values in the enhancing tumor regions and *CP* calculated within the peritumoral regions were best for differentiating lymphomas from metastases (AUC = 0.909).

Chiang et al[36] reported that there was significant increase in rCBV and Cho/Cr ratios and significant decrease in ADC values in the adjacent peritumoral regions in high-grade gliomas compared to solitary metastases at 3T MRI. But they found insignificant disparity in Cho/Cr ratio and rCBV within intratumoral regions

between the two tumor groups. They concluded that combination of these advanced MRI techniques could complement the conventional MRI findings in differentiating metastases from high-grade gliomas.

Law et al[75] measured rCBV, Cho/Cr ratio and Cho/NAA ratio from intratumoral regions of gliomas. They used them together in grading of gliomas to achieve high sensitivity (93.3%), specificity (60%), positive predictive value (87.5%) and negative predictive value (75%) compared to the conventional MRI.

Tsougos et al[93] differentiated glioblastomas from metastases utilizing MRS, DTI and DSC-MRI at 3T MRI. They found that a combination of NAA/Cr, Cho/Cr, Cho/NAA ratios and rCBV in the peritumoral regions differentiated glioblastomas from metastases. They however, observed insignificant difference in ADC and FA values between the two groups.

Correlation of DSC-MRI and DTI at 3T MRI in gliomas, solitary metastases and meningiomas in intratumoral and peritumoral regions was shown by Svolos et al[98]. They reported that a combination of diffusion and perfusion metrics helped to better characterize and classify the tumors. The use of a sophisticated classification scheme could give an optimum diagnostic outcome and it would be practically applicable in clinical decision making.

There was a significant correlation between the degrees of ITSS with rCBVmax in gliomas in a study by Park et al[99]. The use of SWI with DTI and DSC-MRI has been

described as useful in glioma grading and diagnosing brain tumors by Park et al[90]. They observed that ITSS were absent in low-grade gliomas and lymphomas in their study. ITSS showed 100% specificity in differentiating glioblastomas from lymphomas and low-grade gliomas. They found that ITSS grade was lower in metastases compared to glioblastomas. Hence, a high ITSS grade (> grade II) was suggestive of glioblastomas rather than metastases. The use of SWI and ADC in combination with DSC-MRI achieved 84% sensitivity and 60% specificity in differentiating glioblastomas from metastases and 86.7% sensitivity and 100% specificity in distinguishing glioblastomas from lymphomas.

The combination of DTI and DSC-MRI may be utilized to gauge the treatment effects.[28, 100] Early response to antiangiogenesis treatment will cause decrease in rCBV though size of the contrast-enhancing part of the tumor may remain the same. There will be increase in water diffusion causing increase in ADC values within the gliomas after 1 month of therapy in patients responding to chemotherapy and radiotherapy.[101] Mardor et al[102] reported that treatment responders showed increase in ADC values 1 week after treatment of malignant brain lesions (mostly metastases).

Tsolaki et al[103] supported the use of intelligent systems like clinical decision support systems (CDSS) for automatic processing, representation, classification and evaluation of MRI data based on advanced MRI techniques. They advocated it to

become a part of the routine clinical work and be used as an assistant diagnostic tool, thus aiding in interpretation of MRI findings and help in decision making.

MATERIALS AND METHODS

Subjects included were ≥ 19 years of age with intra-axial high-grade cerebral tumors referred from the Neurosurgery and Neurology departments of Sree Chitra Tirunal Institute for Medical Sciences and Technology to our department for advanced MRI and subsequently undergoing biopsy or surgical excision.

This study included both retrospective and prospective analysis of data. The retrospective study period was from January 2009 to May 2013 and the prospective data was collected from June 2013 to June 2015. Approval for the study was obtained from the Ethical Committee of the institute (IEC Numbers- SCT/IEC-490/July-2013 and SCT/IEC-498/Aug-2013).

We obtained informed written consent from all the study patients and/or their bystanders included in the prospective analysis. Consent waiver was permitted by the Ethical Committee for patients included in the retrospective analysis. We did not include normal volunteers, pregnant women and students/staff of the institute in the study. Subjects were not excluded based on their gender, race or ethnicity.

The Inclusion and Exclusion criteria were as follows:

Inclusion criteria:

1) Patients ≥ 19 years of age with high-grade intra-axial cerebral tumors and subsequently undergoing biopsy or surgical excision
2) Patients giving informed consent.

Exclusion criteria:

1) Patients not giving informed consent

2) Patients with contraindication to contrast study (allergy, renal failure etc.)
3) Patients who underwent chemotherapy or radiotherapy before the MRI examination
4) Patients who underwent prior surgery or biopsy.

STUDY PROTOCOL-

We collected, stored and analyzed the data of patients fulfilling the inclusion and exclusion criteria according to the following procedure:

- All MR images were obtained using 1.5T superconducting MR scanner Magnetom Avanto (Siemens, Germany) with a 12-channel phased array head coil.
- MRI was done in all these patients as per the tumor protocol of our institution which included T1-weighted imaging, T2-weighted imaging, FLAIR imaging, DWI, SWI, contrast-enhanced T1-weighted imaging, DSC-MRI, DTI and MRS.
- Histopathological evaluation was done in these patients after stereotactic biopsy or surgical resection of the tumors. Patients with high-grade lesions on histopathology were included in the study by one radiologist.
- The included patients were then analyzed by another radiologist (blinded to histopathology findings) for DTI metrics (FA, *p*, *q*, *L*, *CL*, *CP*, and *CS*), ITSS in SWI (in pre- and postcontrast images) and DSC-MRI parameters (rCBV, rCBF, rPSR) using Siemens software.

MRI protocol:

- T1-weighted SE images: TR- 468, TE- 11, slice thickness- 5 mm, matrix size- 320 x 83, NEX- 1.

- T2-weighted FSE images: TR- 5860, TE- 110, matrix size- 320 x 83, slice thickness- 5mm, NEX- 1.
- DTI (SE-EPI sequence): TR- 4800, TE- 126, slice thickness- 5 mm, matrix size- 178 x 178, FOV- 230 mm, b-values- 0 and 1,000 s/mm^2
- SWI (3D GRE flow compensated sequence): TR- 49, TE- 40, slice thickness- 2.1 mm, matrix size- 448 x 290, FOV- 230 mm, flip angle- 15°.
- DSC-MRI (T2*-weighted GRE-EPI sequence): TR- 1850, TE- 43, slice thickness- 5 mm, matrix size- 128 x 100, number of averages- 1, contrast agent- gadodiamide (dose- 0.1mmol/kg body weight) at a rate of 5ml/sec followed by saline injection of 20 ml.
- A separate workstation was used for postprocessing (Leonardo, Siemens) and DTI maps (FA, λ_1, λ_2, λ_3, *CP, CL* and *CS*) and DSC-MRI maps (CBV, CBF) were generated for analysis.
- ROIs were drawn by hand of 3-4 pixel size for DTI analysis and 21-25 pixel size for DSC-MRI analysis.
- At least 9-10 ROIs were drawn in all the tumors in three study regions: intratumoral, adjacent peritumoral and opposite normal cerebral white matter. The term adjacent peritumoral region was applied to the region just next to (within 5-10 mm) the enhancing tumor region.
- The maps of eigenvalues (λ_1, λ_2, λ_3) were used for calculation of *p, q* and *L.*
- The mean values of the DTI metrics (FA, *p, q, L, CP, CL* and *CS*) were calculated in the three study regions.
- The maximum values of CBV and CBF were chosen in tumor and peritumoral regions and then compared with opposite cerebral white matter to obtain rCBV and rCBF values.
- Signal intensity-time curves were also obtained and rPSR was calculated in tumor and peritumoral regions.

- ITSS were graded on SWI images in tumor regions. In some patients who underwent postcontrast SWI images, the precontrast and postcontrast SWI images were also compared.

STATISTICAL ANALYSIS

- Chi-square test was utilized to test the difference in age and gender distribution of the three study groups- high-grade glioma, metastasis and PCNSL.
- ANOVA was used to analyze the difference in DTI metrics (FA, *p*, *q*, *L*, *CP, CS* and *CL*) and DSC-MRI parameters (rCBV, rCBF, rPSR) in the tumor and adjacent peritumoral regions between the study cohorts.
- The ordinal data of the grades of ITSS within the tumor regions on SWI images was analyzed using ordinal regression.
- A *P* value of < 0.05 was considered as cutoff for level of statistical importance. All *P* values were 2- tailed.
- Receiver operating characteristic (ROC) analysis was done to ascertain the sensitivity, specificity and area under curve (AUC) of the parameters with $P < 0.05$.
- Statistical analysis was done by means of SPSS software (statistical package for social sciences, Chicago, Illinois), version 17.0 and MedCalc statistical package (MedCalc software, Mariakerke, Belgium).

RESULTS

There were a total of sixty-six patients with histopathologically proven high-grade tumors. There were three cohorts in the study- high-grade glioma (HGG), metastasis and primary central nervous system lymphoma. There were a total of thirty-five patients with high-grade glioma, eighteen patients of metastasis and thirteen patients of lymphoma who fulfilled the inclusion criteria and formed part of the study population.

I) DEMOGRAPHIC PROFILE:

The age of the patients with high-grade glioma ranged between 19 to 68 years with mean of 43.8 years ± 14.28. The patients with metastasis had age ranging from 35 to 71 years and mean of 53 years ± 9.77. Primary central nervous system lymphoma patients had age between 26 to 67 years with mean of 49.3 years ± 10.91. Age-wise distribution of the study population is shown in Fig 1:

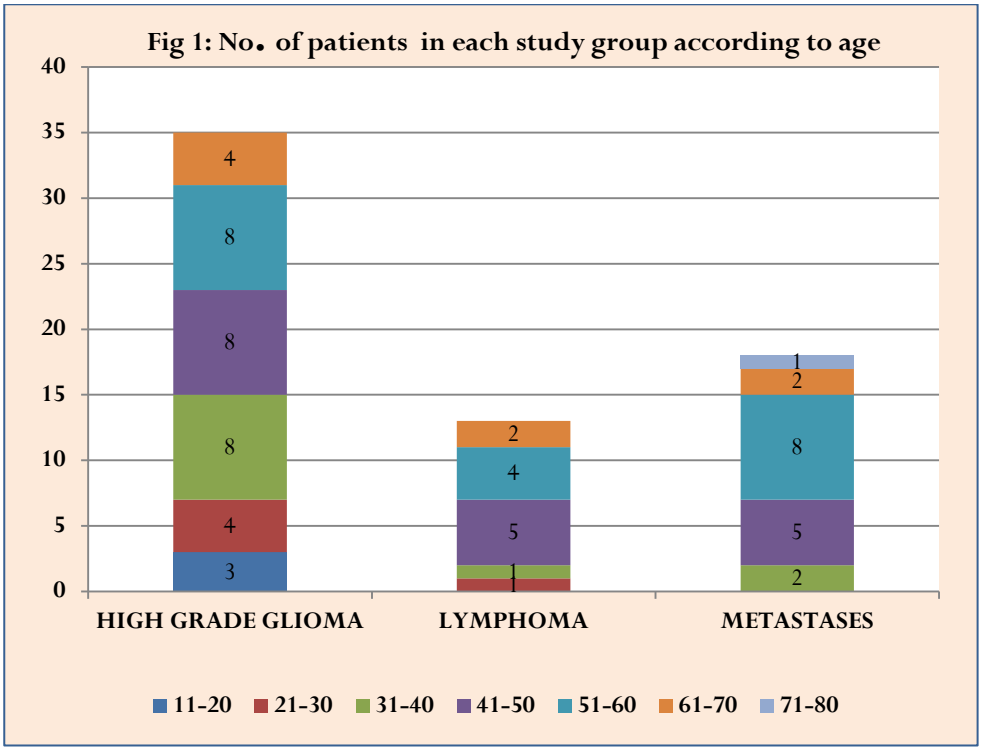

Chi-square test was done to analyze the difference in age distribution between the three groups. There was no statistical difference in the age distribution between the study groups with $P > 0.05$ as shown in Table 1.

Table 1: Study groups - age distribution	*P* value
High-grade glioma versus metastases	0.21
High-grade glioma versus lymphoma	0.61
Metastases versus lymphoma	0.71

The study population consisted of 63.64% of males and 36.36% of females. The gender distribution in the study population is shown in Fig 2:

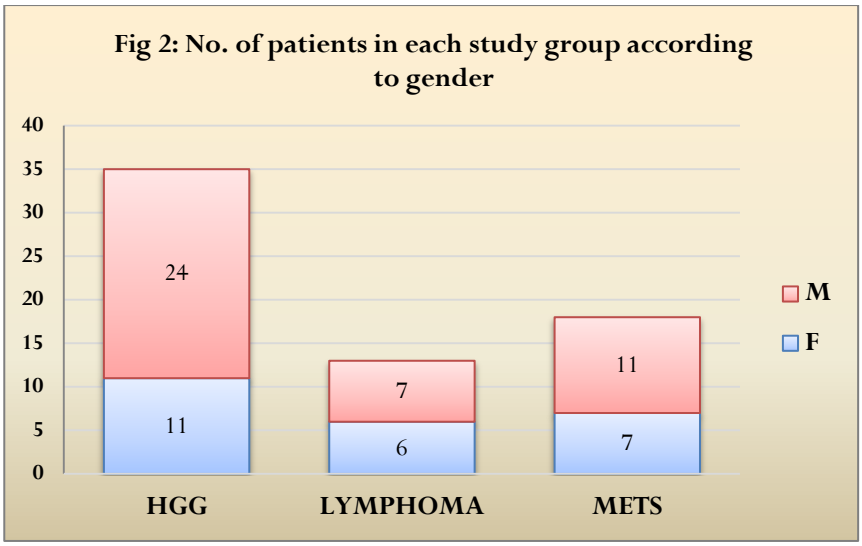

Chi-square test was done to evaluate the difference in gender distribution between the three study groups. It showed that there was no gender predilection in the study groups with $P > 0.05$ as shown in Table 2.

Table 2: Study groups - gender distribution	*P* value
High-grade glioma versus metastases	0.78
High-grade glioma versus lymphoma	0.34
Metastases versus lymphoma	0.29

II) CLINICAL FEATURES:

Almost all the patients had more than one symptom at the time of presentation. The most common symptom was headache present in 38 of the total 66 patients (57.6%). The frequency of the various clinical symptoms is shown in Table 3 as follows:

CLINICAL FEATURES	HGG	METASTASES	LYMPHOMA	NO. OF PTS.
HEADACHE	17	12	9	**38**
WEAKNESS	13	2	7	22
SEIZURE	15	9	2	26
VISUAL COMPLAINTS	8	2	2	12
MEMORY LOSS	8	2	1	11
GAIT UNSTEADINESS	2	0	1	3
LOSS OF CONSCIOUSNESS	1	0	2	3
BEHAVIOURAL CHANGE	1	0	2	3
TREMOR	1	0	0	1
DIFFICULTY FINDING WORDS	1	0	0	1
VOMITING	5	5	1	11
URINARY INCONTINENCE	2	0	0	2
PARESTHESIA	0	1	2	3
SLURRING SPEECH	0	1	0	1
NUMBNESS	0	1	0	1
ALTERED SENSORIUM	0	0	1	1

III) ADVANCED MRI FINDINGS:

1) DIFFUSION TENSOR IMAGING:

DTI was done in all the patients except in one patient each in the metastases and lymphoma groups. The DTI metrics in enhancing tumor regions, adjacent peritumoral white matter regions and contralateral white matter regions in the three study groups are represented in boxplots.

The horizontal bars at the ends of the vertical lines indicate the range of values of each parameter. The margins of the boxes in the boxplot charts represent the 25^{th} and 75^{th} percentiles of values of each parameter. The line between the green and purple regions in each box represents the mean value of each parameter. The purple region within each box represents the values above the mean value of each parameter and green region within each box represents the values below the mean value of each parameter.

a) **Fractional Anisotropy (FA):**

The mean FA values in tumor and adjacent peritumoral regions were reduced in comparison to contralateral white matter regions in all three tumor groups. The range of FA values in the tumor groups are shown in boxplots in Fig 3 (values are in x 10^{-3}) as follows:

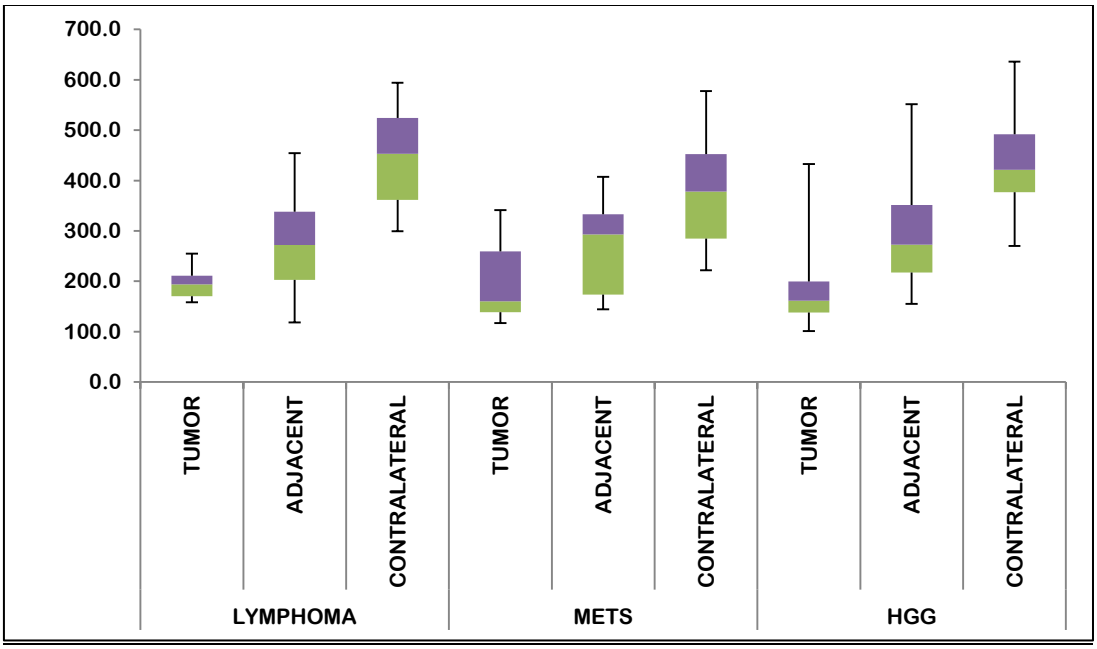

b) ***p*- pure isotropic component of diffusion:** There was increase in mean *p* values in the tumor and peritumoral regions in comparison to opposite white matter in high-grade gliomas and metastases and in the peritumoral regions in lymphomas but not in the tumor regions of lymphomas. The range of *p* values are shown in boxplots in Fig 4 (values are in x 10^{-3} mm^2/s) as follows:

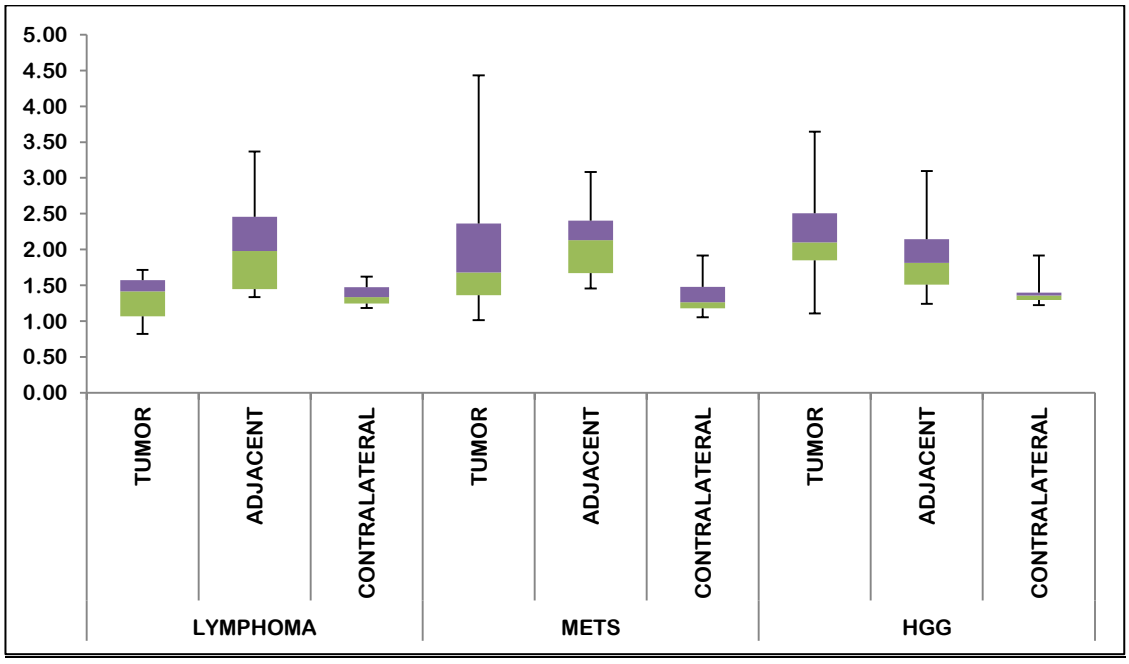

c) ***q*- pure anisotropic component of diffusion:** The mean *q* value was lower in tumor regions compared to contralateral white matter in all the three tumor groups. There was decrease in mean *q* value in peritumoral regions in comparison to contralateral white matter in high-grade gliomas and lymphomas but not in metastases. The range of *q* values in the tumor groups are shown in boxplots in Fig 5 (values are in x 10^{-3} mm^2/s) as follows:

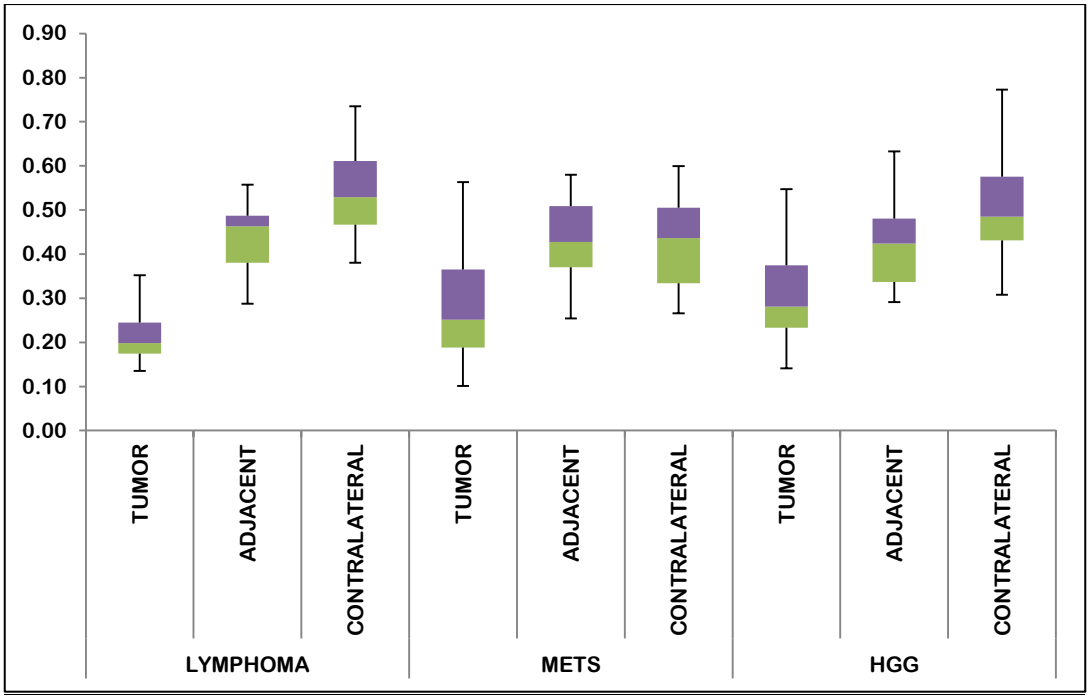

d) ***L*- total magnitude of diffusion:** There was increase in mean *L* value in tumor regions in comparison to contralateral white matter in high-grade gliomas and metastases but was decreased in tumor region in lymphomas. The mean *L* value was increased in peritumoral regions compared to contralateral white matter in all the three tumor groups. The range of *L* values in the tumor groups are shown in boxplots in Fig 6 (values are in x 10^{-3} mm^2/s) as follows:

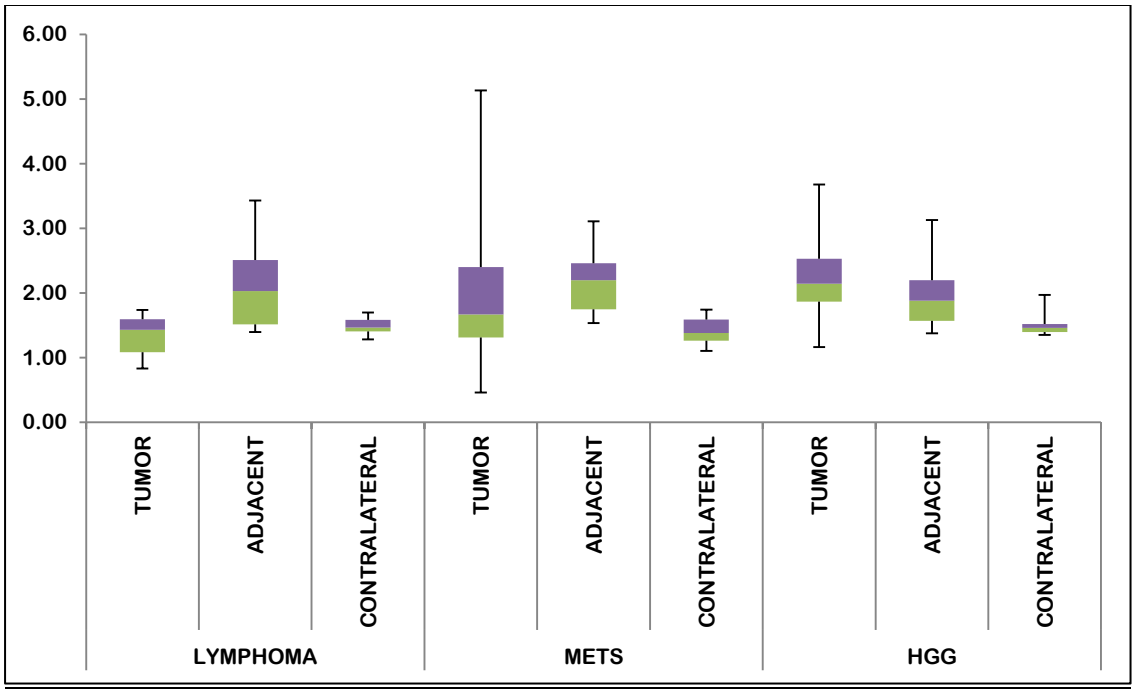

e) *CL*- linear anisotropy- There was decrease in mean *CL* values in tumor and peritumoral regions in comparison to contralateral white matter in all three tumor types. The range of C*L* values in the tumor groups are shown in boxplots in Fig 7 (values are in x 10^{-3} mm^2/s) as follows:

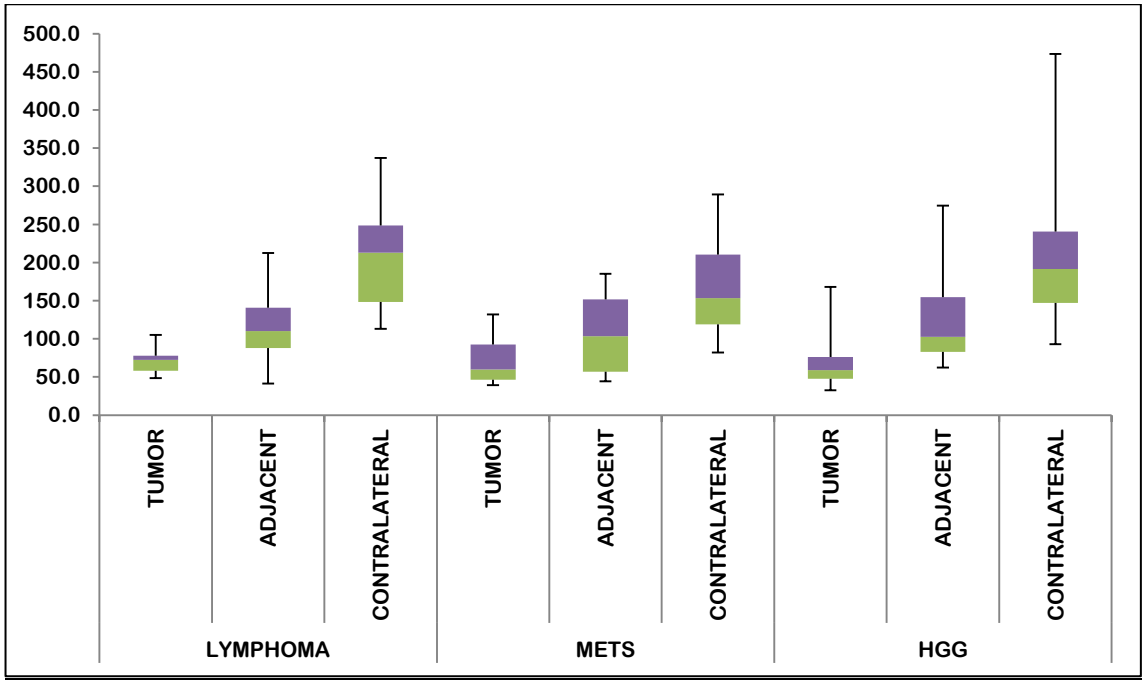

f) ***CP*- planar anisotropy:** There was decrease in mean *CP* values in tumor and peritumoral regions in all three tumor types compared to contralateral white matter. The range of *CP* values in the tumor groups are shown in boxplots in Fig 8 (values are in x 10^{-3} mm^2/s) as follows:

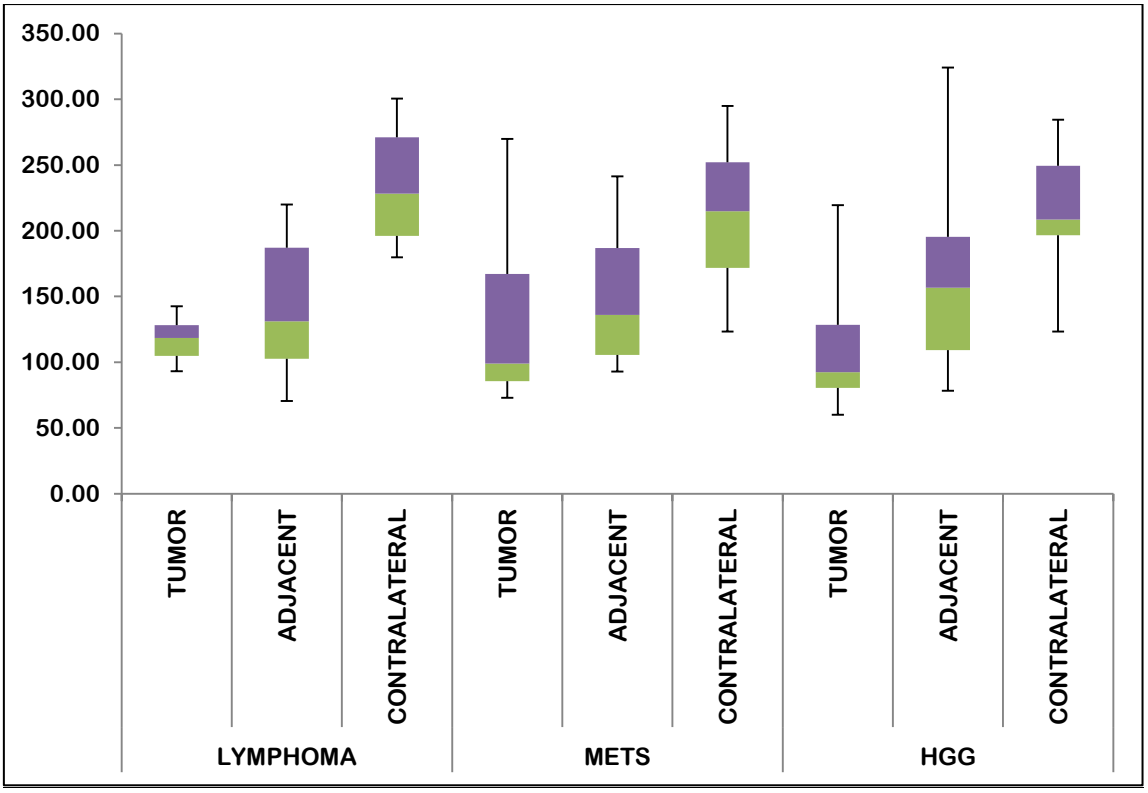

g) ***CS*- spherical anisotropy:** The mean *CS* values were increased in tumor and peritumoral regions in all three tumor types into contralateral white matter The range of *CS* values in the tumor groups are shown in boxplots in Fig 9 (values are in x 10^{-3} mm^2/s) as follows:

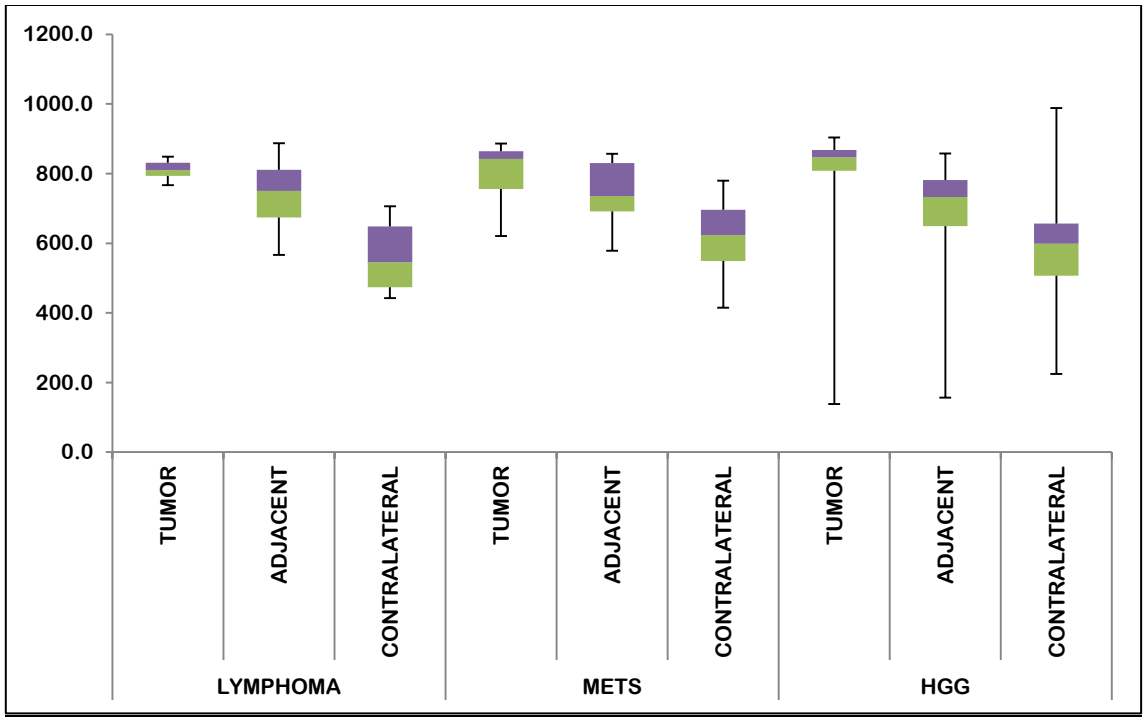

A) COMPARISON WITHIN THE STUDY GROUPS:

Each of the three study regions was compared with each other in all the three study groups.

1) HIGH-GRADE GLIOMA:

A) TUMOR VERSUS PERITUMORAL REGION: All the metrics were significantly different except for *CL* as shown in Table 4 below:

DTI PARAMETERS (MEAN VALUES)	TUMOR REGION	PERITUMORAL REGION	*P* VALUE
FA	183.14 ± 72.1	291.58 ± 96.2	**<0.001**
p	2.19 ± 0.61	1.88 ± 0.43	**0.004**
q	0.31 ± 0.10	0.42 ± 0.08	**<0.001**
L	2.22 ± 0.61	1.94 ± 0.41	**0.007**
CP	104.7 ± 35.8	162 ± 57.3	**<0.001**
CS	797.3 ± 168.5	699.8 ± 135.2	**0.006**
CL	65.97 ± 28.8	117.7 ± 50.3	0.061

B) TUMOR VERSUS CONTRALATERAL NORMAL WHITE MATTER REGION: All the metrics were significantly different as shown in Table 5 below:

DTI PARAMETERS (MEAN VALUES)	TUMOR REGION	CONTRALATERAL WHITE MATTER	*P* VALUE
FA	183.14 ± 72.1	425.5 ± 85.7	**<0.001**
p	2.19 ± 0.61	1.37 ± 0.12	**<0.001**
q	0.31 ± 0.10	0.51 ± 0.1	**<0.001**
L	2.22 ± 0.61	1.48 ± 0.12	**<0.001**
CP	104.7 ± 35.8	215.2 ± 36.3	**<0.001**
CS	797.3 ± 168.5	584.4 ± 133.5	**<0.001**
CL	65.97 ± 28.8	200.4 ± 81.1	**<0.001**

C) PERITUMORAL REGION VERSUS CONTRALATERAL NORMAL WHITE MATTER REGION: All the metrics were significantly different as shown in Table 6 below:

DTI PARAMETERS (MEAN VALUES)	PERITUMORAL REGION	CONTRALATERAL WHITE MATTER	*P* VALUE
FA	291.58 ± 96.2	425.5 ± 85.7	**<0.001**
p	1.88 ± 0.43	1.37 ± 0.12	**<0.001**
q	0.42 ± 0.08	0.51 ± 0.1	**0.001**
L	1.94 ± 0.41	1.48 ± 0.12	**<0.001**
CP	162 ± 57.3	215.2 ± 36.3	**<0.001**
CS	699.8 ± 135.2	584.4 ± 133.5	**0.001**
CL	117.7 ± 50.3	200.4 ± 81.1	**<0.001**

2) METASTASES:

A) TUMOR VERSUS PERITUMORAL REGION: The mean FA, *q* and *CL* were significantly different as shown in Table 7 below:

DTI PARAMETERS (MEAN VALUES)	TUMOR REGION	PERITUMORAL REGION	*P* VALUE
FA	193.4 ± 71.8	262.42 ± 89.03	**0.027**
p	1.97 ± 0.85	2.13 ± 0.48	0.407
q	0.29 ± 0.12	0.43 ± 0.09	**<0.001**
L	1.93 ± 1.05	2.19 ± 0.46	0.280
CP	126.3 ± 59.07	148.6 ± 49.8	0.233
CS	809.3 ± 76.8	751.6 ± 81.5	0.059
CL	70.68 ± 28.5	104.6 ± 46.9	**0.032**

B) TUMOR VERSUS CONTRALATERAL NORMAL WHITE MATTER REGION: All metrics were significantly different as shown in Table 8 below:

DTI PARAMETERS (MEAN VALUES)	TUMOR REGION	CONTRALATERAL WHITE MATTER	*P* VALUE
FA	193.4 ± 71.8	379.1 ± 100.6	**<0.001**
p	1.97 ± 0.85	1.35 ± 0.23	**0.003**
q	0.29 ± 0.12	0.43 ± 0.10	**<0.001**
L	1.93 ± 1.05	1.44 ± 0.21	**0.038**
CP	126.3 ± 59.07	214.3 ± 51.8	**<0.001**
CS	809.3 ± 76.8	617.1 ± 100.1	**<0.001**
CL	70.68 ± 28.5	168.3 ± 54.6	**<0.001**

C) PERITUMORAL REGION VERSUS CONTRALATERAL NORMAL WHITE MATTER REGION: FA, *p, L, CP, CS* and *CL* were significantly different as shown in Table 9 below:

DTI PARAMETERS (MEAN VALUES)	PERITUMORAL REGION	CONTRALATERAL WHITE MATTER	*P* VALUE
FA	262.42 ± 89.03	379.1 ± 100.6	**<0.001**
p	2.13 ± 0.48	1.35 ± 0.23	**<0.001**
q	0.43 ± 0.09	0.43 ± 0.10	0.884
L	2.19 ± 0.46	1.44 ± 0.21	**0.002**
CP	148.6 ± 49.8	214.3 ± 51.8	**0.001**
CS	751.6 ± 81.5	617.1 ± 100.1	**<0.001**
CL	104.6 ± 46.9	168.3 ± 54.6	**<0.001**

3) LYMPHOMA:

A) TUMOR VERSUS PERITUMORAL REGION: All metrics except *CP* were significantly different as shown in Table 10 below:

DTI PARAMETERS (MEAN VALUES)	TUMOR REGION	PERITUMORAL REGION	*P* VALUE
FA	196.01 ± 27.6	273.9 ± 89.2	**0.018**
p	1.34 ± 0.28	2.06 ± 0.65	**<0.001**
q	0.21 ± 0.06	0.44 ± 0.07	**<0.001**
L	1.36 ± 0.28	2.12 ± 0.64	**<0.001**
CP	116.9 ± 14.9	143.9 ± 50.6	0.098
CS	811.2 ± 24.4	740.5 ± 88.8	**0.027**
CL	70.75 ± 14.8	114.5 ± 43.1	**0.032**

B) **TUMOR VERSUS CONTRALATERAL NORMAL WHITE MATTER REGION:** FA, *q*, *CP, CS* and *CL* were significantly different as shown in Table 11 below:

DTI PARAMETERS (MEAN VALUES)	TUMOR REGION	CONTRALATERAL WHITE MATTER	*P* VALUE
FA	196.01 ± 27.6	452.4 ± 93.8	**<0.001**
p	1.34 ± 0.28	1.36 ± 0.13	0.915
q	0.21 ± 0.06	0.54 ± 0.10	**<0.001**
L	1.36 ± 0.28	1.48 ± 0.12	0.493
CP	116.9 ± 14.9	233.7 ± 41.8	**<0.001**
CS	811.2 ± 24.4	555.2 ± 91.5	**<0.001**
CL	70.75 ± 14.8	210.1 ± 69.1	**<0.001**

C) PERITUMORAL REGION VERSUS CONTRALATERAL NORMAL WHITE MATTER REGION: All metrics were significantly different as shown in Table 12 below:

DTI PARAMETERS (MEAN VALUES)	PERITUMORAL REGION	CONTRALATERAL WHITE MATTER	*P* VALUE
FA	273.9 ± 89.2	452.4 ± 93.8	**<0.001**
p	2.06 ± 0.65	1.36 ± 0.13	**<0.001**
q	0.44 ± 0.07	0.54 ± 0.10	**0.005**
L	2.12 ± 0.64	1.48 ± 0.12	**0.001**
CP	143.9 ± 50.6	233.7 ± 41.8	**<0.001**
CS	740.5 ± 88.8	555.2 ± 91.5	**<0.001**
CL	114.5 ± 43.1	210.1 ± 69.1	**<0.001**

B) COMPARISON BETWEEN THE STUDY GROUPS: The study groups were compared by combining two groups together forming three pairs. Each of the DTI parameters were compared between the two study groups in each pair in the tumor and peritumoral regions. The lesion-to-brain ratios were calculated by dividing the mean values in tumor and peritumoral regions with that of contralateral regions.

1) TUMOR REGION OF HIGH-GRADE GLIOMA AND METASTASES: There was no statistical difference in the metrics between these two groups as shown in Table 13 below:

DTI PARAMETERS (MEAN VALUES)	HIGH-GRADE GLIOMA	METASTASES	*P* VALUE
FA	183.14 ± 72.1	193.4 ± 71.8	0.602
p	2.19 ± 0.61	1.97 ± 0.85	0.245
q	0.31 ± 0.10	0.29 ± 0.12	0.386
L	2.22 ± 0.61	1.93 ± 1.05	0.180
CP	104.7 ± 35.8	126.3 ± 59.07	0.079
CS	797.3 ± 168.5	809.3 ± 76.8	0.761
CL	65.97 ± 28.8	70.68 ± 28.5	0.613

2) LESION-TO-BRAIN RATIO IN TUMOR REGION OF HIGH-GRADE GLIOMA AND METASTASES: It was not statistically different for all the parameters between the two study groups as shown in Table 14 as follows:

DTI PARAMETERS	HIGH-GRADE GLIOMA	METASTASES	*P* VALUE
FA	0.4304	0.5102	0.074
p	1.5986	1.4592	0.319
q	0.6078	0.6744	0.408
L	1.5	1.3402	0.212
CP	0.4865	0.5893	0.081
CS	1.3643	1.3114	0.705
CL	0.3291	0.4199	0.446

3) **PERITUMORAL REGION OF HIGH-GRADE GLIOMA AND METASTASES:** There was no statistical difference in the metrics between these two groups as shown in Table 15 as follows:

DTI PARAMETERS (MEAN VALUES)	HIGH-GRADE GLIOMA	METASTASES	*P* VALUE
FA	291.58 ± 96.2	262.42 ± 89.03	0.294
p	1.88 ± 0.43	2.13 ± 0.48	0.084
q	0.42 ± 0.08	0.43 ± 0.09	0.803
L	1.94 ± 0.41	2.19 ± 0.46	0.084
CP	162 ± 57.3	148.6 ± 49.8	0.407
CS	699.8 ± 135.2	751.6 ± 81.5	0.135
CL	117.7 ± 50.3	104.6 ± 46.9	0.361

4) **LESION-TO-BRAIN RATIO IN PERITUMORAL REGION OF HIGH-GRADE GLIOMA AND METASTASES:** There was no statistical difference in DTI metrics between these two groups except for *p* value as shown in Table 16 which is as follows:

DTI PARAMETERS	HIGH-GRADE GLIOMA	METASTASES	*P* VALUE
FA	0.6852	0.6922	0.823
p	1.3722	1.5772	**0.032**
q	0.8235	1.0	0.067
L	1.31	1.5208	0.233
CP	0.7528	0.6935	0.701
CS	1.1975	1.2179	0.802
CL	0.5873	0.6215	0.967

5) **TUMOR REGION OF HIGH-GRADE GLIOMA AND LYMPHOMA:** There was statistical difference in *p*, *q* and *L* between these two groups as shown in Table 17 below:

DTI PARAMETERS (MEAN VALUES)	HIGH-GRADE GLIOMA	LYMPHOMA	*P* VALUE
FA	183.14 ± 72.1	196.01 ± 27.6	0.564
p	2.19 ± 0.61	1.34 ± 0.28	**0.000**
q	0.31 ± 0.10	0.21 ± 0.06	**0.005**
L	2.22 ± 0.61	1.36 ± 0.28	**0.001**
CP	104.7 ± 35.8	116.9 ± 14.9	0.376
CS	797.3 ± 168.5	811.2 ± 24.4	0.754
CL	65.97 ± 28.8	70.75 ± 14.8	0.657

6) **LESION-TO-BRAIN RATIO IN TUMOR REGION OF HIGH-GRADE GLIOMA AND LYMPHOMA:** There was statistical difference in lesion-to-brain ratio of *p*, *q* and *L* between these two groups as shown in Table 18 below:

DTI PARAMETERS (MEAN VALUES)	HIGH-GRADE GLIOMA	LYMPHOMA	*P* VALUE
FA	0.4304	0.4332	0.829
p	1.5986	0.9852	**0.000**
q	0.6078	0.3889	**0.000**
L	1.5	0.9189	**0.000**
CP	0.4865	0.5002	0.775
CS	1.3643	1.4611	0.205
CL	0.3291	0.3367	0.750

7) **PERITUMORAL REGION OF HIGH-GRADE GLIOMA AND LYMPHOMA:** There was no statistical difference in the parameters between these two groups as shown in Table 19 below:

DTI PARAMETERS (MEAN VALUES)	HIGH-GRADE GLIOMA	LYMPHOMA	*P* VALUE
FA	291.58 ± 96.2	273.9 ± 89.2	0.573
p	1.88 ± 0.43	2.06 ± 0.65	0.271
q	0.42 ± 0.08	0.44 ± 0.07	0.641
L	1.94 ± 0.41	2.12 ± 0.64	0.262
CP	162 ± 57.3	143.9 ± 50.6	0.325
CS	699.8 ± 135.2	740.5 ± 88.8	0.297
CL	117.7 ± 50.3	114.5 ± 43.1	0.846

8) **LESION-TO-BRAIN RATIO IN PERITUMORAL REGION OF HIGH-GRADE GLIOMA AND LYMPHOMA:** There was no statistical difference in the parameters between these two groups as shown in Table 20 below:

DTI PARAMETERS (MEAN VALUES)	HIGH-GRADE GLIOMA	LYMPHOMA	*P* VALUE
FA	0.6852	0.6055	0.369
p	1.3722	1.5147	0.253
q	0.8235	0.8148	0.588
L	1.31	1.4324	0.292
CP	0.7528	0.6157	0.158
CS	1.1975	1.3337	0.140
CL	0.5873	0.5449	0.654

9) **TUMOR REGION OF METASTASES AND LYMPHOMA:** The *p* and *L* values were significantly different between metastases and lymphoma as shown in Table 21 below:

DTI PARAMETERS (MEAN VALUES)	METASTASES	LYMPHOMA	*P* VALUE
FA	193.4 ± 71.8	196.01 ± 27.6	0.918
p	1.97 ± 0.85	1.34 ± 0.28	**0.012**
q	0.29 ± 0.12	0.21 ± 0.06	0.060
L	1.93 ± 1.05	1.36 ± 0.28	**0.037**
CP	126.3 ± 59.07	116.9 ± 14.9	0.544
CS	809.3 ± 76.8	811.2 ± 24.4	0.968
CL	70.68 ± 28.5	70.75 ± 14.8	0.998

10) **LESION-TO-BRAIN RATIO IN TUMOR REGION OF METASTASES AND LYMPHOMA:** The *p*, *q* and *L* values were significantly different between metastases and lymphoma as shown in Table 22 below:

DTI PARAMETERS (MEAN VALUES)	METASTASES	LYMPHOMA	*P* VALUE
FA	0.5102	0.4332	0.173
p	1.4592	0.9852	**0.014**
q	0.6744	0.3889	**0.02**
L	1.3402	0.9189	**0.031**
CP	0.5893	0.5002	0.245
CS	1.3114	1.4611	0.110
CL	0.4199	0.3367	0.270

11) **PERITUMORAL REGION OF METASTASES AND LYMPHOMA:** There was no significant difference in all the parameters as shown in Table 23 below:

DTI PARAMETERS (MEAN VALUES)	METASTASES	LYMPHOMA	*P* VALUE
FA	262.42 ± 89.03	273.9 ± 89.2	0.744
p	2.13 ± 0.48	2.06 ± 0.65	0.694
q	0.43 ± 0.09	0.44 ± 0.07	0.827
L	2.19 ± 0.46	2.12 ± 0.64	0.711
CP	148.6 ± 49.8	143.9 ± 50.6	0.821
CS	751.6 ± 81.5	740.5 ± 88.8	0.799
CL	104.6 ± 46.9	114.5 ± 43.1	0.586

12) **LESION-TO-BRAIN RATIO IN PERITUMORAL REGION OF METASTASES AND LYMPHOMA:** There was no significant difference in all the parameters except for *q* value as shown in Table 24 below:

DTI PARAMETERS (MEAN VALUES)	METASTASES	LYMPHOMA	*P* VALUE
FA	0.6922	0.6055	0.324
p	1.5772	1.5147	0.583
q	1.0	0.8148	**0.02**
L	1.5208	1.4324	0.935
CP	0.6935	0.6157	0.397
CS	1.2179	1.3337	0.244
CL	0.6215	0.5449	0.573

C) ROC ANALYSIS OF DTI PARAMETERS:

The *p*, *q* and *L* values in tumor region had high accuracy, sensitivity and specificity in differentiating high-grade gliomas from lymphomas. The cutoff values for *p*, *q* and *L* were calculated to be > 1.7144, > 0.2104 and > 1.7356 respectively with values above the cutoff levels more predictive of high-grade gliomas.

For differentiating metastases from lymphomas, *p* and *L* values in the tumor region and lesion-to-brain ratio of *q* in the tumor and peritumoral regions were found to be statistically significant. The cutoff values for *p* and *L* in tumor regions were found to be > 1.6236 and > 1.6649 respectively and for lesion-to-brain ratio of *q* in tumor and peritumoral regions as > 0.4697 and > 0.8041 with values above the cutoff levels more predictive of metastases.

For differentiating high-grade gliomas from metastases, lesion-to-brain ratio of *p* in peritumoral region with cutoff value of ≤ 1.7146 was found to have high accuracy and sensitivity but low specificity. Values below the cutoff level were more predictive of high-grade gliomas.

Table 25: ROC analysis of DTI parameters

STUDY GROUPS	REGION	DTI METRICS	CUTOFF VALUES	SENSITIVITY (%)	SPECIFICITY (%)	AUC (%)
HGG VS LYMPHOMA	TUMOR	*p*	> 1.7144	80	100	0.9
HGG VS LYMPHOMA	TUMOR	*q*	> 0.2104	91.4	66.7	0.83
HGG VS LYMPHOMA	TUMOR	*L*	> 1.7356	80	100	0.90
LYMPHOMA VS METASTASES	TUMOR	*p*	> 1.6236	58.8	91.7	0.75
LYMPHOMA VS METASTASES	TUMOR	*L*	> 1.6649	52.9	91.7	0.69
LYMPHOMA VS METASTASES	TUMOR LESION-TO-BRAIN RATIO	*q*	> 0.4697	76.5	83.3	0.81
LYMPHOMA VS METASTASES	PERITUMORAL LESION-TO-BRAIN RATIO	*q*	> 0.8041	88.2	66.7	0.76
HGG VS METASTASES	PERITUMORAL LESION-TO-BRAIN RATIO	*P*	≤ 1.7146	88.6	52.9	0.67

2) DSC-MRI:

DSC-MRI was available in twenty-four patients with high-grade glioma and in twelve patients each of metastasis and lymphoma. The values of all its parameters (rCBV, rCBF and rPSR) measured in the three study groups are represented in box-plots. The horizontal lines at the ends of the vertical lines denote the range of

values of each parameter. The borders of the boxes in the boxplot charts denote the 25th and 75th percentiles of values of each parameter. The stripe between the green and purple regions in each box represents the mean value of each parameter. The purple region within each box represents the values above the mean value of each parameter and green region within each box represents the values below the mean value of each parameter.

A) **Fig 10: Boxplot chart showing rCBV and rCBF in tumor regions of the tumor groups:** The mean maximum rCBV values in tumor regions were 5.52 ± 3 in high-grade gliomas, 6.2 ± 3 in metastases and 4.18 ± 1.95 in lymphomas. The mean maximum rCBF values within the tumor regions were 5.23 ± 3.2 in high-grade gliomas, 5.7 ± 3.05 in metastases and 4.15 ± 1.07 in lymphomas.

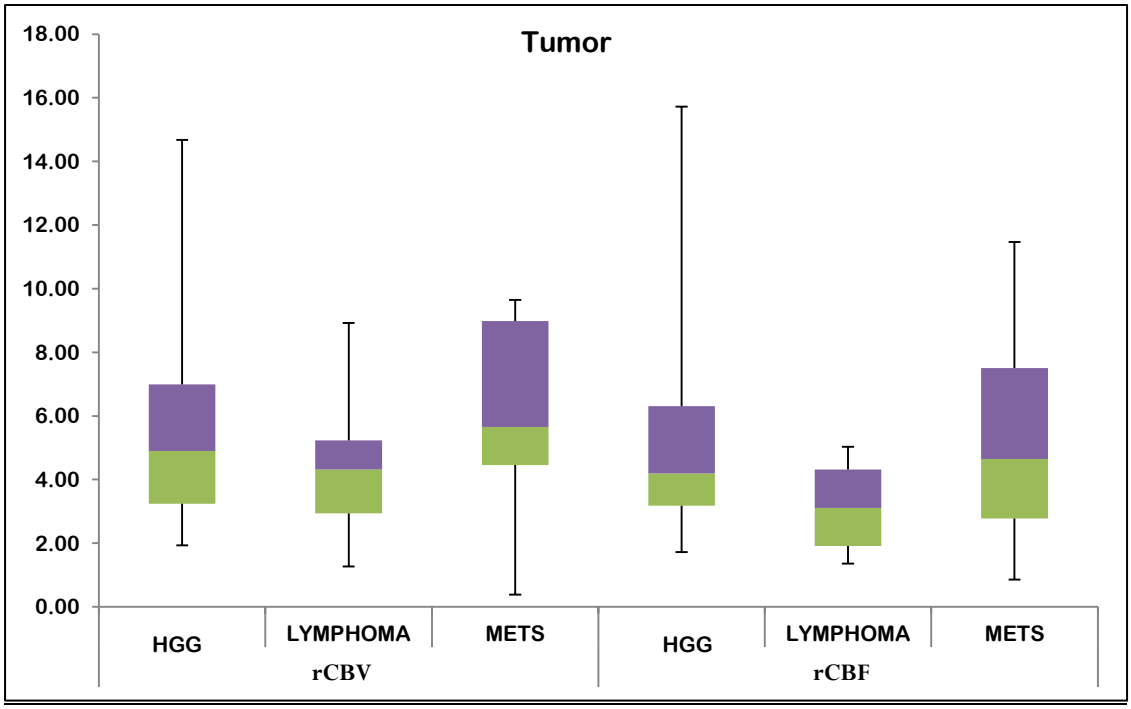

B) **Fig 11: Boxplot chart showing rCBV and rCBF in adjacent peritumoral regions of the tumor groups:** The mean maximum rCBV values in adjacent peritumoral regions were 0.93 ± 0.47 in high-grade gliomas, 0.59 ± 0.42 in metastases and 0.65 ± 0.29 in lymphomas. The mean maximum rCBF values within the adjacent peritumoral regions were 0.86 ± 0.51 in high-grade gliomas, 0.6 ± 0.29 in metastases and 0.63 ± 0.18 in lymphomas.

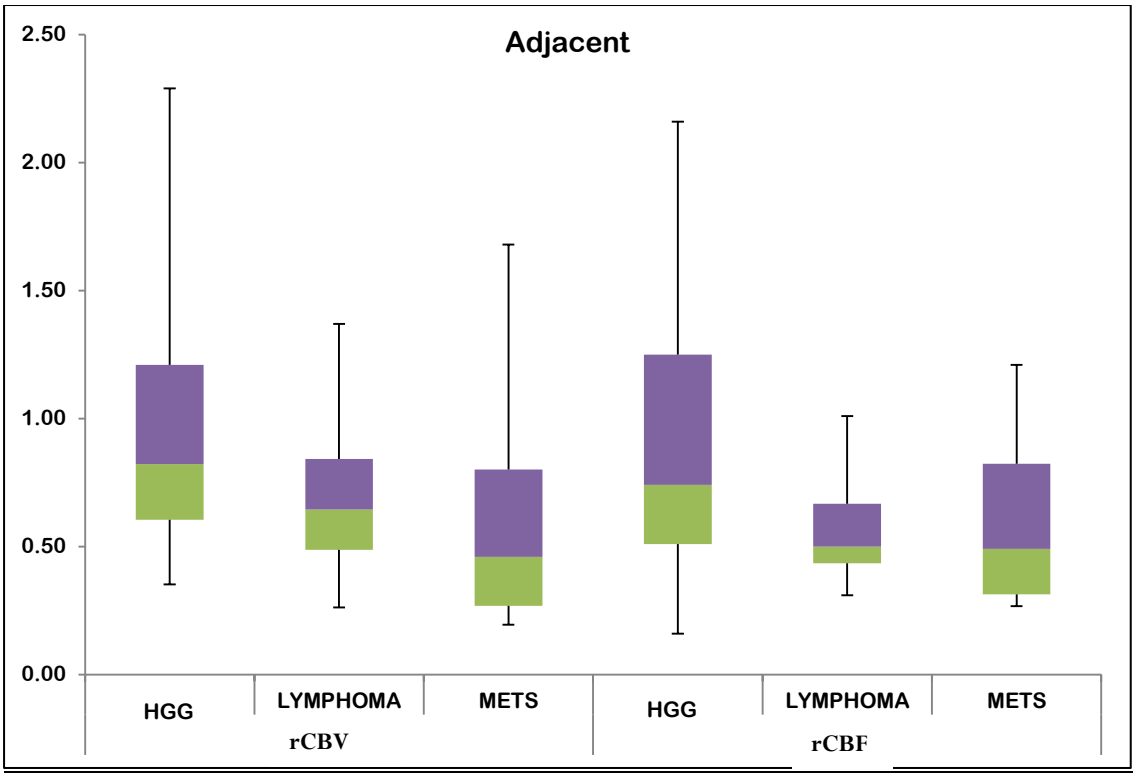

C) **Fig 12: Boxplot chart showing rPSR in tumor and adjacent peritumoral regions of the tumor groups:** The mean rPSR values in enhancing tumor regions were 101.02 ± 14.9 in high-grade gliomas, 81.67 ± 23.6 in metastases and 150.72 ± 63.5 in lymphomas. The mean rPSR values in adjacent peritumoral regions were 99.34 ± 11.3 in high-grade gliomas, 101.03 ± 19.5 in metastases and 101.18 ± 17.02 in lymphomas.

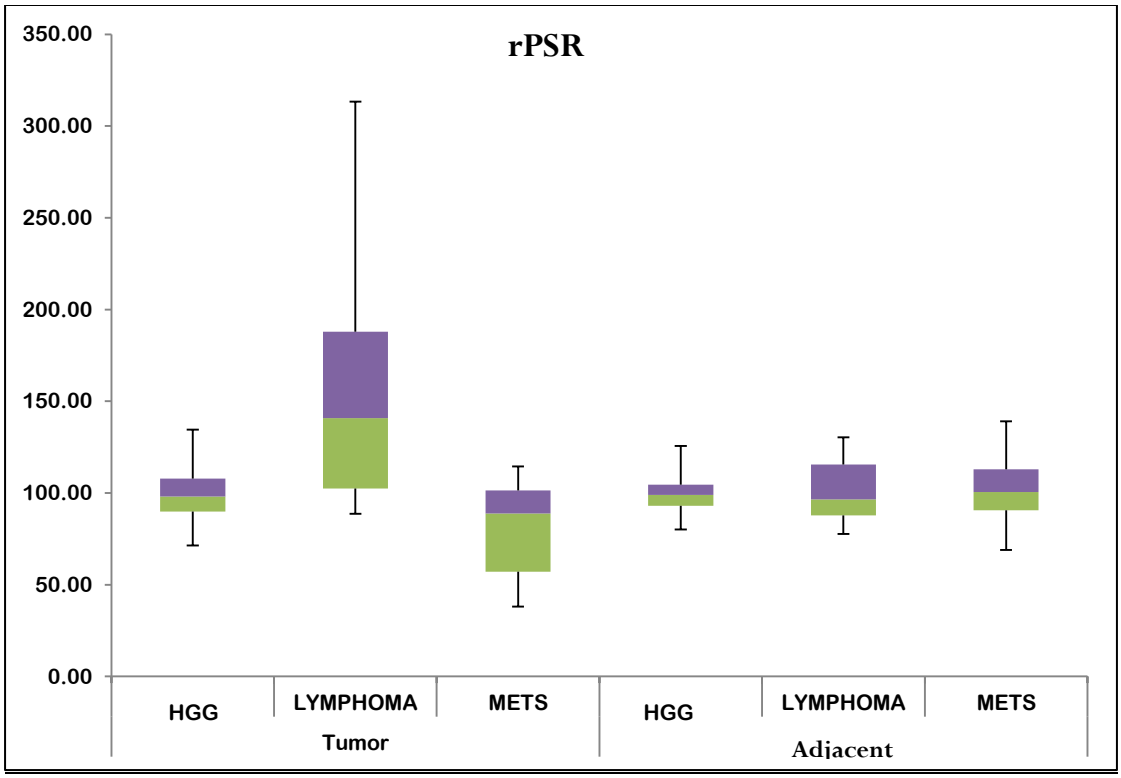

D) COMPARISON OF THE TUMOR AND ADJACENT PERITUMORAL REGIONS WITHIN THE STUDY GROUPS FOR rCBV, rCBF AND rPSR.

ANOVA showed significant difference in rCBV and rCBF between the tumor and adjacent peritumoral regions in all the three study groups ($P < 0.001$). The rPSR was however, significant only in lymphomas between the tumor and peritumoral regions ($P = 0.010$) and not in high-grade gliomas and metastases ($P = 0.587$ and 0.053 respectively).

E) COMPARISON WAS DONE BETWEEN THE THREE STUDY GROUPS IN TUMOR AND ADJACENT PERITUMORAL REGIONS:

ANOVA showed significant difference in rCBV in adjacent peritumoral regions between the three study groups ($P < 0.03$). The rPSR in tumor regions was also significantly different between the study cohorts ($P < 0.01$). There was

no statistical difference between the intratumoral rCBV and rCBF and the peritumoral rCBF and rPSR between the tumor groups.

F) ROC ANALYSIS OF DSC-MRI PARAMETERS:

The rCBV in peritumoral regions and rPSR in tumor regions were found to have higher accuracy, sensitivity and specificity for differentiating between the tumor types.

The cutoff values for peritumoral rCBV for differentiating high-grade gliomas from metastases, lymphomas from metastases and high-grade gliomas from lymphomas were calculated to be ≤ 0.38, > 0.38 and > 0.79 respectively.

High-grade gliomas had higher peritumoral rCBV compared to lymphomas and metastases. Lymphomas had higher rCBV in peritumoral region compared to metastases.

The cutoff values for intratumoral rPSR for differentiating high-grade gliomas from metastases, lymphomas from metastases and high-grade gliomas from lymphoma were calculated to be > 85.94, > 103.4 and > 134.49 respectively.

Lymphomas had higher rPSR compared to high-grade gliomas and metastases. High-grade gliomas had higher rPSR than metastases.

Table 26: ROC analysis of DSC-MRI parameters

TUMORS	REGION	DSC-MRI PARAMETERS	CUTOFF VALUE	SENSITIVITY (%)	SPECIFICITY (%)	AUC (%)
HGG VS METASTASES	PERITUMORAL	rCBV	≤ 0.38	50	95.8	0.75
HGG VS LYMPHOMA	PERITUMORAL	rCBV	> 0.79	54.2	75	0.65
LYMPHOMA VS METASTASES	PERITUMORAL	rCBV	> 0.38	91.7	50	0.64
HGG VS LYMPHOMA	TUMOR	rPSR	> 134.49	53.8	100	0.79
METASTASES VS LYMPHOMA	TUMOR	rPSR	> 103.4	75	91.7	0.89
HGG VS METASTASES	TUMOR	rPSR	> 85.94	91.7	50	0.74

3) SWI:

The ITSS in precontrast SWI images in tumor regions of all three study groups were divided into four grades. The SWI images were not available in one patient with high-grade glioma and one patient with lymphoma; hence there were thirty-four patients in high-grade glioma group, eighteen patients with metastasis and twelve patients with lymphoma with available precontrast SWI images.

Table 27: The grades of ITSS on precontrast SWI in different groups:

ITSS	HIGH-GRADE GLIOMA	METASTASES	LYMPHOMA
GRADE 0	5 (14.71%)	8 (44.45%)	12 (100%)
GRADE I	1 (2.94%)	4(22.22%)	0%
GRADE II	10 (29.41%)	2(11.11)	0%
GRADE III	18 (52.94%)	4 (22.22%)	0%

Ordinal regression was done for comparing the difference in ITSS grades between the study groups. There was significant difference between the metastases and high-grade gliomas for absence (grade 0) of ITSS compared to presence of ITSS (grades I, II and III) as shown in Table 28 below:

Odds ratio	Standard Error	*P* value	95% Confidence Interval
0.2155	0.6779	0.0236	0.0571 - 0.8137

There was no statistically significant difference in the grades I - III between the tumor regions of high-grade gliomas and metastases as shown in Table 29 below:

Odds ratio	Standard Error	*P* value	95% Confidence Interval
0.4074	0.7504	0.2315	0.0936 - 1.7733

The ordinal regression could not be done for comparing lymphomas with metastases and high-grade gliomas as there were no patients with ITTS in lymphoma group.

ROC analysis was done for comparing the three study groups for different grades of ITSS. It showed that grade III ITSS had the highest predictive value for differentiating the study groups.

Postcontrast SWI was done in 9 cases. All the cases were of high-grade glioma. On comparison with the precontrast SWI images, it showed no difference in the grades of ITSS.

IV) HISTOPATHOLOGY FINDINGS:

Histopathological confirmation was done in all the patients. Forty-six patients underwent surgical excision and 20 patients were biopsied.

Table 30: Distribution of surgical procedures

	HIGH-GRADE GLIOMA	METASTASES	LYMPHOMA
SURGICAL EXCISION	27	16	3
BIOPSY	8	2	10

REPRESENTATIVE CASES

Case 1

History:

32 year old female patient, presented with complaints of insidious onset, gradually progressive moderate to severe bifrontal headache for last 1 year. She developed 3 episodes of seizure in last 1 year.

On examination:

She had bilateral papilledema. No neurological deficits were noted.

Conventional MRI:

An ill-defined solid-cystic lesion was noted in left frontotemporal and basal ganglia region with mass effect and heterogeneous contrast enhancement. The solid part measured 53x40x47mm with extensive perilesional edema. It was hyperintense on T2-weighted and FLAIR images. There was mild diffusion restriction within the lesion. MRS showed elevated choline peak and presence of lactate peak within the lesion.

Advanced MR imaging:

DTI: Tumor area showed reduced FA, increased *p, L, CS* and reduced *q, CP* and *CL* compared to contralateral white matter. The peritumoral area showed reduced FA, increased *p, L* and *CS* and reduced *q, CP* and *CL* as compared to the contralateral normal appearing white matter.

DSC-MRI: The lesion showed areas of increased perfusion. The rCBV was 12.1 and rCBF was 10.7. The rCBV and rCBF in peritumoral region were 0.55 and 0.56. The signal intensity-time curve showed rapid fall below baseline with rapid

recovery not reaching baseline. The rPSR was 87.82 in tumor region and 98.3 in peritumoral region.

SWI: blooming was noted within the lesion (ITSS – grade III).

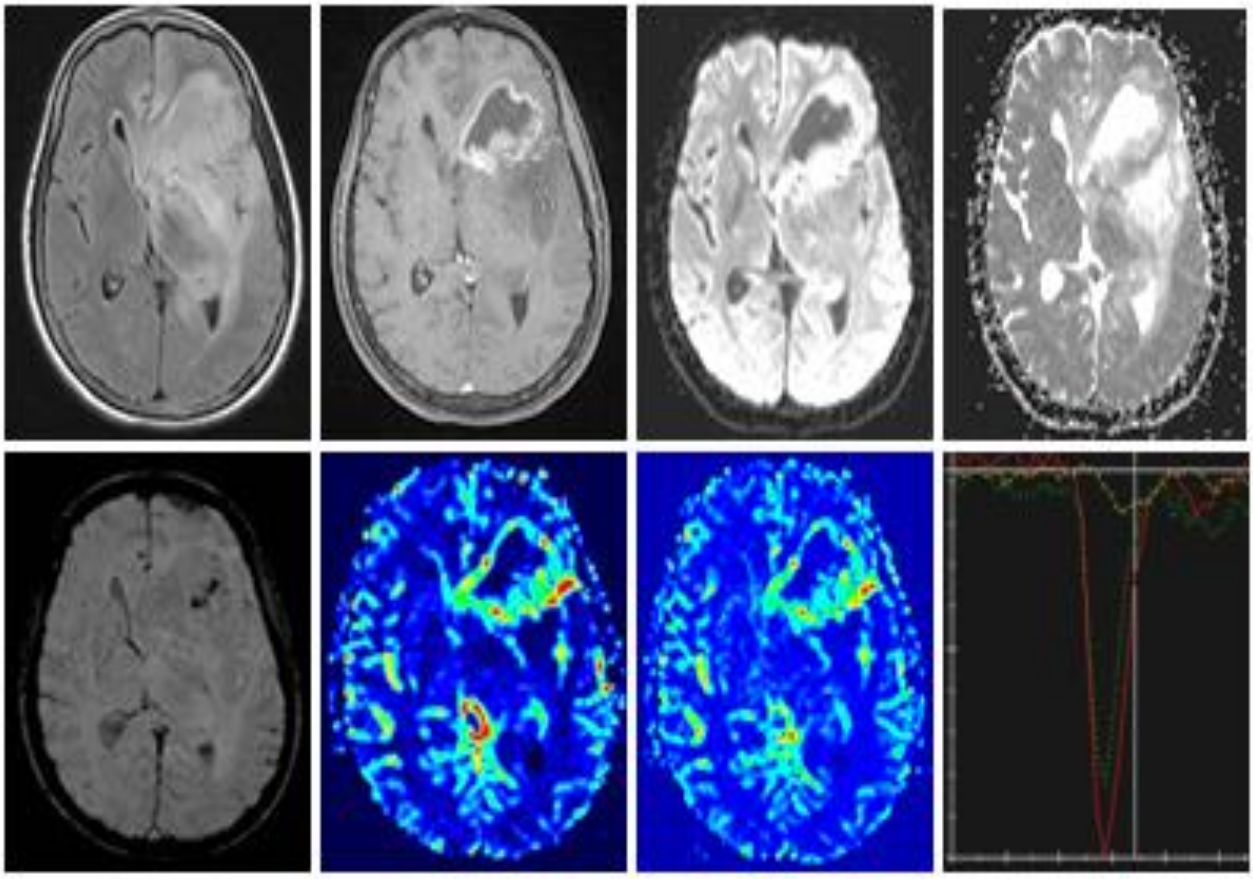

Surgery:

Left pterional craniotomy and near total excision of the lesion was performed.

Histopathology:

Glioblastoma multiforme.

Case 2

History:

41 year old female complained of headache for last 2 years. It was insidious in onset, mild to moderate in intensity and was holocranial. For last 2 weeks she developed weakness in right upper and lower limbs.

On examination:

Bilateral papilledema was noted. No neurological deficit was present.

Conventional MRI:

Multiple T2 hypointense and FLAIR isointense lesions were noted in parietooccipital lobes and splenium of corpus callosum. They showed homogeneous contrast enhancement. Diffusion restriction was present within these lesions. Mild perilesional edema was noted. MRS showed increased choline peak and reduced NAA peak.

Advanced MR imaging:

DTI: Tumor area showed reduced FA, increased *p, L, CS* and reduced *q, CP* and *CL* compared to contralateral white matter. The peritumoral area showed reduced FA, increased *p, L* and *CS*, almost similar *q* and reduced *CP* and *CL* as compared to the opposite cerebral white matter.

DSC-MRI: The lesion showed mildly increased perfusion. The rCBV was 4.43 and rCBF was 3.4. The rCBV and rCBF in peritumoral region were 0.84 and 0.54. The signal intensity-time curve showed minimal fall below baseline with rapid recovery above baseline. The rPSR was 152.38 in tumor region and 89.8 in peritumoral region.

SWI: No SWI blooming was noted within the lesion (ITSS - grade 0).

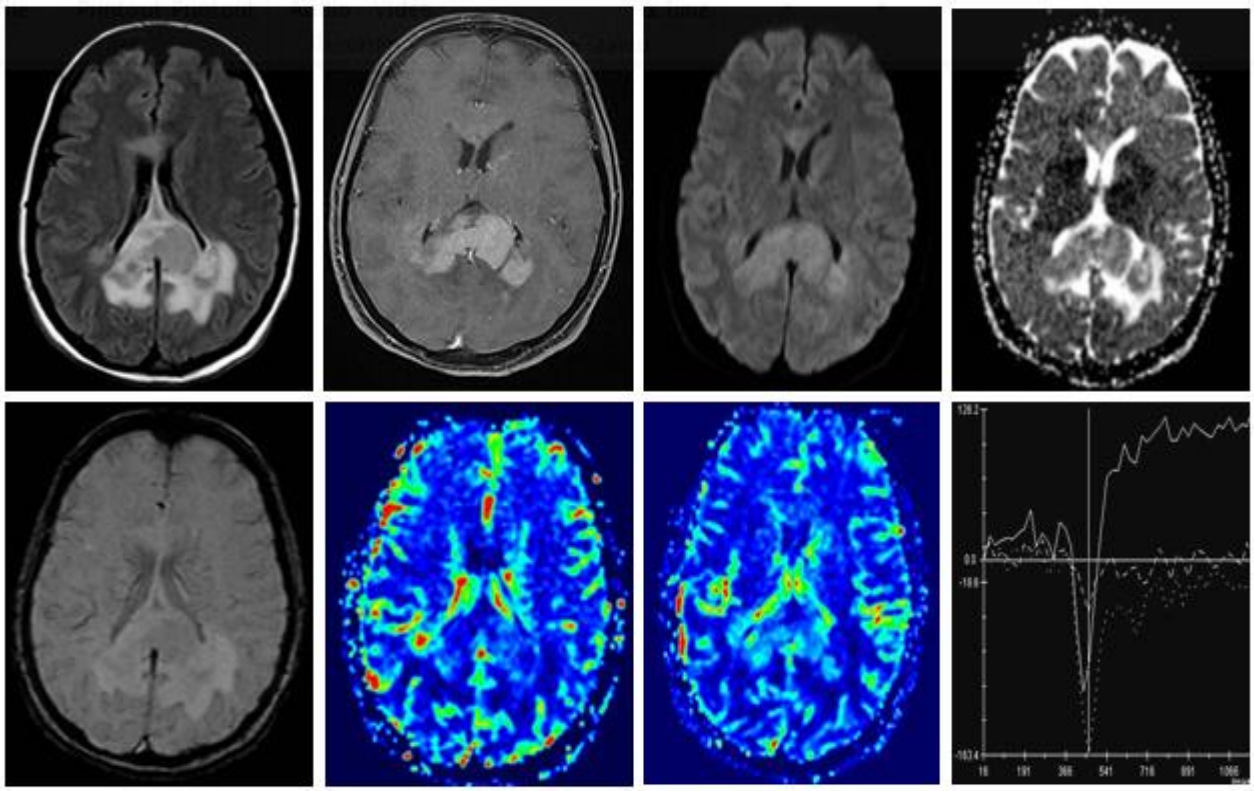

Surgery:

Biopsy from the lesion.

Histopathology:

Primary central nervous system lymphoma.

Case 3

History:

55 year old male with no comorbidities presented with complaints of right hemicranial headache for last 2 years. It was mild to moderate, intermittent and relieved with medications.

On examination:

No focal neurological signs were noted.

Conventional MRI:

There was a T2 heterogeneous lesion in right temporal lobe measuring 26x27x27mm with moderate heterogeneous contrast enhancement, mild diffusion restriction, elevated choline peak and prominent lipid peak.

Advanced MR imaging:

DTI: Tumor area showed reduced FA, increased *CS* and reduced *p, q, L, CP* and *CL* compared to normal appearing contralateral white matter. The peritumoral area showed reduced FA, increased *p, L* and *CS* and reduced *q, CP* and *CL* as compared to the contralateral white matter.

DSC-MRI: The lesion showed areas of increased perfusion. The rCBV was 9.65 and rCBF was 7.3. The rCBV and rCBF in peritumoral region were 0.54 and 0.3. The signal intensity-time curve showed rapid fall below baseline with rapid recovery below baseline. The rPSR was 74.2 in tumor region and 98.5 in peritumoral region.

SWI: blooming was noted within the lesion (ITSS – grade III).

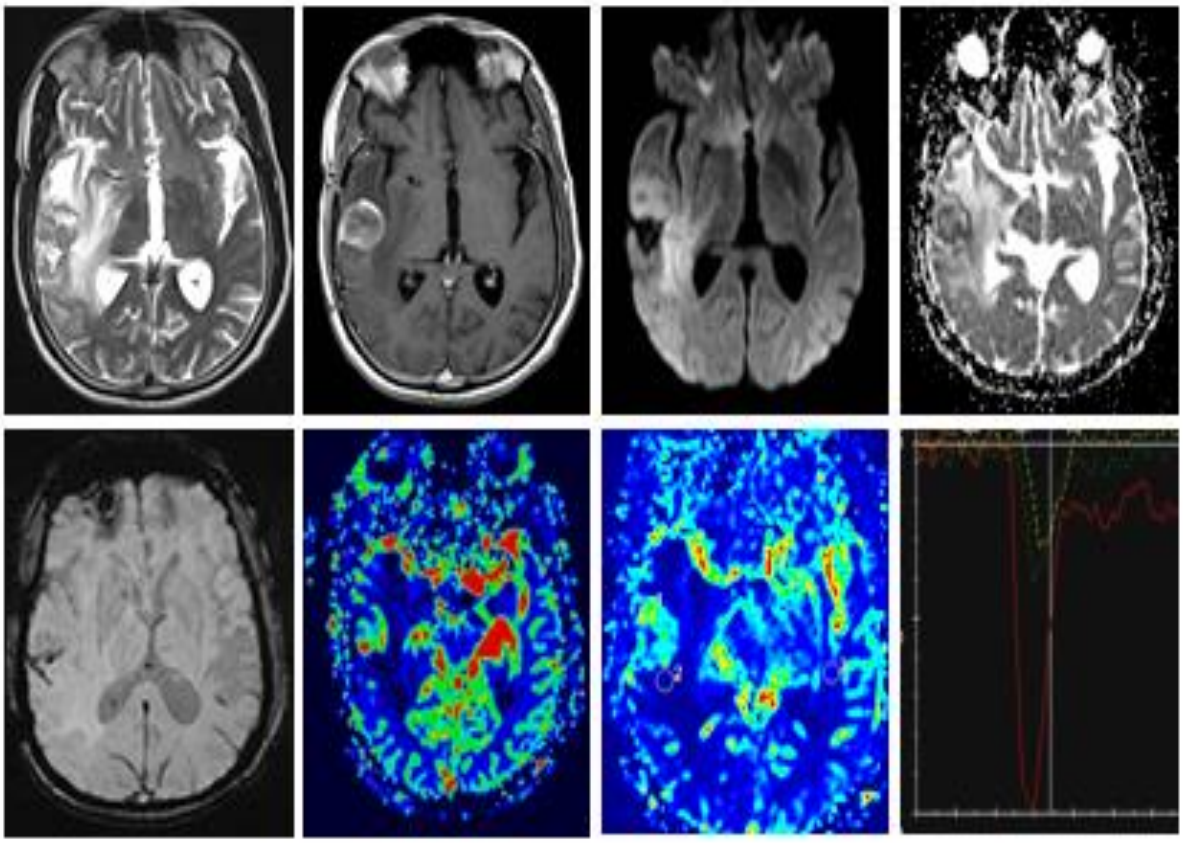

Surgery:

He underwent right temporal craniotomy and gross total decompression.

Histopathology:

Metastasis from poorly differentiated lung carcinoma.

Case 4

History:

61 year old male patient, known hypertensive, diabetic and post-percutaneous transluminal coronary angioplasty (PTCA) status (for LAD artery thrombosis), presented with c/o acute onset gradually progressive weakness of left upper and lower limbs for last 2 months. He also had one episode of simple partial seizure with tonic-clonic movements of left upper and lower limbs.

On examination:

He had bilateral papilledema with grade 0/5 power in left upper and lower limbs and 3/5 power in right upper and lower limbs. Left UMN facial palsy was also noted.

Conventional MRI:

Peripheral enhancing T2 hyperintense lesions were seen in right temporal, parietal and occipital lobes with moderate perilesional edema and enhancing peripheral nodular component. Mild diffusion restriction was noted in solid component. MRS showed increased choline peak with lactate peak. Ill-defined T2 hyperintense lesion with diffusion restriction, contrast enhancement and increased perfusion was also noted in splenium of corpus callosum.

Advanced MR imaging of right temporal lesion:

DTI: Tumor area showed reduced FA, increased *p, L, CS* and reduced *q, CP* and *CL* compared to contralateral normal white matter. The peritumoral area showed reduced FA, reduced *q, CP,CL* and similar *p, L* and increased *CS* as compared to the contralateral white matter.

DSC-MRI: There was increased perfusion in the periphery of the lesion. The rCBV was 3.08 and rCBF was 3.15 in the tumor region. The rCBV and rCBF in

peritumoral region were 0.62 and 0.536. Signal intensity-time curve showed steep fall with rapid rise above baseline. The rPSR was 134.5 in tumor region and 99.73 in peritumoral region.

SWI: No SWI blooming was noted within the lesion (ITSS - grade 0).

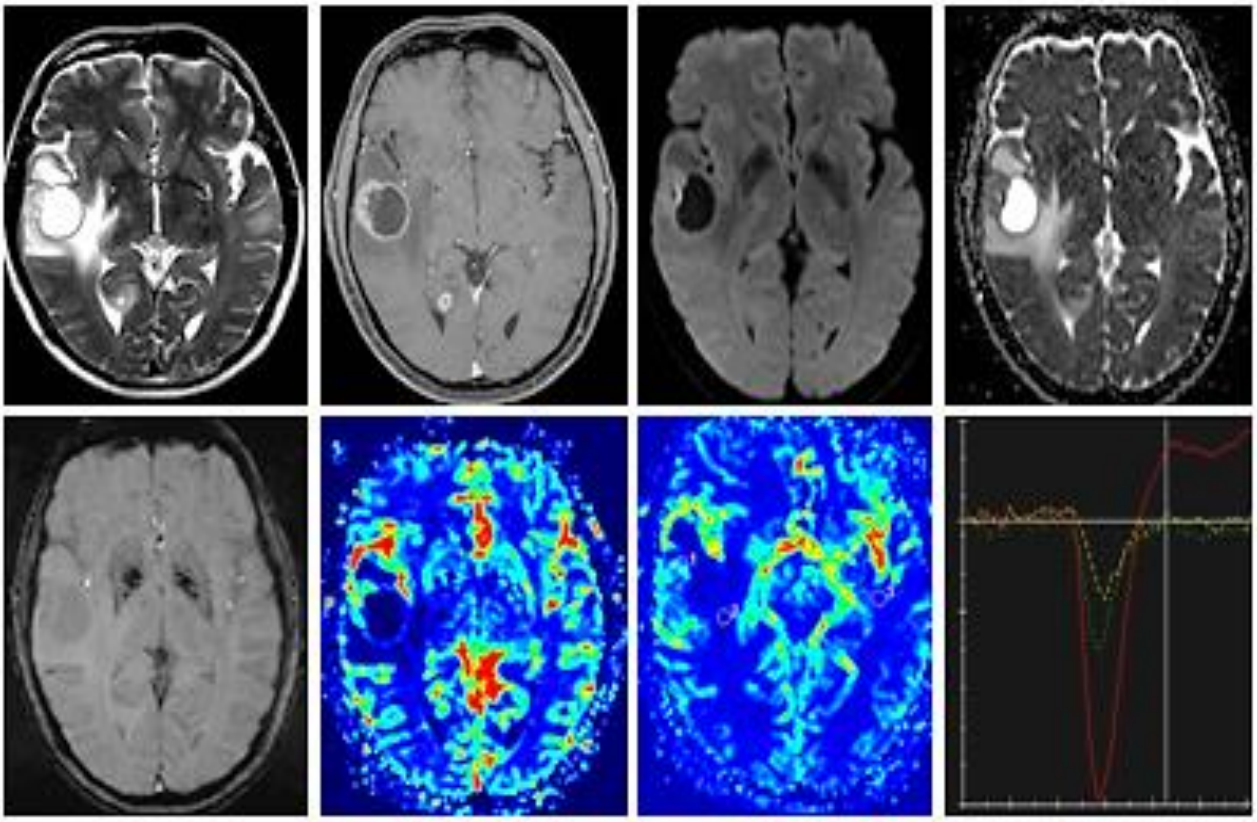

Surgery:

Right frontotemporal craniotomy with gross total decompression of the lesions was done.

Histopathology:

Glioblastoma multiforme with oligodendroglial component.

Case 5

History:

67 year old male, known hypertensive, dyslipidemic, CAD (post CABG status), presented with acute onset weakness and paresthesia in right upper and lower limbs. He was started on anti-tubercular drugs (AKT-4) with steroids (prednisolone-10 mg/day). He improved over 3-4 days. There was history of right eye retinopathy 7-8 years back.

On examination:

Right eye showed no perception of light and left eye had cataract (visual acuity-6/24. No other deficits were seen.

Conventional MRI:

Left frontoparietal ill-defined T2 isointense lesion with moderate perilesional edema, heterogeneous contrast enhancement and diffusion restriction was noted. There was extension to splenium and periventricular region.

Advanced MR imaging:

DTI: Tumor area showed reduced FA, increased *p, L, CS* and reduced *q, CP* and *CL* compared to contralateral white matter. The peritumoral area showed reduced FA, reduced *q, CP, CL* and increased *p, L* and *CS* as compared to the contralateral white matter.

DSC-MRI: There were areas of increased perfusion in the lesion. The rCBV was 4.5 and rCBF was 2.61 in tumor region. The rCBV and rCBF in peritumoral region were 0.47 and 0.48. Signal intensity- time curve showed fall below baseline with rapid recovery above baseline. The rPSR was 155.9 in tumor region and 115.2 in peritumoral region.

SWI: no blooming was noted in the lesion.

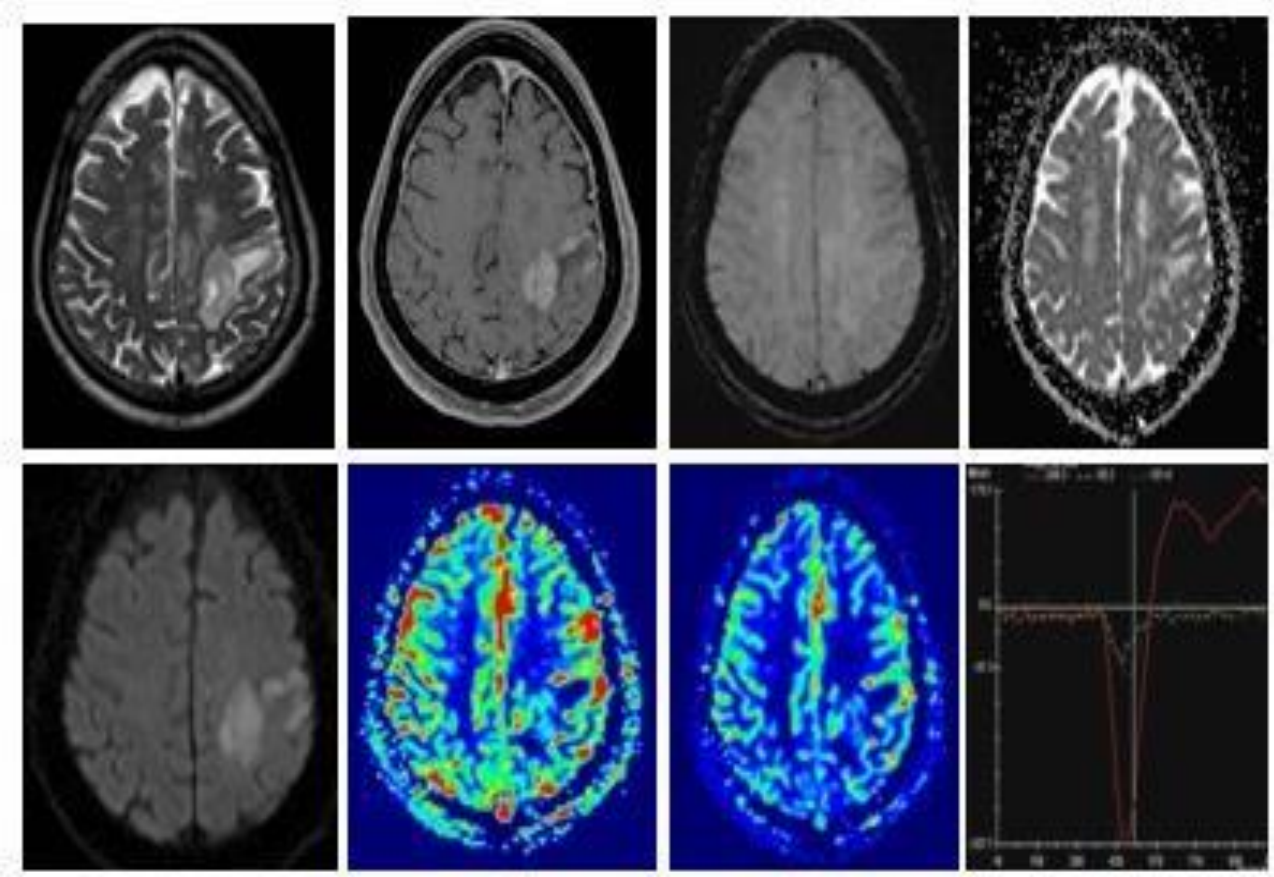

Surgery:

Left parietal burr-hole biopsy was done.

Histopathology:

Primary central nervous system lymphoma.

Case 6

History:

58 year old male patient, known hypertensive, presented with complaints of right sided mild to moderate intermittent headache for last 3 months. It was associated with blurring of vision.

On examination:

There was no evidence of papilledema or any neurological deficit. Visual acuity was normal.

Conventional MRI:

An ill-defined cortical based lesion was noted in right temporooccipital lobe with mixed signal intensity on T2-weighted images, heterogeneous contrast enhancement measuring 35x33x39mm. There was diffusion restriction within the lesion with perilesional edema. MRS showed increased choline peak and presence of lactate peak within it.

Advanced MR imaging:

DTI: Tumor area showed reduced FA, increased *p, L, CS* and reduced *q, CP* and *CL* compared to opposite cerebral white matter. The peritumoral area showed increased FA, *p, q* and *L* and almost similar *CP, CS,* and *CL* as compared to the contralateral normal appearing white matter.

DSC-MRI: The lesion showed increased perfusion. The tumor area had rCBV of 6.13 and rCBF of 3.7. The rCBV and rCBF in peritumoral region were 1.1 and 1.7. Signal intensity- time curve showed rapid fall below baseline with rapid recovery below baseline. The rPSR was 96.11 in tumor region and 84.7 in peritumoral region.

SWI: SWI blooming was noted (ITSS – grade III).

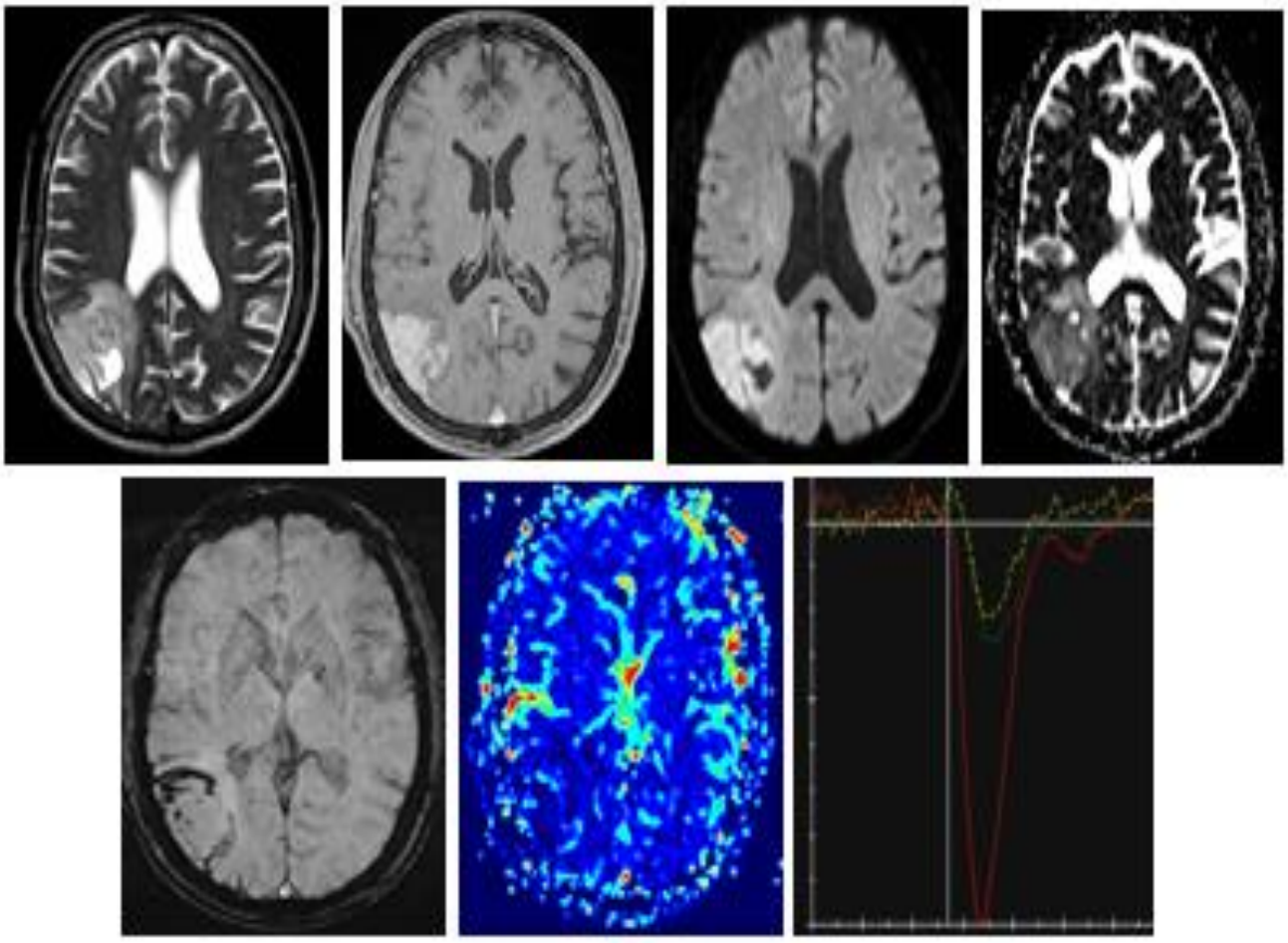

Surgery:

Right parietal craniotomy and decompression was done.

Histopathology:

Oligodendroglioma with polar spongioblastoma like areas (WHO grade III).

Case 7

History:

67 year old male, known hypertensive presented with complaints of 1 episode of seizure 1 month back. It was associated with transient loss of consciousness and postictal drowsiness. He also complained of mild memory impairment in the form of forgetting names easily. He had history of adenocarcinoma of right lung 3 years back for which he underwent thoracotomy and pneumonectomy followed by chemotherapy.

On examination:

There was early papilledema in both eyes. No neurological deficit was present.

Conventional MRI:

A well-defined T2 heterogeneous lesion was seen in left frontal lobe with moderate contrast enhancement, mild diffusion restriction and mild perilesional edema. MRS showed elevation of choline peak and reduction of NAA peak.

Advanced MR imaging:

DTI: Tumor area showed reduced FA, increased *p, L, CP, CS* and reduced *q* and *CL* compared to contralateral white matter. The peritumoral area showed reduced FA, increased *p, L* and *CS*, minimally increased *q* and reduced *CP* and *CL* as compared to the contralateral white matter.

DSC-MRI: The lesion showed areas of increased perfusion. The rCBV was 7.46 and rCBF was 3.65 within the lesion. The rCBV and rCBF in peritumoral region were 0.24 and 0.35. Signal intensity- time curve showed rapid fall below baseline with slow recovery below baseline. The rPSR was 68.02 in tumor region and 67.4 in peritumoral region.

SWI: extensive blooming was noted (ITSS – grade III).

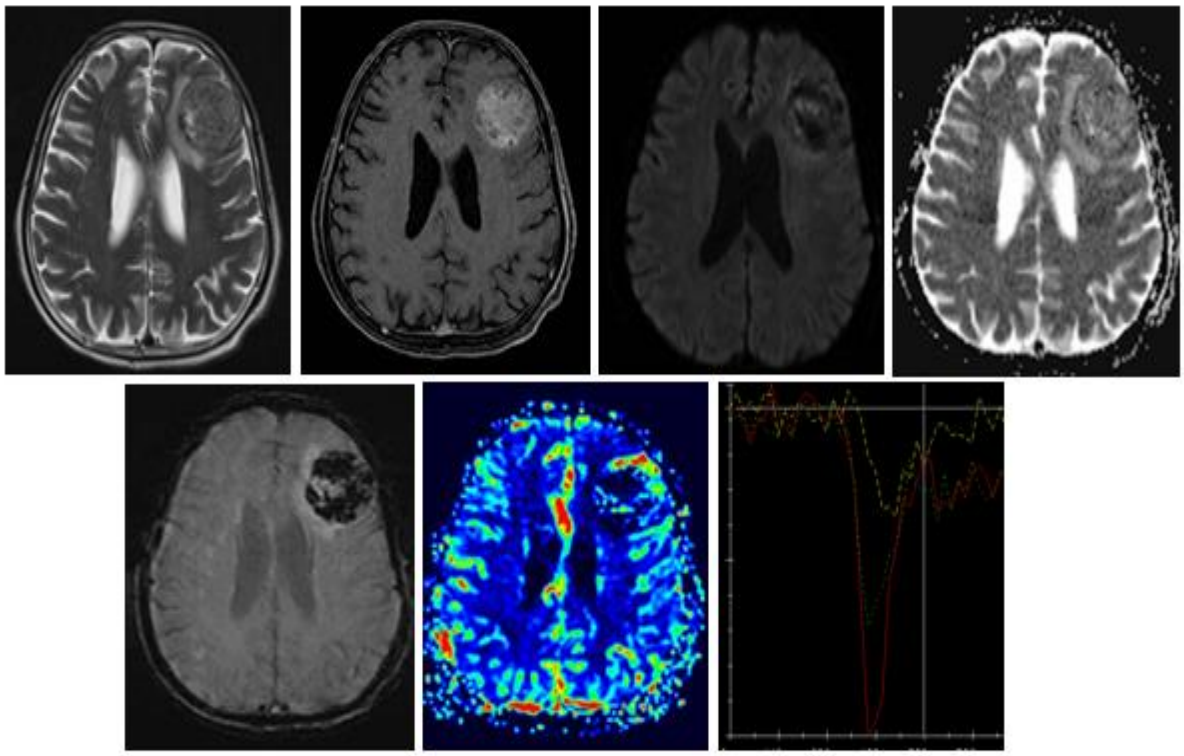

Surgery:

He underwent left frontal craniotomy and excision.

Histopathology:

Well differentiated papillary adenocarcinoma.

DISCUSSION

This study was done with the objective to assess the utility of some of the advanced MRI techniques in differentiating the intra-axial high-grade lesions. We aimed at finding definite quantitative measures that would favor a particular diagnosis and would eventually help in better management of these diseases.

Among the patients with high-grade glioma, 51.43% patients had glioblastoma multiforme and 48.57% had grade III glioma including anaplastic astrocytoma, anaplastic oligoastrocytoma and anaplastic oligodendroglioma. In the metastases group, 7 cases (38.89%) had primary from lung carcinoma, 5 cases (27.78%) from breast carcinoma and 6 cases (33.34%) from unknown primary source. There was no statistical difference in the age and gender distribution between the study groups ($P > 0.05$).

In our study, high-grade gliomas and metastases showed significant increase in *p, L* and *CS* and remarkable decrease in FA, *q, CP* and *CL* in tumor regions compared to opposite cerebral white matter. In the peritumoral regions, high-grade gliomas showed statistical increase in *p, L* and *CS* and significant decrease in FA, *q, CP* and *CL*. In peritumoral region in metastases, similar findings were noted except for insignificant change in *q*. These findings are almost similar to the study published by Wang et al[58] assessing FA, *p, q* and *L* except the unremarkable change in *q* found in their study.

We found that tumor regions in lymphomas differed from high-grade gliomas and metastases by the insignificant increase in *p* and *L*. The peritumoral regions in lymphomas also showed remarkable increase in *p, L* and *CS* and significant decrease in FA, *q, CP* and *CL* compared to contralateral white matter.

There was reduction in FA in tumor regions in all three tumor types compared to opposite cerebral white matter, being lower in high-grade gliomas compared to metastases and lymphomas. However, there was no statistical difference in intratumoral FA between the tumor groups. This finding differed from study reported by Toh et al[46] which showed significantly lower FA in lymphomas compared to glioblastomas ($P < 0.001$). Our study included both grade III and grade IV gliomas which could be a reason for the lack of statistical significance.

In our study, peritumoral region showed low FA in all the three tumor types compared to opposite cerebral white matter. It was higher in high-grade gliomas compared to metastases and lymphomas but this was not statistically significant. Similar finding was reported by Lu et al[21] who compared peritumoral FA between metastases and high-grade gliomas. Meta-analysis done by Jiang et al[8] showed no significant difference in intratumoral FA between high-grade gliomas and metastases but the peritumoral FA was significantly higher in high-grade gliomas compared to metastases. Wang et al[55] have observed that intratumoral FA was the single best predictor for discriminating glioblastomas from metastases, dissimilar to our study.

Wang et al[58] found that *q* and FA were significantly lower in gross tumor regions ($P < 0.001$) and *q* was significantly lower in peritumoral margins ($P < 0.001$) in glioblastoma multiforme compared to metastases. In our study, there was no significant difference between the tumor and peritumoral regions in *p, q* and *L* between high-grade gliomas and metastases. There was however, significant difference in the lesion-to-brain ratio of *p* in peritumoral regions between high-grade gliomas and metastases. Wang et al[58] also found significant overlap in values of all parameters in the tumor and peritumoral regions within the 2 groups similar to our study. We are of the notion that the lack of direct labeled histologic correlation with the ROIs used for parametric measurements may have led to disparities in the findings.

We found that there was remarkable decrease in *CP* and *CL* and increase in *CS* in tumor and peritumoral regions in all three tumor types. However, there was considerable overlap in the values of these parameters between the tumor groups. Hence, they were not helpful in differentiating between these lesions.

ROC analysis showed that a combination of *p, q* and *L* in tumor region had high accuracy, sensitivity and specificity for differentiating high-grade gliomas from lymphomas. For differentiating metastases from lymphomas, *p* and *L* in tumor regions and lesion-to-brain ratio of *q* in tumor and peritumoral regions were found to be statistically significant. For differentiating high-grade gliomas from

metastases, lesion-to-brain ratio of *p* in peritumoral region was found to have highest accuracy and sensitivity but low specificity. We could not compare these findings due to lack of comparative similar studies simultaneously comparing all these metrics in these three high-grade lesions.

Various studies have published different values of mean rCBV in high-grade gliomas. It was found to be higher in grade IV gliomas compared to grade III gliomas (mean rCBVmax 5.5 and 4.03 respectively) by Cha et al[64] similar to our study (mean rCBVmax 6.3 and 4.56 respectively). In metastases, Cho et al[79] found mean rCBVmax of 8.34 which is near to values measured in our study (6.2 ± 3). Lymphomas have been found to demonstrate significantly lower rCBV (mean rCBVmax 1.44) compared to glioblastomas by Cha et al[64]. However, in our study the mean rCBVmax in lymphomas was higher (4.18 ± 1.95). The possible reason for this observation could be the fact that measurement of CBV with leakage correction decreases the difference in rCBV between high-grade gliomas and lymphomas as presented by Toh et al[81].

In our study, there was no statistical difference in rCBV in tumor regions between the three tumor groups as there was considerable overlap in the values. Calli et al[26] also found no significant difference in mean rCBV between metastases and lymphomas and high-grade gliomas. There was significant difference in rCBV in adjacent peritumoral regions between the three study groups in our study ($P <$

0.05). Cha et al[64] also found significant difference in peritumoral rCBV between high-grade gliomas and metastases.

Cha et al[67] reported significantly lower rPSR in intratumoral as well as peritumoral regions in metastases compared to glioblastomas. Lymphomas exhibit higher rPSR compared to glioblastomas as reported by Hartmann et al[68] due to extensive leakage of contrast. Similar observations were seen in our study. Mangla et al[69] suggested a cutoff value of > 136 for rPSR to differentiate lymphomas from glioblastomas. This cutoff value is almost same as our study which shows a cutoff value of > 134.49 for differentiating high-grade gliomas from lymphomas. They also suggested a minimum rPSR of < 40 to be specific for metastases. In our study, none of the patients with high-grade gliomas and lymphomas had rPSR < 71.3 and < 88.69 respectively and one of the patients with metastases had rPSR of 38.06 which fits the criteria suggested by Mangla et al[69]. A combination of rCBV in peritumoral regions and rPSR in tumor regions was found to be more accurate with higher sensitivity and specificity for differentiating the tumor types.

We found that ITSS were present in 85.3% of patients with high-grade gliomas (94.45% of glioblastomas and 75% of grade III gliomas), 55.55% of metastatic lesions and 0% lymphoma cases. Kim et al[91] found ITSS in 100% of glioblastomas, 40% of anaplastic astrocytomas, 73% of metastases and 0% of lymphoma patients, which is comparable to our study. We found that grade III ITSS had the highest predictive

value for differentiating the tumor types, similar to Kim et al[91]. Grade 0 ITSS was more suggestive of lymphomas.

In our study, it was observed that high-grade gliomas can be differentiated from lymphomas by a combination of DTI parameters (intratumoral *p*, *q* and *L*), intratumoral rPSR, peritumoral rCBV and ITSS. For differentiating high-grade gliomas from metastases, the measurements of lesion-to-brain ratio of *p* in peritumoral region, peritumoral rCBV, intratumoral rPSR and ITSS were useful. The combination of intratumoral *p* and *L*, lesion-to-brain ratio of *q* in tumor and peritumoral regions, peritumoral rCBV, intratumoral rPSR and ITSS were helpful in differentiating metastases from lymphomas.

Strengths of our study: We have excluded the patients who had previously undergone biopsy/surgery or chemotherapy/radiotherapy in our study. We have excluded the hemorrhagic, necrotic, cystic and calcified areas within the tumors to reduce the errors in measurements. We have used similar study protocols and software for processing the DTI, SWI and DSC-MRI source data in all the study patients to ensure generation of parameters suitable for comparison. Similar dose of contrast agent was used for all the patients. We did not give preload dose of contrast for DSC-MRI to obtain better signal intensity-time curves. We have measured at least 9-10 ROIs for calculation of mean values within each region to reduce the measurement bias. The postprocessing and measurements of the quantitative and semi-quantitative parameters were done by single radiologist

blinded to the clinical and histopathological findings. The immediate adjacent peritumoral region was selected as this is the site which has been shown to have significant changes between the tumors in previous studies. The maximum values of the rCBV, rCBF and rPSR were selected to enhance the predictive power of the study. High-resolution SWI images were used for accurate assessment and grading of ITSS. Definite quantitative measures were found in our study which favored a particular high-grade lesion. These could potentially increase the diagnostic accuracy; ensure better prognostication and optimal treatment.

Limitations of our study: This was a combined retrospective and prospective observation study. Inclusion of retrospective data might have added some selection bias. The relatively low number of patients in each of the study groups reduced the power of the study. There was non-uniformity in the number of patients in each study cohort, although there was no significant difference in age and gender distribution between them. We have done manual placement of the ROIs which is a less accurate method compared to automatic mirrored ROI placement. The subjective selection of the sites of ROI might have caused variation in the parameters measured. We could not correlate the areas of tumors selected for quantitative measurement with the site of histopathological examination which remains the most important drawback of the study. We could not exclude the possibility of previous steroid treatment in patients selected retrospectively which might have been a confounding factor for changes in advanced MRI parameters.

CONCLUSION

This was an analytical observational cohort study having both prospective and retrospective cases. The advanced MRI techniques including DTI, SWI and DSC-MRI were used for assessing intra-axial high-grade lesions with histopathological evaluation as gold standard. The study cohorts included high-grade gliomas, metastases and primary central nervous system lymphomas. A total of sixty-six patients were included in the study. It was found that a combination of DTI metrics, DSC-MRI parameters and ITSS grades on SWI had high accuracy, sensitivity and specificity in differentiating between these high-grade lesions. This was corroborating with the previously published literature.

The highlight of this study was the recognition of certain specific quantifiable parameters which could collectively distinguish these lesions. The intratumoral *p*, *q* and *L*, intratumoral rPSR, peritumoral rCBV and ITSS had the highest predictive value in this regard. We determined definite cutoff values which can augment the diagnostic precision and confidence. The intratumoral *p*, *q* and *L* values showed highest accuracy in discriminating high-grade gliomas from lymphomas. The considerable increase in peritumoral rCBV in high-grade gliomas implied adjacent tumor infiltration discerning it from vasogenic edema seen in metastases and lymphomas. We estimated particular limits for rPSR values which could enhance

the differentiating ability. Absence of ITSS was distinctive of lymphomas whereas existence of grade III ITSS suggested greater likelihood of high-grade gliomas.

This study emphasizes that the combined measurement and analysis of DTI, SWI and DSC-MRI parameters from the tumor, adjacent peritumoral white matter and normal appearing opposite cerebral hemispheric white matter regions can improve the diagnostic performance of MRI in brain tumor imaging. Thus it can play a major role in treatment planning, deciding specific sites for biopsy and estimating prognosis and clinical outcome of these patients. We are of the opinion that further studies are warranted which could find out the exact correlation between the sites of biopsy and areas quantitatively measured on MRI to aid in further comprehension of the biological behavior and prognosis of these high-grade lesions.

REFERENCES

1. Stiles, C. D. Cancer of the central nervous system. Review of an AACR special conference in cancer research with the joint section on tumors of the AANS/CNS (San Diego, CA, June 7-11, 1997). Biochim. Biophys. Acta 1377, R1–10 (1998).

2. Ohgaki, H. Epidemiology of brain tumors. Methods Mol. Biol. Clifton NJ 472, 323–342 (2009).

3. Cha, S. Update on Brain Tumor Imaging: From Anatomy to Physiology. Am. J. Neuroradiol. 27, 475–487 (2006).

4. Preston-Martin, S. Epidemiology of primary CNS neoplasms. Neurol. Clin. 14, 273–290 (1996).

5. Werner, M. H., Phuphanich, S. & Lyman, G. H. The increasing incidence of malignant gliomas and primary central nervous system lymphoma in the elderly. Cancer 76, 1634–1642 (1995).

6. Nayak, L., Lee, E. Q. & Wen, P. Y. Epidemiology of brain metastases. Curr. Oncol. Rep. 14, 48–54 (2012).

7. Nguyen, T. D. & DeAngelis, L. M. Brain metastases. Neurol. Clin. 25, 1173–1192, x–xi (2007).

8. Jiang, R. et al. The value of diffusion tensor imaging in differentiating high-grade gliomas from brain metastases: a systematic review and meta-analysis. PloS One 9, e112550 (2014).

9. Haldorsen, I. S., Espeland, A. & Larsson, E.-M. Central nervous system lymphoma: characteristic findings on traditional and advanced imaging. AJNR Am. J. Neuroradiol. 32, 984–992 (2011).

10. Schlegel, U., Schmidt-Wolf, I. G. & Deckert, M. Primary CNS lymphoma: clinical presentation, pathological classification, molecular pathogenesis and treatment. J. Neurol. Sci. 181, 1–12 (2000).

11. Osborn, A. in Osborn's Brain: Imaging, Pathology and Anatomy 472–500 (Wolters Kluwer, Lippincott Williams and Wilkins, 2012).

12. Sepulveda Sanchez, J. M. et al. Classification of oligodendroglial tumors based on histopathology criteria is a significant predictor of survival--clinical, radiological and pathologic long-term follow-up analysis. Clin. Neuropathol. 28, 11–20 (2009).

13. Aldape, K., Zadeh, G., Mansouri, S., Reifenberger, G. & von Deimling, A. Glioblastoma: pathology, molecular mechanisms and markers. Acta Neuropathol. (Berl.) 129, 829–848 (2015).

14. Wen, P. Y. & Kesari, S. Malignant gliomas in adults. N. Engl. J. Med. 359, 492–507 (2008).

15. Bruner, J. M. Neuropathology of malignant gliomas. Semin. Oncol. 21, 126–138 (1994).

16. Osborn, A. in Osborn's Brain: Imaging, Pathology and Anatomy 645–652 (Wolters Kluwer, Lippincott Williams and Wilkins, 2012).

17. Lee, E. K. et al. Intracranial metastases: spectrum of MR imaging findings. Acta Radiol. Stockh. Swed. 1987 53, 1173–1185 (2012).

18. Osborn, A. in Osborn's Brain: Imaging, Pathology and Anatomy 745–755 (Wolters Kluwer, Lippincott Williams and Wilkins, 2012).

19. Stupp, R., Tonn, J.-C., Brada, M., Pentheroudakis, G. & ESMO Guidelines Working Group. High-grade malignant glioma: ESMO Clinical Practice Guidelines for diagnosis, treatment and follow-up. Ann. Oncol. Off. J. Eur. Soc. Med. Oncol. ESMO 21 Suppl 5, v190–193 (2010).

20. Law, M. et al. Comparison of cerebral blood volume and vascular permeability from dynamic susceptibility contrast-enhanced perfusion MR imaging with glioma grade. AJNR Am. J. Neuroradiol. 25, 746–755 (2004).

21. Lu, S., Ahn, D., Johnson, G. & Cha, S. Peritumoral diffusion tensor imaging of high-grade gliomas and metastatic brain tumors. AJNR Am. J. Neuroradiol. 24, 937–941 (2003).

22. Essig, M. et al. MR imaging of neoplastic central nervous system lesions: review and recommendations for current practice. AJNR Am. J. Neuroradiol. 33, 803–817 (2012).

23. Chen, X. Z. et al. Differentiation between brain glioblastoma multiforme and solitary metastasis: qualitative and quantitative analysis based on routine MR imaging. AJNR Am. J. Neuroradiol. 33, 1907–1912 (2012).

24. Tang, Y. M., Ngai, S. & Stuckey, S. The solitary enhancing cerebral lesion: can FLAIR aid the differentiation between glioma and metastasis? AJNR Am. J. Neuroradiol. 27, 609–611 (2006).

25. Christoforidis, G. A. et al. Visualization of Microvascularity in Glioblastoma Multiforme With 8-T High-Spatial-Resolution MR Imaging. Am. J. Neuroradiol. 23, 1553–1556 (2002).

26. Calli, C. et al. Perfusion and diffusion MR imaging in enhancing malignant cerebral tumors. Eur. J. Radiol. 58, 394–403 (2006).

27. Mori, S. & Barker, P. B. Diffusion magnetic resonance imaging: its principle and applications. Anat. Rec. 257, 102–109 (1999).

28. Provenzale, J. M., Mukundan, S. & Barboriak, D. P. Diffusion-weighted and perfusion MR imaging for brain tumor characterization and assessment of treatment response. Radiology 239, 632–649 (2006).

29. Stadnik, T. W. et al. Diffusion-weighted MR imaging of intracerebral masses: comparison with conventional MR imaging and histologic findings. AJNR Am. J. Neuroradiol. 22, 969–976 (2001).

30. Sugahara, T. et al. Usefulness of diffusion-weighted MRI with echo-planar technique in the evaluation of cellularity in gliomas. J. Magn. Reson. Imaging JMRI 9, 53–60 (1999).

31. Yang, D. et al. Cerebral gliomas: prospective comparison of multivoxel 2D chemical-shift imaging proton MR spectroscopy, echoplanar perfusion and diffusion-weighted MRI. Neuroradiology 44, 656–666 (2014).

32. Kono, K. et al. The role of diffusion-weighted imaging in patients with brain tumors. AJNR Am. J. Neuroradiol. 22, 1081–1088 (2001).

33. Pauleit, D. et al. Can the apparent diffusion coefficient be used as a noninvasive parameter to distinguish tumor tissue from peritumoral tissue in cerebral gliomas? J. Magn. Reson. Imaging JMRI 20, 758–764 (2004).

34. Krabbe, K. et al. MR diffusion imaging of human intracranial tumours. Neuroradiology 39, 483–489 (1997).

35. Lee, E. J. et al. Diagnostic value of peritumoral minimum apparent diffusion coefficient for differentiation of glioblastoma multiforme from solitary metastatic lesions. AJR Am. J. Roentgenol. 196, 71–76 (2011).

36. Chiang, I. C. et al. Distinction between high-grade gliomas and solitary metastases using peritumoral 3-T magnetic resonance spectroscopy, diffusion, and perfusion imagings. Neuroradiology 46, 619–627 (2004).

37. Guo, A. C., Cummings, T. J., Dash, R. C. & Provenzale, J. M. Lymphomas and high-grade astrocytomas: comparison of water diffusibility and histologic characteristics. Radiology 224, 177–183 (2002).

38. Barajas, R. F., Rubenstein, J. L., Chang, J. S., Hwang, J. & Cha, S. Diffusion-weighted MR imaging derived apparent diffusion coefficient is predictive of clinical outcome in primary central nervous system lymphoma. AJNR Am. J. Neuroradiol. 31, 60–66 (2010).

39. Mascalchi, M. et al. Diffusion-weighted MR of the brain: methodology and clinical application. Radiol. Med. (Torino) 109, 155–197 (2005).

40. Wang, S., Kim, S. & Melhem, E. R. in Functional Brain Tumor Imaging (ed. Pillai, J. J.) 27–38 (Springer New York, 2014). at <http://link.springer.com/10.1007/978-1-4419-5858-7_2>

41. Svolos, P. et al. The role of diffusion and perfusion weighted imaging in the differential diagnosis of cerebral tumors: a review and future perspectives. Cancer Imaging 14, 20 (2014).

42. Sternberg, E. J., Lipton, M. L. & Burns, J. Utility of diffusion tensor imaging in evaluation of the peritumoral region in patients with primary and metastatic brain tumors. AJNR Am. J. Neuroradiol. 35, 439–444 (2014).

43. Price, S. J. et al. Tissue signature characterisation of diffusion tensor abnormalities in cerebral gliomas. Eur. Radiol. 14, 1909–1917 (2004).

44. Deng, Z. et al. Quantitative analysis of glioma cell invasion by diffusion tensor imaging. J. Clin. Neurosci. Off. J. Neurosurg. Soc. Australas. 17, 1530–1536 (2010).

45. Green, H. A. L. et al. Increased anisotropy in acute stroke: a possible explanation. Stroke J. Cereb. Circ. 33, 1517–1521 (2002).

46. Toh, C.-H. et al. Primary cerebral lymphoma and glioblastoma multiforme: differences in diffusion characteristics evaluated with diffusion tensor imaging. AJNR Am. J. Neuroradiol. 29, 471–475 (2008).

47. Wieshmann, U. C. et al. Reduced anisotropy of water diffusion in structural cerebral abnormalities demonstrated with diffusion tensor imaging. Magn. Reson. Imaging 17, 1269–1274 (1999).

48. Le Bihan, D. et al. Diffusion tensor imaging: concepts and applications. J. Magn. Reson. Imaging JMRI 13, 534–546 (2001).

49. Morita, K. et al. Diffusion tensor analysis of peritumoral edema using lambda chart analysis indicative of the heterogeneity of the microstructure within edema. J. Neurosurg. 102, 336–341 (2005).

50. Kimura, T., Ohkubo, M., Igarashi, H., Kwee, I. L. & Nakada, T. Increase in glutamate as a sensitive indicator of extracellular matrix integrity in peritumoral edema: a 3.0-tesla proton magnetic resonance spectroscopy study. J. Neurosurg. 106, 609–613 (2007).

51. Lu, S. et al. Diffusion-tensor MR imaging of intracranial neoplasia and associated peritumoral edema: introduction of the tumor infiltration index. Radiology 232, 221–228 (2004).

52. Kinoshita, M. et al. Diffusion tensor-based tumor infiltration index cannot discriminate vasogenic edema from tumor-infiltrated edema. J. Neurooncol. 96, 409–415 (2010).

53. Liang, R. et al. Potential role of fractional anisotropy derived from diffusion tensor imaging in differentiating high-grade gliomas from low-grade gliomas: a meta-analysis. Int. J. Clin. Exp. Med. 7, 3647–3653 (2014).

54. Byrnes, T. J. D., Barrick, T. R., Bell, B. A. & Clark, C. A. Diffusion tensor imaging discriminates between glioblastoma and cerebral metastases in vivo. NMR Biomed. 24, 54–60 (2011).

55. Wang, S. et al. Diagnostic utility of diffusion tensor imaging in differentiating glioblastomas from brain metastases. AJNR Am. J. Neuroradiol. 35, 928–934 (2014).

56. Scherer, H. Structural development in gliomas. Am J Cancer 34, 333–351 (1938).

57. Chepuri, N. B. et al. Diffusion anisotropy in the corpus callosum. AJNR Am. J. Neuroradiol. 23, 803–808 (2002).

58. Wang, W., Steward, C. E. & Desmond, P. M. Diffusion tensor imaging in glioblastoma multiforme and brain metastases: the role of p, q, L, and fractional anisotropy. AJNR Am. J. Neuroradiol. 30, 203–208 (2009).

59. Smitha, K. A., Gupta, A. K. & Jayasree, R. S. Total magnitude of diffusion tensor imaging as an effective tool for the differentiation of glioma. Eur. J. Radiol. 82, 857–861 (2013).

60. Muthusami, P., Basti, R. S., Thomas, B., Kapilamoorthy, T. R. & Kesavadas, C. Glioma progression as revealed by diffusion tensor metrics. Neurol. India 60, 355–357 (2012).

61. Price, S. J. et al. Improved Delineation of Glioma Margins and Regions of Infiltration with the Use of Diffusion Tensor Imaging: An Image-Guided Biopsy Study. Am. J. Neuroradiol. 27, 1969–1974 (2006).

62. Sinha, S., Bastin, M. E., Wardlaw, J. M., Armitage, P. A. & Whittle, I. R. Effects of dexamethasone on peritumoural oedematous brain: a DT-MRI study. J. Neurol. Neurosurg. Psychiatry 75, 1632–1635 (2004).

63. Heiss, W.-D., Raab, P. & Lanfermann, H. Multimodality assessment of brain tumors and tumor recurrence. J. Nucl. Med. Off. Publ. Soc. Nucl. Med. 52, 1585–1600 (2011).

64. Cha, S. et al. Intracranial mass lesions: dynamic contrast-enhanced susceptibility-weighted echo-planar perfusion MR imaging. Radiology 223, 11–29 (2002).

65. Chavhan, G. B., Babyn, P. S., Thomas, B., Shroff, M. M. & Haacke, E. M. Principles, Techniques, and Applications of T2*-based MR Imaging and Its Special Applications. Radiographics 29, 1433–1449 (2009).

66. Welker, K. et al. ASFNR recommendations for clinical performance of MR dynamic susceptibility contrast perfusion imaging of the brain. AJNR Am. J. Neuroradiol. 36, E41–51 (2015).

67. Cha, S. et al. Differentiation of glioblastoma multiforme and single brain metastasis by peak height and percentage of signal intensity recovery derived from dynamic susceptibility-weighted contrast-enhanced perfusion MR imaging. AJNR Am. J. Neuroradiol. 28, 1078–1084 (2007).

68. Hartmann, M. et al. Distinguishing of primary cerebral lymphoma from high-grade glioma with perfusion-weighted magnetic resonance imaging. Neurosci. Lett. 338, 119–122 (2003).

69. Mangla, R. et al. Percentage signal recovery derived from MR dynamic susceptibility contrast imaging is useful to differentiate common enhancing malignant lesions of the brain. AJNR Am. J. Neuroradiol. 32, 1004–1010 (2011).

70. Liao, W. et al. Differentiation of primary central nervous system lymphoma and high-grade glioma with dynamic susceptibility contrast-enhanced perfusion magnetic resonance imaging. Acta Radiol. Stockh. Swed. 1987 50, 217–225 (2009).

71. Fan, G. G., Deng, Q. L., Wu, Z. H. & Guo, Q. Y. Usefulness of diffusion/perfusion-weighted MRI in patients with non-enhancing supratentorial brain gliomas: a valuable tool to predict tumour grading? Br. J. Radiol. 79, 652–658 (2006).

72. Sugahara, T. et al. Correlation of MR imaging-determined cerebral blood volume maps with histologic and angiographic determination of vascularity of gliomas. AJR Am. J. Roentgenol. 171, 1479–1486 (1998).

73. Knopp, E. A. et al. Glial neoplasms: dynamic contrast-enhanced T2*-weighted MR imaging. Radiology 211, 791–798 (1999).

74. Shin, J. H. et al. Using relative cerebral blood flow and volume to evaluate the histopathologic grade of cerebral gliomas: preliminary results. AJR Am. J. Roentgenol. 179, 783–789 (2002).

75. Law, M. et al. Glioma grading: sensitivity, specificity, and predictive values of perfusion MR imaging and proton MR spectroscopic imaging compared with conventional MR imaging. AJNR Am. J. Neuroradiol. 24, 1989–1998 (2003).

76. Aronen, H. J. et al. Cerebral blood volume maps of gliomas: comparison with tumor grade and histologic findings. Radiology 191, 41–51 (1994).

77. Preul, C. et al. Differentiation of cerebral tumors using multi-section echo planar MR perfusion imaging. Eur. J. Radiol. 48, 244–251 (2003).

78. Law, M. et al. Gliomas: predicting time to progression or survival with cerebral blood volume measurements at dynamic susceptibility-weighted contrast-enhanced perfusion MR imaging. Radiology 247, 490–498 (2008).

79. Cho, S. K. et al. Perfusion MR imaging: clinical utility for the differential diagnosis of various brain tumors. Korean J. Radiol. 3, 171–179 (2002).

80. Hakyemez, B. et al. Evaluation of different cerebral mass lesions by perfusion-weighted MR imaging. J. Magn. Reson. Imaging JMRI 24, 817–824 (2006).

81. Toh, C. H., Wei, K.-C., Chang, C.-N., Ng, S.-H. & Wong, H.-F. Differentiation of primary central nervous system lymphomas and glioblastomas: comparisons of diagnostic performance of dynamic susceptibility contrast-enhanced perfusion MR

imaging without and with contrast-leakage correction. AJNR Am. J. Neuroradiol. 34, 1145–1149 (2013).

82. Boxerman, J. L., Schmainda, K. M. & Weisskoff, R. M. Relative cerebral blood volume maps corrected for contrast agent extravasation significantly correlate with glioma tumor grade, whereas uncorrected maps do not. AJNR Am. J. Neuroradiol. 27, 859–867 (2006).

83. Kickingereder, P. et al. Evaluation of microvascular permeability with dynamic contrast-enhanced MRI for the differentiation of primary CNS lymphoma and glioblastoma: radiologic-pathologic correlation. AJNR Am. J. Neuroradiol. 35, 1503–1508 (2014).

84. Chinchure, S. et al. Mean intensity curve on dynamic contrast-enhanced susceptibility-weighted perfusion MR imaging--review of a new parameter to differentiate intracranial tumors. J. Neuroradiol. J. Neuroradiol. 38, 199–206 (2011).

85. Geer, C. P. et al. Does MR perfusion imaging impact management decisions for patients with brain tumors? A prospective study. AJNR Am. J. Neuroradiol. 33, 556–562 (2012).

86. Çoban, G. et al. Prognostic Value of Dynamic Susceptibility Contrast-Enhanced and Diffusion-Weighted MR Imaging in Patients with Glioblastomas. AJNR Am. J. Neuroradiol. 36, 1247–1252 (2015).

87. Young, G. S. & Setayesh, K. Spin-echo echo-planar perfusion MR imaging in the differential diagnosis of solitary enhancing brain lesions: distinguishing solitary metastases from primary glioma. AJNR Am. J. Neuroradiol. 30, 575–577 (2009).

88. Jackson, A. et al. Abnormalities in the recirculation phase of contrast agent bolus passage in cerebral gliomas: comparison with relative blood volume and tumor grade. AJNR Am. J. Neuroradiol. 23, 7–14 (2002).

89. Sehgal, V. et al. Clinical applications of neuroimaging with susceptibility-weighted imaging. J. Magn. Reson. Imaging JMRI 22, 439–450 (2005).

90. Park, S. M., Kim, H. S., Jahng, G.-H., Ryu, C.-W. & Kim, S. Y. Combination of high-resolution susceptibility-weighted imaging and the apparent diffusion coefficient: added value to brain tumour imaging and clinical feasibility of non-contrast MRI at 3 T. Br. J. Radiol. 83, 466–475 (2010).

91. Kim, H. S., Jahng, G.-H., Ryu, C. W. & Kim, S. Y. Added value and diagnostic performance of intratumoral susceptibility signals in the differential diagnosis of

solitary enhancing brain lesions: preliminary study. AJNR Am. J. Neuroradiol. 30, 1574–1579 (2009).

92. Mittal, S., Wu, Z., Neelavalli, J. & Haacke, E. M. Susceptibility-weighted imaging: technical aspects and clinical applications, part 2. AJNR Am. J. Neuroradiol. 30, 232–252 (2009).

93. Tsougos, I. et al. Differentiation of glioblastoma multiforme from metastatic brain tumor using proton magnetic resonance spectroscopy, diffusion and perfusion metrics at 3 T. Cancer Imaging Off. Publ. Int. Cancer Imaging Soc. 12, 423–436 (2012).

94. Opstad, K. S. et al. Differentiation of metastases from high-grade gliomas using short echo time 1H spectroscopy. J. Magn. Reson. Imaging JMRI 20, 187–192 (2004).

95. Lee, E. J., Ahn, K. J., Lee, E. K., Lee, Y. S. & Kim, D. B. Potential role of advanced MRI techniques for the peritumoural region in differentiating glioblastoma multiforme and solitary metastatic lesions. Clin. Radiol. 68, e689–697 (2013).

96. Hilario, A. et al. The added value of apparent diffusion coefficient to cerebral blood volume in the preoperative grading of diffuse gliomas. AJNR Am. J. Neuroradiol. 33, 701–707 (2012).

97. Wang, S. et al. Differentiation between glioblastomas, solitary brain metastases, and primary cerebral lymphomas using diffusion tensor and dynamic susceptibility contrast-enhanced MR imaging. AJNR Am. J. Neuroradiol. 32, 507–514 (2011).

98. Svolos, P. et al. Investigating brain tumor differentiation with diffusion and perfusion metrics at 3T MRI using pattern recognition techniques. Magn. Reson. Imaging 31, 1567–1577 (2013).

99. Park, M. J. et al. Semiquantitative assessment of intratumoral susceptibility signals using non-contrast-enhanced high-field high-resolution susceptibility-weighted imaging in patients with gliomas: comparison with MR perfusion imaging. AJNR Am. J. Neuroradiol. 30, 1402–1408 (2009).

100. Tsien, C. et al. Parametric response map as an imaging biomarker to distinguish progression from pseudoprogression in high-grade glioma. J. Clin. Oncol. Off. J. Am. Soc. Clin. Oncol. 28, 2293–2299 (2010).

101. Hein, P. A., Eskey, C. J., Dunn, J. F. & Hug, E. B. Diffusion-weighted imaging in the follow-up of treated high-grade gliomas: tumor recurrence versus radiation injury. AJNR Am. J. Neuroradiol. 25, 201–209 (2004).

102. Mardor, Y. et al. Early detection of response to radiation therapy in patients with brain malignancies using conventional and high b-value diffusion-weighted magnetic resonance imaging. J. Clin. Oncol. Off. J. Am. Soc. Clin. Oncol. 21, 1094–1100 (2003).

103. Tsolaki, E. et al. Clinical decision support systems for brain tumor characterization using advanced magnetic resonance imaging techniques. World J. Radiol. 6, 72–81 (2014).

ANNEXURES

ANNEXURE 1: PROFORMA

CLINICAL DATA:

SERIAL NO.	AGE	GENDER	CLINICAL SYMPTOMS	LOCATION OF LESION

DTI METRICS IN TUMOR REGION:

FA	*p*	*q*	*L*	*CP*	*CS*	*CL*

SWI IN TUMOR REGION:

ITSS GRADE	PRECONTRAST	POSTCONTRAST

DSC-MRI IN TUMOR REGION:

rCBV	rCBF	rPSR

DTI METRICS IN PERITUMORAL REGION:

FA	*p*	*q*	*L*	*CP*	*CS*	*CL*

SWI IN PERITUMORAL REGION:

ITSS GRADE	PRECONTRAST	POSTCONTRAST

DSC-MRI IN PERITUMORAL REGION:

rCBV	rCBF	rPSR

DTI METRICS IN CONTRALATERAL WHITE MATTER:

FA	*p*	*q*	*L*	*CP*	*CS*	*CL*

SWI IN CONTRALATERAL WHITE MATTER:

ITSS GRADE	PRECONTRAST	POSTCONTRAST

DSC-MRI IN CONTRALATERAL WHITE MATTER:

rCBV	rCBF	rPSR

ANNEXURE 2: MASTER CHART

SL.No	Age	Sex	Clinical symptom	Location	SWI	DTI (MEAN VALUES)								DSC-MRI			Surgery	HP
						AREA	FA	*p*	*q*	*L*	*CP*	*CS*	*CL*	rCBV	rCBF	rPSR		
1	49	M	1,4, 6,11	RT F	0	T	133.87	2.09	0.22	2.11	88.18	867.76	43.93	3.53	3.39	99.23	1	1A
						A	222.15	1.63	0.32	1.68	148.11	776.26	75.58	0.74	0.5	96.61		
						C	269.93	1.91	0.42	1.97	123.37	758.33	118.28					
2	57	M	4,7	RT TO	3	T	161.41	2.51	0.32	2.53	92.49	847.22	60.21	4	2.57	127	1	1B
						A	286.32	2.02	0.47	2.07	198.68	706.63	94.71	0.82	0.92	100		
						C	387.95	1.4	0.48	1.48	151.68	656.95	191.4					
3	58	F	2,3	RT F	2	T	178.78	1.85	0.27	1.87	128.37	817.20	54.41	4.82	4.10	98.90	2	1B
						A	267.08	1.94	0.43	1.99	171.68	736.99	91.44	1.88	1.43	98.73		
						C	384.94	1.29	0.43	1.37	243.76	609.04	147.12					
4	59	M	2	RT F	3	T	164.59	2.04	0.27	2.06	98.14	841.64	60.14	5.24	5.78	109.23	1	1B
						A	256.97	2.23	0.44	2.28	123.41	764.64	111.90	0.41	0.34	83.40		
						C	345.43	1.41	0.41	1.48	201.22	671.64	139.40					
5	36	F	1,3	RT F	3	T	108.84	2.20	0.19	2.21	77.99	889.40	32.67	5.37	4.28	118.56	1	1A
						A	536.66	1.30	0.63	1.47	324.08	433.33	242.68	0.74	0.86	96.44		
						C	278.18	1.36	0.31	1.40	187.94	719.03	92.94					
6	50	M	3	RT FP	3	T	228.70	1.69	0.30	1.72	151.89	771.92	76.19	4.45	4.11	83.56	1	1A
						A	385.32	1.43	0.45	1.51	238.27	604.37	157.40	0.82	0.86	80.18		
						C	394.40	1.32	0.47	1.41	209.88	618.29	172.07					
7	46	F	3	LT FT	3	T	154.89	2.07	0.44	2.14	86.10	855.06	58.84	-	-	-	1	1A
						A	188.87	1.86	0.29	1.89	114.44	817.22	69.48	-	-	-		
						C	381.30	1.53	0.52	1.62	199.29	629.22	171.22					
8	60	M	5,8	LT F	0	T	141.23	2.45	0.28	2.46	70.26	873.07	56.56	2.95	2.82	104.67	1	1A
						A	359.72	1.81	0.51	1.90	199.92	645.84	154.16	1.15	0.57	102.30		
						C	336.09	1.55	0.44	1.61	152.19	699.63	148.28					
9	53	F	1	RT F	2	T	270.57	2.12	0.46	5.13	167.74	731.03	101.27	8.97	11.47	103.40	1	2
						A	296.00	2.34	0.58	2.42	191.81	701.76	106.46	0.82	0.84	104.56		
						C	499.67	1.27	0.55	1.38	289.33	493.00	216.89					
10	63	M	1,2	LT FP	3	T	199.00	2.37	0.40	2.41	119.52	807.79	72.77	8.23	6.48	88.53	1	1B
						A	314.14	1.82	0.45	1.88	185.39	691.41	123.27	0.62	0.39	87.11		
						C	454.40	1.41	0.57	1.54	205.70	570.03	224.39					

SL.No	Age	Sex	Clinical symptom	Location	SWI	DTI (MEAN VALUES)								DSC-MRI			Surgery	HP
						AREA	FA	*p*	*q*	*L*	*CP*	*CS*	*CL*	rCBV	rCBF	rPSR		
11	41	M	1,2, 12	RT F	0	T	165.99	2.88	0.39	2.91	73.79	855.01	71.18	3.15	1.72	95.52	1	1A
						A	351.49	1.61	0.48	1.68	220.67	649.21	130.36	0.73	0.54	105.00		
						C	361.13	1.49	0.46	1.56	256.93	623.48	119.60					
12	61	M	2,3	RT T, P,O	0	T	132.22	2.02	0.22	2.04	88.10	868.22	43.62	3.08	3.15	134.49	1	1B
						A	250.74	1.44	0.30	1.48	143.74	760.00	96.14	0.62	0.54	99.73		
						C	413.68	1.41	0.51	1.51	177.40	622.84	139.40					
13	36	F	3	LT F	2	T	207.39	2.20	0.37	2.24	110.62	808.46	80.98	-	-	-	1	1A
						A	402.26	1.44	0.50	1.54	186.39	627.82	185.96	-	-	-		
						C	455.88	1.25	0.49	1.35	240.59	556.13	203.16					
14	39	M	1,8, 13	LT P	0	T	208.67	1.02	0.17	1.04	124.33	798.56	76.00	5.53	4.21	88.89	2	3
						A	253.78	2.37	0.49	2.42	103.44	778.78	116.67	0.48	0.45	86.08		
						C	572.00	1.24	0.65	1.42	240.67	442.67	315.22					
15	57	F	1,2, 14	LT F	3	T	274.11	2.24	0.47	2.30	232.05	762.85	116.02	8.99	7.14	81.47	1	2
						A	316.03	1.71	0.43	1.77	222.14	674.21	103.62	0.38	0.49	139.00		
						C	361.13	1.49	0.46	1.56	256.93	623.48	119.60					
16	46	F	2,3, 4	LT FP	-	T	199.00	1.45	0.23	1.47	95.56	821.33	82.33	3.18	3.63	106.00	1	1A
						A	315.56	1.51	0.41	1.57	109.00	735.22	154.78	0.83	1.13	97.60		
						C	421.44	1.30	0.48	1.39	201.56	598.89	198.56					
17	52	M	1,5, 15	LT P	0	T	160.41	2.48	0.32	2.51	87.91	849.93	62.03	4.40	3.91	91.83	2	2
						A	297.76	1.55	0.38	1.60	241.45	723.55	120.73	0.27	0.27	106.69		
						C	269.93	1.92	0.43	1.97	123.38	758.33	118.29					
18	37	M	2	LT T	3	T	224.51	1.74	0.32	1.77	160.80	769.42	69.93	7.57	9.56	97.18	2	1B
						A	231.44	1.98	0.36	2.02	169.70	760.02	70.03	1.46	2.16	85.22		
						C	278.18	1.36	0.31	1.40	187.94	719.03	92.94					
19	48	M	7	LT T	0	T	217.89	0.98	0.17	0.99	142.56	784.00	72.67	1.63	1.36	88.69	2	3
						A	454.44	1.41	0.56	1.52	220.00	566.44	212.33	1.37	1.01	77.71		
						C	510.78	1.35	0.61	1.50	300.44	471.67	226.67					
20	19	F	10	LT F	2	T	432.74	1.22	0.45	1.31	219.40	160.00	620.20	7.99	5.15	89.08	1	1A
						A	551.72	1.24	0.57	1.38	269.78	454.89	274.49	0.99	0.94	99.27		
						C	538.67	1.24	0.58	1.38	258.44	266.89	473.44					

SL.No	Age	Sex	Clinical symptom	Location	SWI	DTI (MEAN VALUES)								DSC-MRI			Surgery	HP
						AREA	FA	*p*	*q*	*L*	*CP*	*CS*	*CL*	rCBV	rCBF	rPSR		
21	28	M	1,2, 4	RT FT	2	T	351.33	1.11	0.33	1.16	138.22	138.22	168.16	2.64	2.17	93.62	2	1B
						A	251.11	1.49	0.30	1.52	156.56	156.56	84.89	0.89	0.55	96.46		
						C	426.56	1.29	0.49	1.38	224.89	224.89	191.22					
22	20	M	2,3	LT FP	0	T	261.44	2.38	0.52	2.44	123.33	764.00	111.78	4.27	6.98	88.57	2	1A
						A	321.44	1.74	0.48	1.81	101.67	732.67	164.78	0.50	0.92	107.00		
						C	502.56	1.51	0.68	1.66	196.56	988.11	258.44					
23	52	M	4,6, 11	RT O	0	T	164.00	1.42	0.19	1.44	115.56	835.11	48.33	1.27	2.14	200.80	1	3
						A	219.22	1.97	0.33	2.01	120.00	788.11	90.89	0.26	0.33	115.70		
						C	446.33	1.18	0.46	1.28	202.22	574.67	222.00					
24	46	F	1,4	RT T	3	T	138.22	2.23	0.25	2.25	95.22	861.57	43.14	6.29	5.06	71.30	1	1B
						A	206.84	2.09	0.34	2.12	123.68	800.48	75.89	0.60	0.45	91.75		
						C	432.33	1.29	0.48	1.40	219.11	580.11	199.89					
25	58	M	1,4	RT TO	3	T	101.27	2.08	0.17	2.09	60.12	903.86	36.01	6.13	3.70	96.11	1	1A
						A	402.26	1.73	0.44	1.79	195.32	687.93	116.68	1.10	1.70	84.70		
						C	329.00	1.39	0.37	1.44	202.56	672.89	123.33					
26	71	M	3	LT O	0	T	-	-	-	-	-	-	-	7.46	3.65	38.06	1	2
						A	-	-	-	-	-	-	-	0.24	0.34	126.55		
						C	-	-	-	-	-	-	-					
27	62	F	1,2, 4, 5	LT F	0	T	196.67	1.59	0.25	1.61	104.11	816.44	78.33	8.92	5.00	145.89	2	3
						A	344.44	1.34	0.38	1.40	186.67	668.67	144.00	0.92	0.66	110.61		
						C	331.33	1.38	0.38	1.44	189.44	676.56	132.89					
28	52	M	3	RT F	0	T	148.33	1.87	0.21	1.88	72.89	866.22	60.00	-	-	-	1	2
						A	377.89	1.46	0.47	1.54	181.89	649.56	167.44	-	-	-		
						C	386.78	1.52	0.51	1.61	189.44	635.56	174.44	-	-	-		
29	34	M	1,3	LT P	2	T	160.01	2.09	0.26	2.11	81.32	854.94	63.67	1.93	2.20	108.10	1	1A
						A	241.97	1.69	0.33	1.72	134.27	770.11	95.52	1.23	1.41	108.80		
						C	528.78	1.34	0.64	1.50	217.78	498.11	283.22					
30	43	M	1, 16	RT F	0	T	191.11	1.71	0.26	1.74	107.11	820.00	71.78				2	3
						A	118.56	3.37	0.45	3.43	70.44	887.22	41.33	3.77	3.28	198.57		
						C	459.44	1.41	0.56	1.53	249.33	544.67	205.22	0.79	0.65	121.42		

SL.No	Age	Sex	Clinical symptom	Location	SWI	DTI (MEAN VALUES)								DSC-MRI			Surgery	HP
						AREA	FA	*p*	*q*	*L*	*CP*	*CS*	*CL*	rCBV	rCBF	rPSR		
31	36	M	3	LT F	1	T	130.44	2.34	0.25	2.36	82.33	873.60	44.00	7.23	9.13	88.93	1	1A
						A	206.74	2.15	0.34	2.18	109.19	807.84	82.96	1.10	1.77	84.73		
						C	495.33	1.33	0.59	1.45	205.56	548.33	245.22					
32	57	F	2,8	RT F, BG	0	T	212.11	1.21	0.21	1.22	131.89	792.33	74.89	3.2	0.7	313.25	2	3
						A	236.56	2.48	0.48	2.54	130.22	775.67	93.22	3.7	0.48	103.24		
						C	345.89	1.62	0.47	1.70	193.89	660.89	144.33					
33	50	M	3,6, 9	LT F	2	T	145.37	3.07	0.36	3.10	89.02	861.11	52.14	-	-	-	1	1A
						A	395.27	1.46	0.48	1.54	234.84	602.14	163.00	-	-	-		
						C	484.00	1.31	0.53	1.42	284.33	504.33	210.11	-	-	-		
34	35	M	1	LT F	1	T	213.44	1.42	0.24	1.43	119.11	798.78	81.00	1.48	2.20	61.2	2	2
						A	314.56	2.12	0.50	2.18	136.11	717.67	145.22	0.28	0.69	115		
						C	468.22	1.23	0.49	1.34	230.89	545.22	222.78					
35	45	M	1	RT T	-	T	190.56	1.36	0.21	1.38	128.44	808.00	62.67	3.43	1.85	100.64	1	3
						A	290.11	2.13	0.49	2.19	187.33	707.89	103.56	0.66	0.31	87.71		
						C	594.00	1.32	0.74	1.51	215.89	446.11	337.11					
36	54	M	1 4, 5	LT F,C	3	T	140.00	2.10	0.23	2.11	68.19	874.89	57.01	3.41	3.27	106.90	2	1B
						A	298.66	1.74	0.42	1.80	194.33	702.00	103.81	1.31	0.62	103.00		
						C	386.22	1.28	0.42	1.36	251.89	598.78	148.44					
37	53	M	3	LT T	2	T	156.67	4.43	0.56	0.46	94.19	849.31	56.47	5.53	3.08	114.39	1	2
						A	162.90	3.08	0.41	3.11	101.34	842.51	56.33	0.68	0.30	100.00		
						C	378.47	1.40	0.43	1.48	233.81	615.01	151.21					
38	23	M	3	LT F	2	T	141.33	2.05	0.23	2.06	80.56	866.33	51.78	-	-	-	1	1A
						A	391.44	1.54	0.52	1.64	187.33	631.89	179.67	-	-	-		
						C	542.11	1.26	0.63	1.42	249.44	473.67	276.00					
39	55	M	1	RT T	3	T	168.22	1.47	0.20	1.48	95.70	839.57	64.70	9.65	7.27	74.2	1	2
						A	144.42	2.20	0.26	2.21	93.79	856.88	49.22	0.54	0.30	98.5		
						C	241.18	1.71	0.30	1.74	146.97	754.89	98.00					
40	41	F	1, 2	LT P, O, C	0	T	255.00	1.62	0.35	1.66	127.2	766.67	105.0	4.43	3.4	152.4	2	3
						A	305.22	1.99	0.48	2.05	132.1	724.44	142.4	0.84	0.54	89.8		
						C	438.22	1.31	0.49	1.40	291.3	546.44	161.1					

SL.No	Age	Sex	Clinical symptom	Location	SWI	DTI (MEAN VALUES)								DSC-MRI			Surgery	HP
						AREA	FA	*p*	*q*	*L*	*CP*	*CS*	*CL*	rCBV	rCBF	rPSR		
41	39	F	1, 11	RT F	3	T	199.33	1.93	0.28	1.95	71.56	835.33	91.78	14.7	15.7	96.37	1	1B
						A	166.00	2.54	0.33	2.56	94.00	756.44	62.56	0.35	0.27	98.57		
						C	423.33	1.28	0.47	1.37	254.2	573.56	171.2					
42	56	M	1, 13	LT T	1	T	248.22	1.31	0.25	1.33	166.4	749.00	83.56	9.35	10.3	55.76	1	2
						A	222.11	2.46	0.45	2.50	126.5	788.67	83.67	1.68	1.21	68.92		
						C	447.22	1.24	0.50	1.35	247.1	552.0	199.3					
43	50	M	3	RT F	3	T	176.86	1.61	0.23	1.64	130.2	818.44	51.30	-	-	-	1	1B
						A	331.60	1.55	0.42	1.61	237.7	654.94	107.2	-	-	-		
						C	413.33	1.38	0.48	1.47	283.7	562.67	152.5	-	-	-		
44	55	M	1, 2	LT T	0	T	-	-	-	-	-	-	-	-	-	-	2	3
						A	-	-	-	-	-	-	-	-	-	-		
						C	-	-	-	-	-	-	-					
45	46	M	1, 11	LT P	3	T	324.92	1.24	0.34	1.29	194.4	673.4	132.2	-	-	-	1	2
						A	407.65	1.63	0.52	1.73	236.4	578.1	185.5	-	-	-		
						C	427.59	1.17	0.44	1.26	237.8	564.8	197.3					
46	38	M	1,3, 4,11	LT P	1	T	117.22	2.09	0.19	2.11	73.89	886.22	39.11	4.7	2.68	55.67	1	2
						A	187.67	2.28	0.35	2.31	155.2	800.00	44.22	0.35	0.49	78.75		
						C	577.78	1.10	0.60	1.26	295.0	415.00	289.1	-	-	-		
47	43	F	1, 3, 11	RT O	1	T	139.53	2.57	0.27	2.58	100.2	855.72	43.90	4.61	5.38	85.94	1	2
						A	151.60	2.04	0.25	2.05	92.98	851.57	55.44	0.89	0.77	90.67		
						C	221.70	1.43	0.27	1.45	137.7	780.06	82.19					
48	61	M	1,2, 5	LT P	3	T	121.54	2.59	0.24	2.61	71.77	882.41	45.87	-	-	-	2	1B
						A	217.69	2.29	0.41	2.33	102.8	804.14	92.92	-	-	-		
						C	469.49	1.35	0.57	1.48	259.9	528.81	211.1					
49	67	M	3,5	LT F	3	T	341.00	1.52	0.35	1.59	269.9	620.5	109.7	7.46	3.65	68.02	1	2
						A	292.90	2.13	0.52	2.20	136.0	735.9	128.0	0.24	0.35	67.4		
						C	445.74	1.14	0.44	1.23	214.7	559.3	226.2					
50	67	M	2,13	LT P	0	T	159.00	1.43	0.19	1.44	93.22	848.89	56.56	4.5	2.61	155.9	2	3
						A	318.67	1.45	0.38	1.49	182.3	688.89	127.6	0.47	0.48	115.2		
						C	493.44	1.20	0.53	1.32	273.1	504.78	221.0					

SL.No	Age	Sex	Clinical symptom	Location	SWI	DTI (MEAN VALUES)								DSC-MRI			Surgery	HP
						AREA	FA	*p*	*q*	*L*	*CP*	*CS*	*CL*	rCBV	rCBF	rPSR		
51	59	M	2,3	LT F	2	T	160.00	2.25	0.29	2.27	108.6	838.33	50.89				2	1B
						A	241.78	1.92	0.38	1.96	115.5	781.11	102.4					
						C	518.89	1.38	0.67	1.56	217.2	498.00	283.4					
52	26	F	1, 2, 3	LT F	0	T	207.11	0.82	0.14	0.83	110.1	807.00	81.67	4.30	4.37	135.7	1	3
						A	197.67	2.98	0.48	3.02	85.00	826.89	87.00	0.40	0.47	130.3		
						C	528.78	1.26	0.60	1.41	264.6	478.22	256.0					
53	48	F	1,11	RT F	0	T	125.90	1.68	0.17	1.69	83.27	873.99	42.70	-	-	-	1	2
						A	219.90	2.21	0.36	2.25	109.9	797.90	92.17	-	-	-		
						C	375.30	1.05	0.34	1.11	209.7	637.00	153.3	-	-	-		
54	70	M	3	LT P	0	T	138.00	1.66	0.19	1.67	92.27	861.56	46.18	-	-	-	1	2
						A	157.17	2.96	0.38	2.98	96.14	846.37	57.52	-	-	-		
						C	457.60	1.47	0.59	16.00	274.5	521.73	203.5					
55	58	F	1, 2	RT FT	0	T	191.78	1.53	0.23	1.54	121.4	812.56	65.11	3.94	3.1	120.3	2	3
						A	351.44	1.45	0.43	1.52	207.7	654.78	136.6	0.76	0.56	87.86		
						C	409.00	1.49	0.53	1.60	203.5	609.33	186.2					
56	33	M	1,5, 11	RT F	3	T	167.84	3.65	0.47	3.68	97.67	839.42	62.71	-	-	-	1	1A
						A	272.76	2.32	0.49	2.37	181.2	723.76	95.02	-	-	-		
						C	562.20	1.37	0.71	1.54	207.3	488.30	304.0					
57	50	F	2, 3,	LT P	0	T	159.56	3.15	0.38	3.18	99.07	842.56	58.44	-	-	-	1	2
						A	349.50	1.64	0.47	1.71	160.6	680.87	158.5	-	-	-		
						C	345.20	1.46	0.41	1.53	211.7	642.48	145.8					
58	68	M	2, 5	RT TP	3	T	187.84	3.44	0.52	3.48	133.7	806.08	60.08	-	-	-	1	1B
						A	212.20	2.33	0.41	2.37	101.2	808.91	89.96	-	-	-		
						C	492.00	1.37	0.60	1.52	252.7	506.8	240.5					
59	53	F	1, 5 11,12	LT F	2	T	124.00	2.69	0.26	2.71	71.11	881.02	47.61	-	-	-	1	1A
						A	170.70	2.53	0.36	2.55	92.57	840.64	66.74	-	-	-		
						C	316.00	1.40	0.37	1.46	197.1	684.08	118.9					
60	19	M	1, 2	LT F	2	T	340.20	1.15	0.33	1.20	172.4	682.11	145.5	4.99	4.96	129.9	2	1B
						A	294.20	1.49	0.37	1.55	183.9	683.08	110.9	1.37	1.29	125		
						C	376.60	1.32	0.43	1.39	192.4	629.62	156.7					

SL.No	Age	Sex	Clinical symptom	Location	SWI	DTI (MEAN VALUES)								DSC-MRI			Surgery	HP
						AREA	FA	*p*	*q*	*L*	*CP*	*CS*	*CL*	rCBV	rCBF	rPSR		
61	49	F	1, 3, 4	RT P	0	T	124.30	1.02	0.10	1.02	76.11	877.33	46.56	5.75	7.58	96.23	1	2
						A	184.10	2.67	0.40	2.69	120.0	818.67	61.38	0.76	0.84	101		
						C	299.91	1.19	0.33	1.37	181.4	700.07	118.3					
62	59	F	1,11	RT FT	0	T	177.70	1.20	0.17	1.22	122.8	819.38	57.77	-	-	-	1	2
						A	378.93	1.81	0.56	1.91	124.1	713.41	162.5	-	-	-		
						C	241.83	1.22	0.30	1.27	162.2	692.92	144.7					
63	32	F	1, 3	LT FT, BG	3	T	130.70	3.30	0.37	3.32	81.48	871.79	46.82	12.1	10.7	87.82	1	1B
						A	155.40	2.76	0.33	2.78	78.19	857.97	64.03	0.54	0.59	98.3		
						C	405.77	1.31	0.47	1.40	184.3	620.88	194.6					
64	29	M	1, 4, 5	RT FT	3	T	260.54	2.64	0.55	2.70	161.7	735.29	103.0	-	-	-	1	1B
						A	336.90	2.10	0.59	2.20	144.2	691.33	164.4	-	-	-		
						C	636.30	1.22	0.77	1.46	208.6	392.39	399.0					
65	23	F	1,5, 11	LT TP	3	T	138.46	1.26	0.14	1.26	86.38	863.66	49.83	5.16	4.92	94.5	1	1B
						A	170.00	3.10	0.43	3.13	98.70	837.72	63.46	0.39	0.16	110		
						C	451.20	1.36	0.54	1.48	224.3	561.23	214.4					
66	48	F	1, 7	RT P	0	T	158.22	1.41	0.18	1.42	97.44	845.56	56.00	5.2	2.86	107.5	2	3
						A	197.00	1.81	0.29	1.84	102.4	818.11	78.78	0.54	0.47	88.5		
						C	299.44	1.54	0.39	1.60	179.9	706.22	113.2					

CODES TO MASTER CHART

CLINICAL SYMPTOMS (CS)	CODES
HEADACHE	1
WEAKNESS	2
SEIZURE	3
VISUAL COMPLAINTS	4
MEMORY LOSS	5
GAIT UNSTEADINESS	6
LOC	7
BEHAVIORAL CHANGE	8
TREMOR	9
DIFF. FINDING WORDS	10
VOMITING	11
URINARY INCONTINENCE	12
PARESTHESIA	13
SLURRING SPEECH	14
NUMBNESS	15
ALTERED SENSORIUM	16

LOCATION OF LESION	CODES
FRONTAL	F
TEMPOROOCCIPITAL	TO
FRONTOPARIETAL	FP
FRONTOTEMPORAL	FT
TEMPOROPARIETAL	TP
TEMPORAL	T
PARIETAL	P
OCCIPITAL	O
BASAL GANGLIA	BG
CORPUS CALLOSUM	C

AREAS STUDIED	FULL FORM
T	INTRATUMOR REGION
A	ADJACENT PERITUMORAL REGION
C	CONTRALATERAL NORMAL WHITE MATTER

HISTOPATHOLOGIC FINDINGS (HP)	CODES
HIGH GRADE GLIOMA – GRADE III	1A
HIGH GRADE GLIOMA – GRADE IV	1B
METASTASES	2
LYMPHOMA	3

SWI (ITSS GRADES)	CODES
GRADE 0	0
GRADE I	1
GRADE II	2
GRADE III	3

SIDE OF LESION	CODES
RIGHT	RT
LEFT	LT

SURGICAL PROCEDURE	CODES
SURGICAL EXCISION	1
BIOPSY OF LESION	2